INTEGRATED LUMINESCENT–CONCENTRATOR PHOTODETECTORS

by

Scott Arthur Evenson

Bachelor of Science (Electrical Engineering)
University of Manitoba, 1990

A THESIS SUBMITTED IN PARTIAL FULFILLMENT
OF THE REQUIREMENTS FOR THE DEGREE OF
MASTER OF APPLIED SCIENCE
in the School
of
Engineering Science

SIMON FRASER UNIVERSITY
September 1994

Approval

Name: Scott Arthur Evenson

Degree: Master of Applied Science

Title of thesis: Integrated Luminescent–Concentrator Photodetectors

Examining Committee: Dr. Glenn H. Chapman
Associate Professor, Engineering Science, Chairman

Dr. Andrew H. Rawicz
Associate Professor, Engineering Science
Senior Supervisor

Dr. M. Parameswaran
Assistant Professor, Engineering Science
Supervisor

Dr. Albert M. Leung
Associate Professor, Engineering Science
Internal Examiner

Date Approved: September 13, 1994

PARTIAL COPYRIGHT LICENSE

I hereby grant to Simon Fraser University the right to lend my thesis, project or extended essay (the title of which is shown below) to users of the Simon Fraser University Library, and to make partial or single copies only for such users or in response to a request from the library of any other university, or other educational institution, on its own behalf or for one of its users. I further agree that permission for multiple copying of this work for scholarly purposes may be granted by me or the Dean of Graduate Studies. It is understood that copying or publication of this work for financial gain shall not be allowed without my written permission.

Title of Thesis/Project/Extended Essay

"Integrated Luminescent - Concentrator Photodetectors

Author:

_____
(signature)

Scott Evenson
(name)

September 13 1994
(date)

Abstract

This research investigates the development of an integrated device that utilizes a **luminescent–concentrator (LC)** to collect luminant energy. LCs offer the possibility to separate different portions of the spectrum and concentrate them at the same time. The response of an **integrated LC photodetector (ILCP)** therefore, is a strong function of these unique characteristics. This thesis presents the theory of photoluminescence and LCs in general, describes the design of a simple ILCP, discusses the two dimensional ray–optic simulation of LC and ILCP elements and details the results of experimentation using several thin film LCs and prototype ILCPs.

An ILCP is a versatile device whose characteristics include: small size, enhanced operation under either direct or diffuse light, the ability to provide wavelength filtering and shifting, improved sensitivity and quantum efficiency and stable spectral response. By tailoring device geometries and through appropriate selection of luminescent materials, ILCPs can be used in many specific applications. For example, an ILCP can be conveniently applied to colorimetric analysis where it could potentially replace complex and costly interference filters in some applications. Furthermore, ILCPs can be fabricated into complex systems. Therefore, by integrating several ILCPs sensitive to different wavelengths on the same substrate, a simple spectral analyzer could be fabricated.

The use of LCs and ILCPs is not restricted to colorimetric applications. For example, this work shows how an LC can be used to couple light from free space into waveguiding structures and how ILCPs can be used in sensors for *photosynthetically active radiation*, *ultraviolet dosimeters*, *LASER positioning* and *early vision systems.* Hence, through continued research, LCs and ILCPs can be applied to a whole range of problems requiring the collection, manipulation, distribution and/or measurement of light.

for **Carrie–Bearsers**

"... a scientist must also be absolutely like a child. If he sees a thing, he must say that he sees it, whether it was what he thought he was going to see or not. See first, think later, then test. But always see first. Otherwise you will only see what you were expecting. Most scientists forget that."

– Wonko the Sane (Adams 1984, page 566).

Acknowledgments

I wish to thank Paul Agnew and Brian Canon (at Quality Color, Delta, British Columbia), Dr. Eva Czyzewska, Dr. Marek Gnatowski (at Polymer Engineering Company Ltd., Burnaby, British Columbia), Dr. Romuald Lakowski, William Li, Dennis Michaelson, Dr. M. Parameswaran, Christopher Phelps (at the Photonics Laboratory, Washington University, St. Louis, Missouri), Brigitte Rabold, Dr. Andrew H. Rawicz, Bill Woods and Tomasz Wysokinski for all their help in the preparation of this work. I would also like to thank my parents *Elmer* and *Catherine Evenson* for the (many) years of support and encouragement they have provided me and for always being there to talk to when I needed them. Thanks also to my sister *Debbie* and her family for their kind thoughts and for helping to make me feel closer to home with their photos and videos. Finally, to my friends *Brad Delanghe*, *Apurva Desai* and *Carrie Underhill*, thanks for your help (from time to time) and for keeping me (mostly) sane to the end of this degree.

Contents

Abstract iii

Acknowledgments vi

Contents vii

List of Tables xi

List of Figures xii

List of Abbreviations xiv

List of Symbols xv

1 Introduction 1

1.1 Motivation 1

1.1.1 Photoreceptor Optics 2

1.1.2 Luminescent–Concentrators 3

1.2 Background 4

1.3 Contributions 5

1.4 Outline 5

2 Photoluminescence 7

2.1 Organic versus Inorganic Luminescence 7

2.2 Excited States of Luminescent Molecules 8

2.2.1 Vibronic Structure 10

2.2.2 Molecular Structure 12

2.3 Photophysical Processes 12
2.3.1 Absorption 13
2.3.2 Radiationless Transitions 13
2.3.3 Emission 15
2.3.4 Energy Migration and Transfer 16
2.4 Characteristics of Photoluminescence 17
2.4.1 Absorption Spectra 17
2.4.2 Emission Spectra 18
2.4.3 Mirror Symmetry 19
2.4.4 Stokes Shift 20
2.4.5 Quantum Efficiency 21
2.4.6 Lifetime 22
2.5 Sensitization and Inhibition 23
2.6 Solvent Effects 25

3 Luminescent–Concentrators 27
3.1 Principle of Operation 28
3.1.1 Flux Input 29
3.1.2 Surface Reflection and Transmission 29
3.1.3 Absorption 31
3.1.4 Emission 32
3.1.5 Total Internal Reflection 33
3.1.6 Flux Output 35
3.2 Loss Mechanisms 36
3.2.1 Transport Losses 36
3.2.2 Transfer Losses 37
3.3 Design Considerations 37
3.3.1 Refractive Indices 38
3.3.2 Dye Concentration 38
3.3.3 Geometry 38
3.3.4 Collection and Coupling 39
3.3.5 Back Reflectors 40

4 Integrated LC Photodetectors 43
4.1 Design 43
4.1.1 Light Pipe versus Waveguide 44
4.1.2 PN Junction Photodiodes 46
4.1.3 External Detection Circuitry 47
4.2 Simulation 48
4.2.1 Modeling Structures 49
4.2.2 Flux Input 49
4.2.3 Surface Transmission 50
4.2.4 Absorption and Emission 50
4.2.5 Internal Reflections 51
4.2.6 Flux Output 51
4.2.7 Results 51
4.3 Experimentation 54
4.3.1 Optical Test Bench 54
4.3.2 LCs 55
4.3.3 Photodiodes 58
4.3.4 ILCPs 60

5 Conclusions 64
5.1 Contributions 64
5.1.1 Advantages 64
5.1.2 Limitations 65
5.2 Future Work 67
5.2.1 Design Improvements 68
5.2.2 Technological Improvements 68
5.2.3 LC Applications 69
5.2.4 ILCP Applications 69

A LC Materials 73
A.1 Luminescent Materials 73
A.2 Matrix Materials 76

B Polymers 78
B.1 Polymer Solvent Systems 79
B.2 Photopolymers 81

C ILCP Fabrication 89
C.1 IC Processing 89
C.2 LC Formation 91

D Glossary 93

References 97

List of Tables

5.1 UV index 71

B.1 UV Polymer Base Resin Formulation 86
B.2 UV Polymer Test Resin Formulations 86

List of Figures

1.1 Luminescent–Concentrator 3
1.2 Integrated Luminescent–Concentrator Photodetector 4

2.1 Energy Band Diagram 10
2.2 Energy Level Diagram 11
2.3 Rhodamine 6G Absorption Spectra 18
2.4 Measurement of Optical Density 19
2.5 Rhodamine 6G Emission Spectra 20
2.6 Stokes Shift in Rhodamine 6G 21

3.1 Luminescent–Concentrator 27
3.2 LC Cross Section 28
3.3 Photon Flow Diagram 29
3.4 Probability of Transmission 31
3.5 Probability of TIR 34
3.6 Collection of Flux Input 40
3.7 Collection of Flux Output 41
3.8 Back Reflector 42

4.1 Integrated Luminescent–Concentrator Photodetector 44
4.2 Modal Concentration in an Asymmetric Slab Waveguide 45
4.3 Silicon Photodiode Responsivity 47
4.4 External Detection Circuitry 48
4.5 ILCP Cross Section 49
4.6 Light Guide Simulation results 52
4.7 ILCP Simulation results 53

4.8 Optical Test Bench 55
4.9 Set Up for LC Test Measurements 56
4.10 Effective LC Device Geometry 57
4.11 Optical Efficiency versus LC Thickness 58
4.12 Output Gain versus Thickness 59
4.13 Experimental Photodiode Responsivity 60
4.14 Set Up for ILCP Test Measurements 61
4.15 ILCP Responsivity 62
4.16 Comparison of ILCP Simulation and Experimental Results 63

5.1 LC Light Coupler 69
5.2 ILCP LASER Positioning System 72

B.1 Creation of Free Radicals for Photopolymerization 82
B.2 Thickness of UV Cured Films 87
B.3 Arithmetic Average Roughness of UV Cured Films 88

C.1 Prototype ILCP 90

List of Abbreviations

%wt : percent weight
AR : anti-reflection
ARROW : anti-resonant reflecting optical waveguide
BOE : buffered oxide etch
CIE : Commission Internationale de l'Eclairage
eV : electron volt (1.602×10^{-19} J)
GaAs : gallium arsenide
IC : integrated circuit
ILCP : integrated luminescent–concentrator photodetector
IR : infrared
LC : luminescent–concentrator
MEK : methyl ethyl ketone
MMA : methyl methacrylate
N_2 : nitrogen
Nd^{3+} : neodymium
OEIC : optoelectronic integrated circuit
PAR : photosynthetically active radiation
PMMA : polymethyl methacrylate
PPFD : photosynthetic photon flux density
PVA : polyvinyl alcohol
Si : silicon
TE : transverse electric
TIR : total internal reflection
TM : transverse magnetic
UO_2^{2+} : uranyl
UV : ultraviolet

List of Symbols

$\alpha(\lambda)$: absorption coefficient of the luminescent material (cm^{-1})

$\alpha_m(\lambda)$: absorption coefficient of the matrix material (cm^{-1})

$\alpha_t(\lambda)$: total absorption coefficient ($\alpha(\lambda) + \alpha_m(\lambda)$ cm^{-1})

Γ : non-polarized intensity reflection coefficient (*probability of reflection*) (-)

Γ_{TE} **and** Γ_{TM} : TE and TM intensity reflection coefficients (-)

δ : fraction of the luminescence lost due to transport losses (-)

$\epsilon(\lambda)$: decadic molar extinction coefficient (l mol^{-1} cm^{-1})

η : luminescent quantum efficiency (-)

θ_c : critical angle for TIR (degrees)

θ_i : incidence angle (degrees)

θ_p : propagation angle (degrees)

θ_t : transmission angle (degrees)

λ : wavelength (m)

λ_i : incident wavelength (m)

ν : frequency ($\frac{c}{\lambda}$ s^{-1})

$\overline{\nu}$: wavenumber ($\frac{1}{\lambda}$ m^{-1})

T : non-polarized intensity transmission coefficient (*probability of transmission*) (-)

τ : decay constant of luminescent emission (s)

T_{TE} **and** T_{TM} : TE and TM intensity transmission coefficients (-)

Φ_a : absorbed photon flux (W)

Φ_e : emitted photon flux (W)

Φ_i : input photon flux (W)

Φ_t : transmitted photon flux (W)

Ψ_i : input photon flux density (W per unit area)

Ψ_o : output photon flux density (W per unit area)

A_e : area of the edge (circumference $\times$ thickness) (m^2)

A_s : area of the input surface (m^2)

C : concentration of the luminescent material (mol l^{-1})

c : speed of light (2.997925×10^8 m s^{-1})

d : thickness (m)

E : energy (J)

E_g : bandgap energy (J)

G_g : geometric gain (-)

G_o : output flux gain (-)

h : Planck's constant (6.624940×10^{-34} J·S)

i : photocurrent (A)

k : Boltzmann's constant (1.380410×10^{-23} J K^{-1})

L : fraction of luminescence not captured by TIR (-)

l_s : path length traveled by a photon (m)

n_1 : refractive index of upper cladding (-)

n_2 : refractive index of core (matrix) (-)

n_3 : refractive index of lower cladding (-)

n_4 : refractive index of (semiconductor) substrate (-)

P : fraction of luminescence captured by TIR (*probability of TIR*) (-)

Q_a : absorption efficiency (*probability of absorption*) (-)

Q_c : collection efficiency (*probability of collection*) (-)

Q_o : optical efficiency (-)

R : photodetector responsivity (A W^{-1})

r_{TE} **and** r_{TM} : TE and TM amplitude reflection coefficients (-)

T : temperature (K)

t : time (s)

Chapter 1

Introduction

The purpose of this thesis is to document the development of an photosensitive device that uses the **Luminescent–Concentrator (LC)** approach to collect and concentrate light energy. The work was motivated by a desire to create an artificial photoreceptor (with properties similar to those found in biological vision systems) that could be fabricated using standard manufacturing processes. To this end, the thesis presents the theory and design of an **integrated LC photodetector (ILCP)** on a silicon substrate and discusses experimental results for several prototype ILCPs.

1.1 Motivation

Photodetectors detect radiant light energy either at a specific or over a broad range of wavelengths and produce an output signal that is proportional to the amount of energy absorbed (Dennis 1986, page 5). For example, because they convert light into electrochemical signals, the photoreceptors found in the retina are the photodetectors of the eye. When light hits one of these biological photoreceptors, chemical changes in its pigments cause electrical impulses to pass along nerves and thus send information to the brain.

There are two main classes of photoreceptor cells in the retina: *Rods* and *Cones*. Rods are the most abundant, having a single morphological type sensitive to light with wavelengths around 496 nm (Leibovic 1990, page 19). Cones are much less abundant than rods and have three morphologically indistinguishable types sensitive to light with wavelengths around 558 nm (red), 531 nm (green) and 419 nm (blue) (Leibovic

1990, page 19). Rods are long (25–50 μm) and thin (1–1.5 μm), while cones are short (6–8 μm) and thick (3–5 μm) except in the fovea where they resemble rods (Shepherd 1990, page 173).

The visible region of the electromagnetic energy spectrum is defined by the response of the photoreceptors in the human eye. Hence, many applications in this region are designed to replace, evaluate or satisfy human visual response. By using a series of filters, the response of other photodetectors (such as silicon photodiodes) can be modified to have a spectral response similar to human photoreceptors. However, other properties must be considered in order to create an artificial photoreceptor.

1.1.1 Photoreceptor Optics

The photoreceptor cells are the input elements of the retina and their function is reasonably well understood. Photons incident on a photoreceptor cell cause a change in its output level. The amount of this change is proportional to the intensity of the input stimuli (number of photons). The photoreceptor cells function to amplify (on the order of one hundred thousand times) and transform photonic input into neuronal output. This is achieved when photoreceptive *pigments* in the outer segment of a photoreceptor cell are *bleached* by photons, causing a chemical reaction, whose byproducts induce hyperpolarization of the cellular membrane (Leibovic 1990, page 18–19).

Photoreceptor optics is the study of how the physical properties of photoreceptors (their structure, arrangement, orientation, shape, size, refractive index and membrane properties) influence their absorption of light and optical characteristics (Menzel and Snyder 1975). The study of photoreceptor optics is closely related to that of optical waveguides. For example, since photoreceptors are composed largely of membrane material they are more dense than the surrounding medium and have a higher refractive index. Therefore, they can contain light by **total internal reflection (TIR)** as is typically the case in an optical lightpipe or waveguide (Snyder, Bossomaier, and Hughes 1990).

The light guiding characteristic of photoreceptors offer the potential for improved optical isolation from neighboring photoreceptors. However, the main advantage of this light guiding, is to minimize the quantity of photopigment required to capture an

individual photon by ensuring that the visual pigment is maximally exposed to the incident light (Snyder, Bossomaier, and Hughes 1990). In addition, cone receptors in the human retina have a shape corresponding approximately to that of a non-imaging concentrator designed for the collecting angle that the pupil of the eye would subtend at the retina under dark adapted conditions (Welford and Winston 1989).

1.1.2 Luminescent–Concentrators

An LC is a non-imaging optical device for collecting and concentrating light energy. As shown in figure 1.1, an LC is a planar optical matrix embedded with a luminescent material whose operation is based on the idea of light pipe trapping of molecular or ionic photoluminescence (Batchelder, Zewail, and Cole 1979). Incident photons absorbed by the luminescent centers inside the optical matrix are subsequently remitted and trapped by TIR. This trapped light is then coupled out of the LC into a photosensitive device.

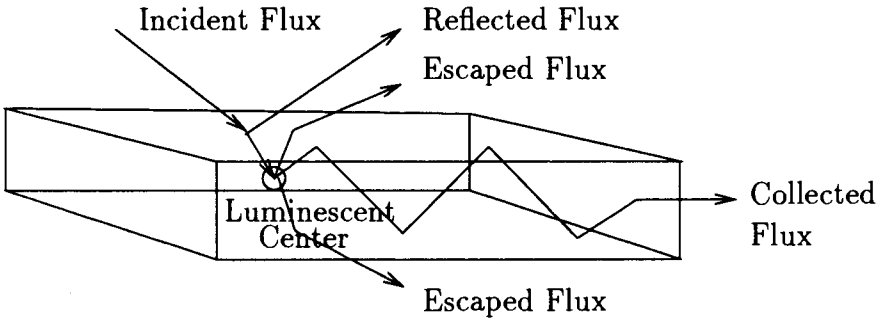

Figure 1.1: Luminescent–Concentrator

As a result of its unique properties, an LC provides concentrated flux that can be spectrally matched to the material characteristics of a given photodetector. In this way, it is possible to make efficient use of photodetectors whose response is optimized for a particular wavelength region (Weber and Lambe 1976). LCs also offer the possibility to separate different portions of the spectrum and concentrate them at the same time (Goetzberger and Greubel 1977). Hence, LCs can be used as spectral elements whose minimum incident flux density can be much less than that required by similar existing devices (Baranow 1991).

The purpose of this thesis is to describe the development of an ILCP. This device, as shown in figure 1.2, consists of a semiconductor substrate (into which planar PN junction photodiodes have been diffused) coated with a thin–film LC. The characteristics of the ILCP include: small size, enhanced operation under either direct or diffuse light, the ability to provide wavelength filtering and shifting, improved spectral sensitivity and quantum efficiency and stable spectral response.

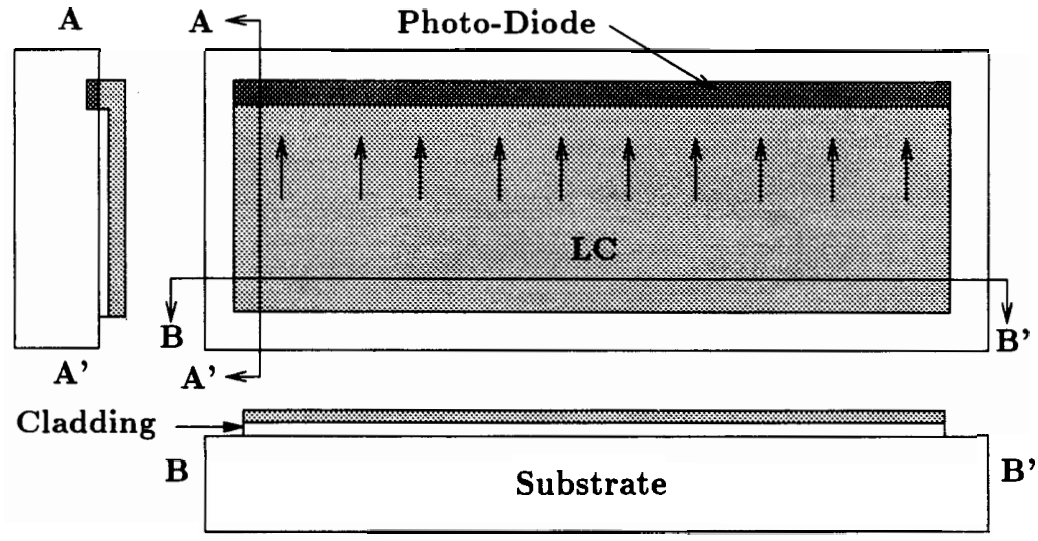

Figure 1.2: Integrated Luminescent–Concentrator Photodetector

By virtue of the photoluminescent energy transfer and light guiding properties of its LC element, an ILCP exhibits some of the optical characteristics of biological photoreceptors. In this case, the absorption and emission of photons by a luminescent material is analogous to the absorption and transduction of photons to electrochemical energy by biological photopigments. Therefore, by matching the spectral response of the LC elements to those of the rods or cones, an ILCP becomes an artificial photoreceptor. Furthermore, by using large scale integration, an array of ILCPs can be made into an imaging photodetector or as part of an artificial retina.

1.2 Background

The application of LCs has been under investigation for several years now (Levin, Cherkasov, and Baranov 1988). Early research attempted to make use of LCs as

radiance amplifiers for scintillation counters, in instrumentation for astronomical observations, in the collection of solar energy and as backlighting elements for liquid crystal displays (Batchelder, Zewail, and Cole 1979). More recently however, it was suggested that LCs can be used to construct optical devices for color or simple spectral analysis (Baranow 1991). Pursuing this idea further, while considering the requirements for an artificial photoreceptor, resulted in the conception of the ILCP (Evenson and Rawicz 1994).

1.3 Contributions

The major contributions made by this thesis are to present the theory of LC's as spectral elements, to show how this theory can be used in the design of LC devices in general and ILCPs in particular and to show how this theory can be modeled using a simple ray–optic algorithm. This thesis also develops various fabrication techniques required to realize thin film LC elements using a photopolymer material, discusses how they can be integrated with electronics on a semiconductor substrate to make an ILCP and, as a final contribution, details experimental results using several prototype ILCPs as proof of concept.

1.4 Outline

Chapter 1 provided a discussion of the motivation and background and stated the contributions made by this research. It now concludes by providing an outline of the remainder of this thesis.

Chapter 2 presents the general theory and characteristics of photoluminescence processes in organic molecules and discusses effects in cascade systems and for various solvent media.

Chapter 3 discusses the theory of LCs in terms of photo flow, describes the various loss mechanisms and details a number of design considerations for the realization of LC devices in general.

Chapter 4 describes the design of a simple ILCP, discusses a two dimensional ray–optic simulation based on this design and presents test results for several experimental thin film LCs and prototype ILCPs.

Chapter 5 provides a general discussion of the research, summarizes the significant ideas presented in this thesis and indicates areas for future work.

Chapter 2

Photoluminescence

Luminescence is the emission of light that is not due to *incandescence* (Merriam–Webster Incorporated 1985). It occurs at low temperatures and can result from chemical, physical, electrical, electromagnetic or biological processes. **Photoluminescence** occurs when a molecule is excited by electromagnetic radiation (photons) to a state where it itself emits such radiation. This type of luminescence can emanate from either organic or inorganic materials.

2.1 Organic versus Inorganic Luminescence

The luminescent mechanism is different for **organic** and **inorganic** materials. Organic materials are held together by Van der Waals forces between molecules and are therefore considered molecular solids. Inorganic materials are held together by ionic or covalent bonds between individual atoms and thus can be regarded as atomic solids (Lumb 1978, page 94). Luminescence in organic materials is associated with excited states of molecules, while in inorganic materials it is associated with either defects or impurities in the atomic lattice or with excited states of isolated atoms or ions. Also, the luminescence spectra of organic materials in the gas, liquid and solid state, unlike inorganic materials, are similar (Lumb 1978, page 94). This thesis considers only uni-molecular luminescence emission from the excited states of organic molecules.

2.2 Excited States of Luminescent Molecules

Photoluminescence from an organic molecules result from electronic transitions involving **π–electrons** (Becker 1969, page 4). These electrons exist as a consequence of a particular configuration of carbon atoms in the molecule that result in the formation of **π–orbitals**. π–electrons are less tightly bound to their parent carbon nuclei and therefore require less excitation energy than other bonding electrons (Lumb 1978, page 96). An excited state is derived by moving one of the electrons from the uppermost filled orbital of the ground state to a vacant orbital of higher energy (Becker 1969, page 1).

An electron in a molecule behaves as if it generates two types of magnetic and mechanical angular momenta that arise from its "spin" and motion about the nucleus. These electrons are added to the orbitals in order of increasing energy and according to the Pauli exclusion principle, only two electrons of opposite spin can occupy each π–orbital. Hence, the overall state of a molecule is a function of its orbital electron configuration and the *total spin* S of a molecule can be found by summing the spins of all the electrons in the various orbitals (Becker 1969, page 4–5).

Organic molecules have an even number of π–electrons so that in the ground (unexcited) state, all the electron spins are paired off and S is equal to zero (Krasovitskii and Bolotin 1988, page 6) (Lumb 1978, page 137). The *level multiplicity* of a molecule is given by the expression $|2S| + 1$. In the ground state the multiplicity is one or **singlet (S)**. If there is a reversal in the spin of one of the electrons, during the transition to an excited state, the total spin becomes unity and the multiplicity becomes three or **triplet (T)** (Krasovitskii and Bolotin 1988, page 6). Hence, electronic energy transitions in luminescence molecules can be described as taking place within either of the following two systems:

1. **Singlet Manifold** with an angular spin momentum of zero
2. **Triplet Manifold** with an angular spin momentum of unity

The nature of the emission process depends on these *state multiplicities* (Becker 1969, page 1).

The Singlet Manifold

The initial state of a molecule before excitation is usually the singlet ground state S_0. Excitation to higher excited states of the singlet manifold S_n results in rapid internal conversion to S_1 from which emission can occur. Following emission, the molecule generally returns to S_0, although frequently in a vibrationally excited form (Becker 1969, page 1). According to **Hund's rule** (Lumb 1978, page 99), for every excited singlet state there is a corresponding triplet state of lower energy (Becker 1969, page 6).

The Triplet Manifold

The lowest excited triplet state T_1 is populated almost entirely by intersystem crossing from S_1. Thus, T_1 can have a similar population to that of S_1 (Lumb 1978, page 137). Although transitions between states of different multiplicity are spin–forbidden processes, the transition probability or **Franck–Condon factor** increases as the energy gap between the respective states decreases [1]. This intersystem crossing process competes with the emission process that occurs due to transitions between S_1 and S_0 (Lumb 1978, page 137). In a manner similar to that in the singlet manifold, excitation to higher excited states of the triplet manifold T_n results in rapid internal conversion to T_1 (Lumb 1978, page 138). The reverse process $T_1 \rightarrow S_0$ is also spin-forbidden and hence T_1 can be regarded as a metastable state having a lifetime in the range of milliseconds to seconds (Lumb 1978, page 137).

Energy Transitions

Figure 2.1 depicts the energy band diagram of a simple luminescent molecule. In the case of a diatomic molecule, the potential energy curve is a function of internuclear distance (Becker 1969, page 1). In a polyatomic molecule, the internuclear distance is replaced by a configurational coordinate (Lumb 1978, page 106). As shown in the figure, at ambient temperatures the unexcited molecule is in its lowest vibrational level S_0. Following the absorption of a photon however, the molecule is raised to an excited state S_n. According to the **Franck–Condon principle** this transition occurs

[1] The $S_1 \rightarrow T_1$ intersystem crossing rate is on the order of 10^6 times greater than that of $S_0 \rightarrow T_1$ (Lumb 1978, page 137).

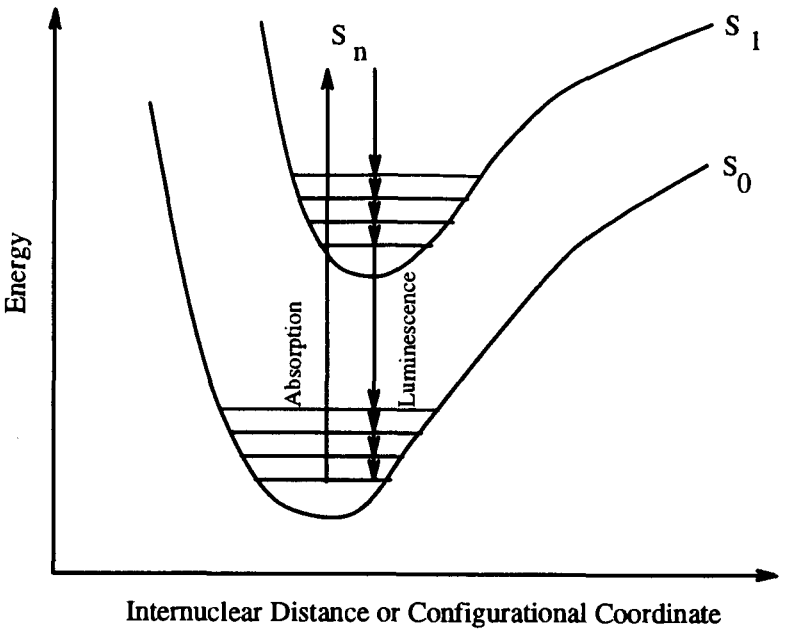

Figure 2.1: Energy Band Diagram

too rapidly for the atomic nuclei to alter their spacing and is therefore represented by a vertical line. Since the bond length of an excited molecule is usually greater than that of its ground state, the molecule is in a highly compressed state. This excess energy is rapidly lost vibrationally to neighboring molecules and the molecule soon relaxes to the lowest level of S_1. At this point, the molecule can drop back to S_0 with the emission of a photon. Again, due to the Frank–Condon principle, this transition is represented by a vertical line on the energy band diagram. The strength of these transitions are determined by the overlap of the vibrational energy bands of the ground and excited states (Lumb 1978, page 104).

2.2.1 Vibronic Structure

The total energy stored in a molecule is equal to the sum of three components:

1. **electronic** energy (E_e)
2. **vibrational** energy (E_v)
3. **rotational** energy (E_r)

Superimposed on each E_e level are vibrational E_v and rotational E_r sub-levels associated with the motion of the main molecular skeleton (Lumb 1978, page 99). Hence,

each electronic absorption transition ΔE_e (on the order of several eV at room temperature) gives rise to an absorption band system where each band corresponds to a different value of ΔE_v (approximately $0.1eV$ at room temperature). This condition is referred to as a **vibronic state** and a transition between two such states is known as a **vibronic transition** (Birks 1970, page 44–45) (Berlman 1971, page 9).

At low temperatures, detailed vibronic structure can be resolved, but at normal temperatures, molecular rotation ($\Delta E_r \approx 0.01$ to $0.001eV$ at room temperature), thermal broadening [2] and/or solvent interaction effects tend to blur this structure (Birks 1970, page 44–45) (Berlman 1971, page 9).

Energy transitions in a luminescent molecule can be studied with the aid of a *Jablonski* or **energy level diagram** (Berlman 1971, page 9)) like that shown in figure 2.2. Here, S, T and V are singlet, triplet and vibrational states respectively. The solid upward arrows represent absorption transitions. The downward pointing arrows represent luminescence transitions. Finally, the dashed lines represent internal conversion transitions.

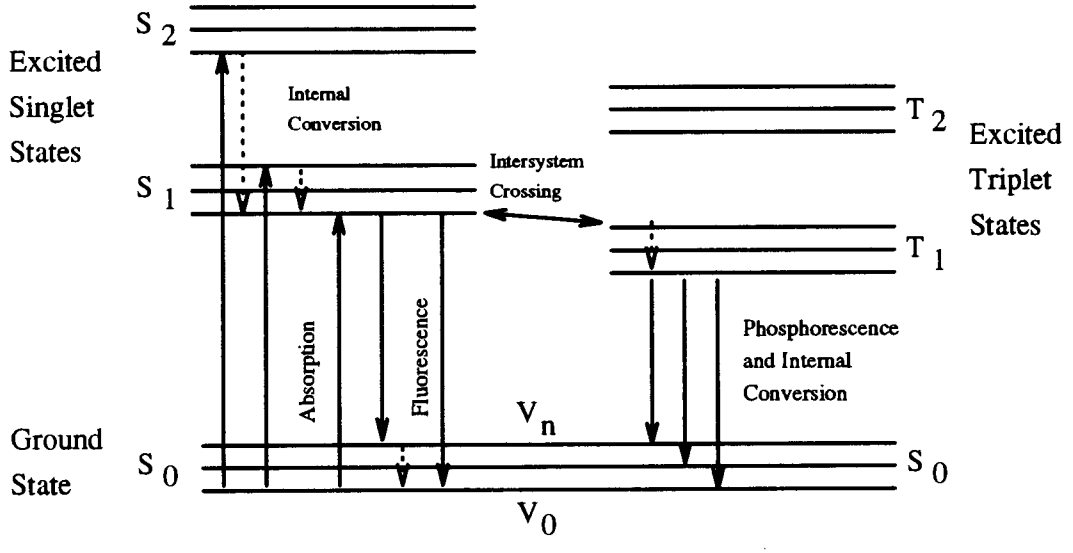

Figure 2.2: Energy Level Diagram

The luminescent properties of an organic molecule depend on the relative arrangement of its singlet and triplet levels and hence its vibronic structure. The nature of

[2] In polyatomic molecules at room temperature, the rotational energy states are very closely spaced and tend to smear out and simply broaden the vibrational bands (Lumb 1978, page 102).

its vibronic transitions however, are also dependent on its molecular structure (Krasovitskii and Bolotin 1988, page 13).

2.2.2 Molecular Structure

The shape of the fluorescence and absorption spectra, their position as a function of wavelength and the strength of the transitions involved are all characteristic of the spatial structure of the luminescent molecule (Berlman 1971, page 67) (Krasovitskii and Bolotin 1988, page 15). For example, transition dipoles of the absorption and emission bands may have a preferential orientation or polarization (Becker 1969, page 80). As the molecular structure becomes more complex (especially in chain compounds), increases in non-radiative energy losses due to molecular rotation and vibration adversely effect luminescence. Conversely, a sufficiently rigid structure minimizes non-radiative loss of the absorbed energy and increases the probability of radiative transitions (Krasovitskii and Bolotin 1988, page 14–15). Furthermore, the effect of molecular structure on the luminescence can vary widely depending on the state of aggregation of the substance, type of solvent, solute concentration, viscosity and temperature (Krasovitskii and Bolotin 1988, page 18).

2.3 Photophysical Processes

A **photophysical process** is a physical process (that is, one that does not involve a chemical change) resulting from the electronic excitation of a molecule or system of molecules by non-ionizing electromagnetic radiation (photons) (Birks 1970, page 29). Referring again to figure 2.2, some of the transitions that can take place in a luminescent molecule include (Berlman 1971, page 10–11):

1. **Absorption:** (electronic excitation) Energy transitions between S_0 and S_n when an incident photon is absorbed.
2. **Internal Conversion:** (electronic relaxation) $S_n \rightarrow S_1$ and $T_n \rightarrow T_1$ transitions, where energy is lost as heat.
3. **Intersystem Crossing:** Energy transitions between excited single and triplet states.

4. **Fluorescence:** Transitions between S_1 and S_0 that result in the immediate emission of a photon.

5. **Phosphorescence:** Transitions between T_1 and S_0 where a photon is released.

2.3.1 Absorption

A transition between two electronic states in a luminescent molecule can be induced by a photon, provided that its frequency (Becker 1969, page 19)

$$\nu = \frac{E_j - E_i}{h} \quad [s^{-1}] \tag{2.1}$$

where h is Planck's constant and E_i and E_j are the energies of the initial and final electronic states respectively. This relation represents the quantization condition for the absorption (or emission) of light (Lumb 1978, page 102). The energy absorbed is equal to the energy of the incident photon as given by the Einstein relationship

$$E = h\nu \quad [J] \tag{2.2}$$

However, in a molecule, the vibrational and rotational energies of the atoms are superimposed on the electronic energy levels of the atoms so that (Lumb 1978, page 102)

$$E = \Delta E_e + \Delta E_v + \Delta E_r \quad [J] \tag{2.3}$$

is also true. Hence from the Franck–Condon Principle the shape of an absorption band will depend largely on the relative location of the potential energy minima of the molecule's electrons (Becker 1969, page 32).

Following electronic excitation to a state S_n, a molecule vibrationally relaxes to S_1. From this state fluorescence emission, continued relaxation to the ground state with no emission, crossing to the triplet state or any combination of these may occur (Becker 1969, page 76).

2.3.2 Radiationless Transitions

Radiationless processes are the result of conversion of electronic energy to vibrational energy between states of the same or different multiplicity, without the emission of a photon. Therefore, these processes are in competition with the radiative processes

responsible for luminescence emission and can be roughly understood as the dissipation of energy in the form of heat (Lumb 1978, page 123). The energy transfer process from the singlet to the triplet state or vice versa is called **intersystem crossing**. Energy lost in other transitions is called **internal conversion** (Becker 1969, page 2).

Internal Conversion

Once excitation has occurred to a level S_n, the molecule immediately begins vibrating and, in an extremely rapid cascading process, descends through the various levels associated with each excited state, until it finally reaches the lowest vibrational level of S_1 (Becker 1969, page 88). The potential energy bands of $S_n...S_1$ do not need to cross but they must be sufficiently close in order to interact strongly (Becker 1969, page 88). This isoenergetic radiationless electronic transition between states of the same multiplicity is called **internal conversion** (Birks 1970, page 143).

At normal temperatures, internal conversion occurs in approximately 10^{-11} seconds. This is slow in comparison with the time of absorption, but it is fast when compared to normal fluorescence (Birks 1970, page 142). Hence, it is assumed that the vibrational relaxation process is fast and that it is the transition between vibronic states that is rate determining (Becker 1969, page 108) [3].

Intersystem Crossing

Intercombination processes involving states of different multiplicity depend on spin–orbit coupling between excited singlet and triplet states (Becker 1969, page 95). This form of radiationless transition is called **intersystem crossing** (Birks 1970, page 144). Since $S_0 \rightarrow T_1$ energy differences are generally much larger than $S_1 \rightarrow T_1$ energy differences, intersystem crossing is considerably more likely than a direct energy transitions from the ground to a triplet state (Becker 1969, page 96).

[3]The radiative lifetime is on the order of 10^{-9} seconds while the period of molecular vibrations is typically 10^{-12} seconds, therefore the molecule normally reaches thermal equilibrium before fluorescence emission occurs (Lumb 1978, page 99).

2.3.3 Emission

Luminescence can originate from any of the excited states (Lumb 1978, page 99). The singlet state is responsible for **fluorescence** processes while the triplet state is responsible for **delayed fluorescence** and **phosphorescence** processes (Lumb 1978, page 137). Fluorescence and phosphorescence differ appreciably in their lifetimes. This property is used to distinguish between the two emissions (Birks 1970, page 201). However, **Kasha's rule** states that the luminescence of an aromatic molecule occurs only from the lowest excited electronic state of a given multiplicity, so that the $S_1 \rightarrow S_0$ fluorescence and the $T_1 \rightarrow S_0$ phosphorescence are the only two molecular luminescences expected (Birks 1970, page 162). Thus, the lowest absorption band and the highest emission band should coincide [4] (Becker 1969, page 87).

Fluorescence

If a molecule can remain in its lowest excited state for 10^{-9} seconds or longer and there are no competing processes, then the situation is favorable for the molecule to emit **fluorescence** (Berlman 1971, page 10). If any non-radiative processes comparable in speed with radiation are possible, the probability of fluorescence diminishes. This non-radiative deactivation of the electron excitation energy may proceed through **internal conversion** or **intersystem crossing** (Krasovitskii and Bolotin 1988, page 10). The transition leading to fluorescence occurs from the lowest vibrational level of S_1 to one of the vibrational levels of S_0. Thus the fluorescent spectrum displays the vibrational spacing of the ground state. Excess vibrational energy in the ground state is lost by internal conversion (Berlman 1971, page 10).

Delayed Fluorescence

Delayed fluorescence although originating from the triplet state has an emission spectrum identical to the normal prompt fluorescence spectrum. It occurs when the long lived triplet state T_1 can be thermally depopulated via S_1 or when pairs of excited triplet molecules interact to produce an excitation energy greater than or equal to S_1 (Lumb 1978, page 100) (Berlman 1971, page 12).

[4] This proves to be true for molecules in vapors, but not true for molecules in solution (Becker 1969, page 87).

Phosphorescence

If an electron is excited into a triplet state, **phosphorescence** due to transitions from the lowest vibrational level of T_1 to the one of the vibrational levels of S_0 can occur. Triplet–triplet internal conversion is analogous to that of the singlet manifold (Birks 1970, page 145). The characteristics of phosphorescence radiation differ from fluorescence in that its lifetime is much longer, its spectrum is composed of much longer wavelengths (since T_1 has less energy than S_1) and its vibrational spacing to S_0 (and hence spectrum) is usually different (Berlman 1971, page 11).

Since T_1 can have a similar population to S_1 it would be expected, that all fluorescent organic molecules are also phosphorescent. Due to its longer lifetime however, the triplet state is very susceptible to quenching by trace impurities and oxygen in particular. In any medium where significant diffusion can occur (such as in a gas or liquid) quenching of the phosphorescence occurs. Thus, phosphorescence is commonly seen in rigid media at low temperatures (Lumb 1978, page 137).

2.3.4 Energy Migration and Transfer

If an acceptor molecule Y is in the vicinity of an excited donor molecule X^* and the energy of an excited state of Y lies below that of X^*, then the energy can be transferred from X^* to Y (Lumb 1978, page 140). **Energy transfer** is the transfer of electronic excitation energy of a molecule or group of molecules to another molecule or group of a different species while **energy migration** is similar to energy transfer, but exists between molecules or groups of the same species (Birks 1970, page 518). Energy migration, causes the excitation energy to become delocalized (Lumb 1978, page 140). Energy transfer and migration may be inter or intramolecular (Birks 1970, page 518) and may involve (Lumb 1978, page 140):

1. **radiative transfer** where the efficiency of transfer depends on the overlap of the emission spectrum of the donor with the absorption spectrum of the acceptor. This type of energy transfer is an important process in solid solutions and most important in solutions with low solute concentrations.

2. **radiationless transfer** occurs when the efficiency of transfer depends on the close proximity of the donor and acceptor and is therefore diffusion controlled.

This type of energy transfer is the most important in solutions with high solute concentrations.

2.4 Characteristics of Photoluminescence

Properties of luminescence systems that can be measured experimentally include (Lumb 1978, page 102):

1. **Absorption, Emission and Excitation spectra**
2. **Lifetimes and Rate parameters**
3. **Quantum Efficiency and Yields**

Other properties, such as the rate parameters of non-radiative processes, can be deduced from these.

2.4.1 Absorption Spectra

The **absorption spectra** of a luminescent molecule depicts the vibrational spacing of S_1 (Lumb 1978, page 104). In a *homogeneous* medium (a medium where the luminescent *absorbing species* is uniformly distributed) the absorption spectra behaves according to the **Beer–Lambert Relationship**, which states that the absorbed photon flux is a function of wavelength such that

$$\Phi_a(\lambda) = \Phi_i(\lambda)(1 - e^{-\alpha(\lambda)l_s}) \quad [W] \tag{2.4}$$

where Φ_i is the incident photon flux, λ is the incident wavelength, α is the absorption coefficient and l_s is the path length of the incident flux in the medium.

For molecules in solution or a solid

$$\alpha(\lambda) = \epsilon(\lambda)Cln(10) \quad [cm^{-1}] \tag{2.5}$$

where $\epsilon(\lambda)$ is the (decadic) **molar extinction coefficient**, and C is the molar concentration of the absorbing species. The absorption spectrum is plotted in terms of ϵ versus frequency ν, wavelength λ or wavenumber $\overline{\nu}$ (Lumb 1978, page 102) as shown in figure 2.3 for rhodamine 6G ($C_{28}H_{31}N_2O_3$) (Berlman 1971, page 412).

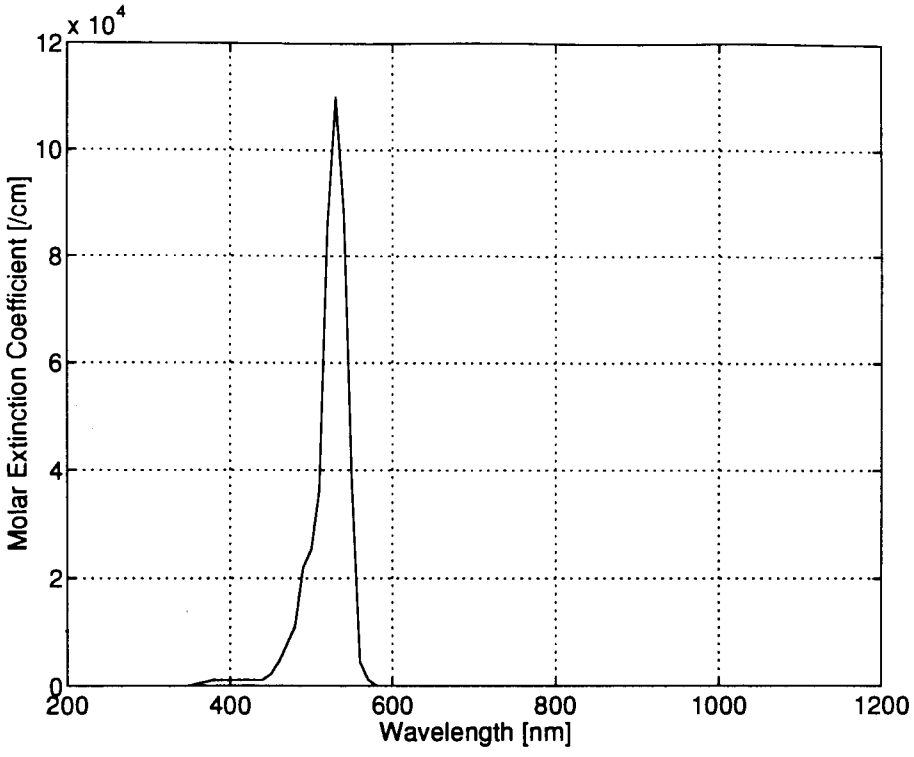

Figure 2.3: Rhodamine 6G Absorption Spectra

ϵ is obtained by measuring the **optical density** of a sample of know concentration C (mol/l) and thickness d (cm) as shown in figure 2.4, since the transmitted flux Φ_t falls off exponentially with thickness

$$\Phi_t(\lambda) = \Phi_i(\lambda)10^{-\epsilon(\lambda)Cd} \quad [W] \tag{2.6}$$

so that (Lumb 1978, page 102)

$$\epsilon(\lambda) = \left(\frac{1}{Cd}\right) Log_{10} \quad [l \cdot mol^{-1}cm^{-1}] \tag{2.7}$$

If the sample is a solution, then the magnitude of the absorption spectra is easily modified by using different concentrations. If the sample is a solid the magnitude of the absorption spectra is a function of specimen thickness.

2.4.2 Emission Spectra

The **emission spectra** is a plot of the distribution of luminescence as a function of wavelength for a given excitation that depicts the vibrational spacing of S_0 (Lumb

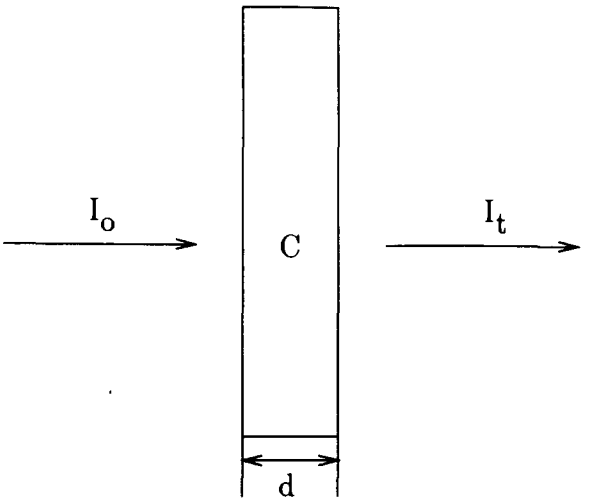

Figure 2.4: Measurement of Optical Density

1978, page 104). In most luminescence systems, the emitted photon is lower in energy than the absorbed photon therefore, quantum efficiencies η greater than 1 are possible, however this is not the usual case (Lumb 1978, page 230). Emission may be either fluorescence or phosphorescence. Figure 2.5 shows the normalized emission spectra of rhodamine 6G (Berlman 1971, page 412).

2.4.3 Mirror Symmetry

When the absorption and fluorescence spectra display similar structured distribution patterns, they are said to possess **mirror symmetry** (Berlman 1971, page 10). This occurs if the nuclear configurations of S_0 and S_1 are sufficiently similar (vibrations in the excited state are comparable to those in the ground state) and is approximately valid for organic luminescent dyes. If the nuclear configurations of S_0 and S_1 are not similar, deviations from this trend may occur (Birks 1970, page 85). For example, differences in the dipole orientation, hydrogen bonding and geometry between the two states can modify this relationship (Becker 1969, page 89), resulting in hindrance to the relaxation processes of the excited or ground states (Lumb 1978, page 106).

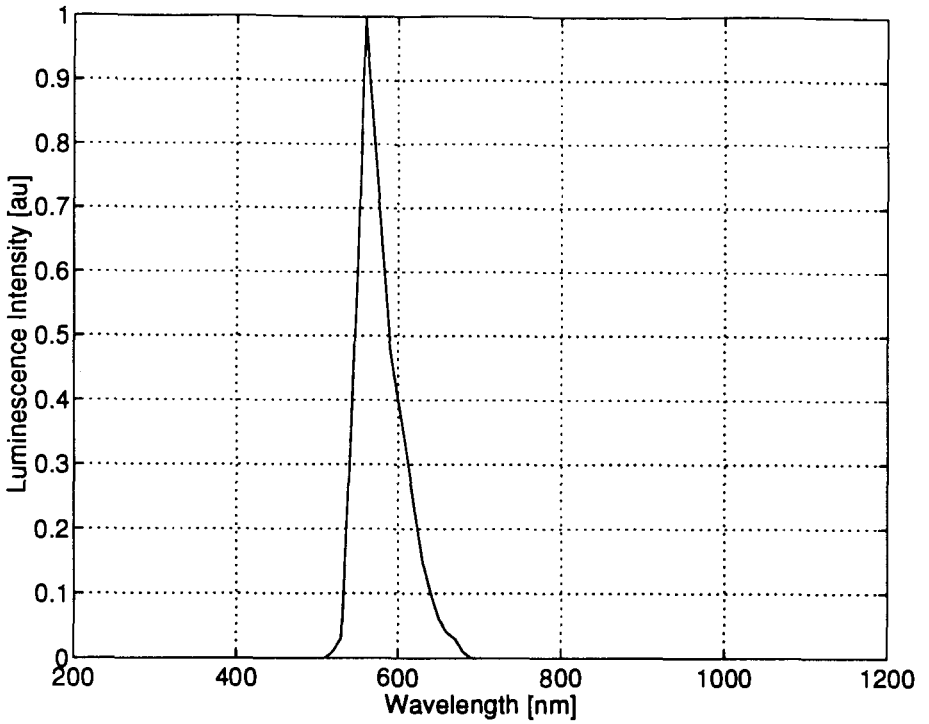

Figure 2.5: Rhodamine 6G Emission Spectra

2.4.4 Stokes Shift

A molecule when excited from S_0 to a vibrationally excited level of S_1 quickly transfers its excess vibrational energy to collisions with neighboring molecules and ends up in the lowest vibrational level of S_1 (Berlman 1971, page 57). From this level, a photon can be emitted and the molecule transferred to a vibrationally excited level of S_0. The difference in the vibrational energy of S_0 occupied by the molecule before absorption and after emission also represents a transfer of vibrational energy (Krasovitskii and Bolotin 1988, page 5). These energy transfer processes represent a loss of some of the excitation energy available for fluorescence, the magnitude of which is determined by the shape of the potential surface of S_0, the change in the equilibrium configuration of the molecule during the electronic transition and by the frequency of the transition (Berlman 1971, page 57). This loss in energy results in a shift in wavelength between the absorbed and emitted radiation and is known as the **Stokes shift**.

In solution, a small Stokes shift results in a large self absorption, while a large

Stokes loss produces the opposite effect (Berlman 1971, page 58). Due to different Stokes shifts, the factors responsible for a particular absorption mechanism (coloration) of organic substances do not always influence the color of their luminescence (Krasovitskii and Bolotin 1988, page 18). Figure 2.6 shows the Stokes shift between the normalized absorption and emission spectra of rhodamine 6G.

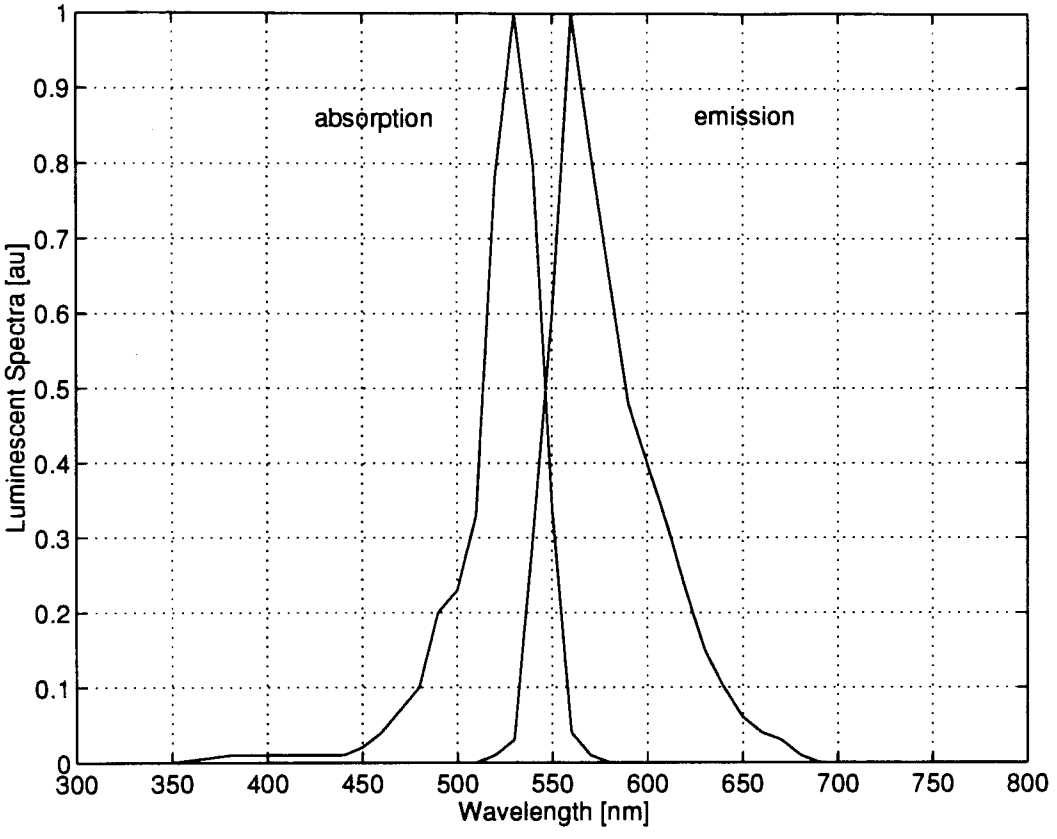

Figure 2.6: Stokes Shift in Rhodamine 6G

2.4.5 Quantum Efficiency

The **quantum efficiency** η of a luminescent material is the probability that an excited molecule will follow a given pathway whether radiative or non-radiative (Lumb 1978, page 109). For example, the **fluorescence quantum yield** or **efficiency** is the ratio of the number of fluorescent photons emitted to the number of exciting photons absorbed (Becker 1969, page 80) (Birks 1970, page 85). Similarly, the **phosphorescence quantum efficiency** is the ratio of the number of phosphorescent photons

emitted from the first excited triplet state to the number of molecules initially excited to a triplet state [5] (Lumb 1978, page 109) (Birks 1970, page 194). For rhodamine 6G in methanol solution at room temperature, the fluorescence quantum efficiency is 0.98 (Baczynski, Marszalek, Walerys, and Zietek 1973).

Vavilov's law states that the quantum efficiency is independent of the initial vibrational and electronic states into which the molecule is excited. That is, the properties of a molecule in dilute solution are independent of the initial vibrational and electronic state to which it is excited (Birks 1970, page 142). This is due to the very efficient process of internal conversion from higher excited states to S_1 or T_1 (Lumb 1978, page 107). However, the occurrence of non-radiative processes tend to lower quantum yields (Krasovitskii and Bolotin 1988, page 5). These competing bimolecular processes include (Birks 1970, page 90):

1. **Collisional impurity quenching:** diffusion controlled collisions between excited dye and impurity molecules in the solution.
2. **Energy transfer quenching:** non-collisional radiationless transfer of energy between excited dye and impurity molecules whose first electronic excited singlet state is lower than that of the dye molecules.
3. **Concentration quenching:** an increase in the molar concentration of the fluorescence dye causes a decrease in the molecular fluorescence due to excimer formation.
4. **Radiative migration:** an overlap of the fluorescence and absorption spectra of the dye molecules resulting in **self-absorption** of part of the fluorescence emission and changes the observed fluorescence lifetime and quantum yield.

2.4.6 Lifetime

Following the removal of the exciting source, fluorescence and phosphorescence emission decay according to a first order rate equation that is exponential with time (Becker 1969, page 77–78)

$$\Phi_e(t) = \Phi_o e^{\frac{-t}{\tau}} \quad [W] \tag{2.8}$$

[5] The **phosphorescence quantum yield** is defined as the ratio of the number of phosphorescence photons emitted to the number of photons absorbed (Birks 1970, page 194).

here, Φ_o is the magnitude of the initial emission and τ is the decay constant of the luminescent emission. The **fluorescence and phosphorescence lifetimes** are defined as the interval during which the strength of the luminescent emission falls to e^{-1} of its initial value (Berlman 1971, page 14). The decay time for emission from S_1 (fluorescence) is very short, being on the order of 10^{-9} seconds. On the other hand, since energy can be stored for a relatively long period of time in a triplet state, the decay time from T_1 (phosphorescence) can be on the order of 10^{-3} to several seconds (Berlman 1971, page 11). For rhodamine 6G in methanol solution at room temperature, the fluorescence decay time is 6.28×10^{-9} seconds (Baczynski, Marszalek, Walerys, and Zietek 1973). This decay time however, will vary depending on the state and type of solvent used.

2.5 Sensitization and Inhibition

Radiative and non-radiative energy transfer in multiple dye luminescent systems are of major practical importance. For example, a technique known as **sensitization** can be used to increase absorption and thereby enhance luminescence emission. Conversely, **inhibition** can be used to decrease emission and therefore to reduce emission. Sensitization and inhibition can also be used to tailor the shape of the absorption and emission spectra respectively.

Sensitization

Cascade Compositions are mixtures where *donor* luminophors luminesce at short wavelengths and *acceptor* chromophores luminesce at longer wavelengths (Krasovitskii and Bolotin 1988, page 12). For example, if a solution contains two species of luminescent molecules X and Y and the first excited singlet state of Y lies below that of X, then energy transfer from X to Y can occur. Thus the fluorescence emission of Y can be increased at the expense of an increase in the concentration of X. This energy transfer process is diffusion controlled (Lumb 1978, page 120).

Using sensitization, a much cheaper and more readily available donor luminophor can be used to compensate for a more expensive acceptor luminophor while producing the same luminescent effect as using only the acceptor but in greater amounts

(Krasovitskii and Bolotin 1988, page 12). Since the effectiveness of energy transfer depends on the amount of overlap of the donor's emission and the acceptor's absorption spectrum (Krasovitskii and Bolotin 1988, page 12) the absorption band of the acceptor should overlap with the fluorescence band of the donor (Krasovitskii and Bolotin 1988, page 11) .

Inhibition

Fluorescence can be quenched by the same mechanisms that are involved in sensitization with the difference that the energy acceptor in this case is a non-fluorescing component (Krasovitskii and Bolotin 1988, page 12). There are three main kinds of quenching processes (Lumb 1978, page 127):

1. **impurity quenching**
2. **concentration quenching**
3. **energy transfer**

The quantum yield of a luminescent molecule may be reduced by the presence of a impurity molecule (Lumb 1978, page 128). This **impurity quenching** processes can take place in a variety of ways, the most common is produced by oxygen dissolved in solution. The detailed mechanics of this process are complicated and may involve the formation of an oxygen organic exciplex. However, the net result is that oxygen enhances non-radiative processes in the luminescent molecule (Lumb 1978, page 129).

At high solute concentrations, the quantum yield often decreases with increasing solute concentration; a phenomenon known as **concentration quenching** (Berlman 1971, page 4) (Lumb 1978, page 130). This is also a diffusion controlled process and is often accompanied by the appearance of a broad structureless luminescent emission at longer wavelengths. This behavior is attributed to the formation of excimers in the solution (Lumb 1978, page 120). Whether the quantum yield of a solution will change with solute concentration depends on the magnitude of the quantum yield of the excimer (Berlman 1971, page 54).

Quenching can also occur by the process of **energy transfer** where a donor excited molecule has its energy transferred to another luminescent or non-luminescent molecule (Lumb 1978, page 130). For example, energy transfer quenching may result

from collisions between solute molecules and any other molecules present in the solution (Becker 1969, page 78). The net effect is a reduction in the strength of the donor emission. This process is a function of the acceptor concentration (Lumb 1978, page 130).

2.6 Solvent Effects

Most studies of luminescence are made in solution. As a result, the luminescent molecules are influenced by the surrounding solvent molecules. Therefore, the photophysical properties of the solution are characteristic of both the luminescent and solvent molecules rather than the luminescent molecules alone (Birks 1970, page 109).

Intermolecular interaction between solvent and solute have a tangible effect on the absorption and emission properties of luminophors. These interactions also create a displacement of bands in the electronic spectra and changes in the quantum yield of photoluminescence (Krasovitskii and Bolotin 1988, page 9). For example, if the luminescent spectra of a molecule exhibits a given vibrational structure in the vapor phase, this structure is normally broader and more diffuse in solution. Furthermore, a change of environment may modify the vibrational spacing and the shape of the spectra envelope of the absorption and emission bands (Birks 1970, page 116) and as a result of dissimilar shifts of the absorption and emission bands, the Stokes shift may differ from one solvent to the next (Krasovitskii and Bolotin 1988, page 10).

Two types of intermolecular interactions responsible for the observed solvent effects include (Birks 1970, page 113):

1. **Universal interactions** due to the collective influence of the solvent as a whole (dielectric constant, refractive index and so on).
2. **Specific interactions** such as the formation of hydrogen bonds, molecular complexes and exciplexes that can result from molecular properties of the solvent and solute.

In a liquid or solid, the solute molecules are in a thermally or spatially disordered environment. Universal interactions may result in a wavelength displacement (or solvent shift) of the absorption and emission spectra relative to the vapor phase (since the refractive index and dielectric constant are higher). Specific interactions due

to dispersion forces and/or collision may result in a broadening of the vibrational structure of the spectra. Finally, excimer interactions may introduce a structureless, red shifted band into the emission spectra (Birks 1970, page 116).

Due to decreased vibrational interactions with neighboring molecules, the spectrum of luminescent molecules in the vapor phase is much sharper than in the liquid or solid phase (Lumb 1978, page 119). However, the quantum yield often increases with an increase in solvent viscosity. For example, the quantum yield is often higher in solid than in liquid or vapor solutions since as the viscosity of the solution increases, the probability of non-radiative loss of excitation energy through internal conversion decreases (Krasovitskii and Bolotin 1988, page 10). Also, in rigid solutions molecular diffusion and excimer formation are inhibited (Birks 1970, page 373) so that the long lived triplet state has a greater probability of emitting to S_0 without being quenched by trace impurities (Lumb 1978, page 121).

Due to the reorientation of polar solvent molecules, the energy of an excited state of a dye molecule is lower in a liquid solution than in the vapor phase. This is due to an increased dipole moment of the excited dye molecules that occurs only after the fast optical transition from the stabilized ground state and an unstabilized excited state. The lifetime of the excited state is longer than the reorientation time of the solvent molecules. Therefore, the fluorescence transition occurs between a stabilized excited state and an unstabilized ground state. The stabilized ground state is reached by slow relaxation of the solvent reorientation. Therefore, the red shift of the absorption band is smaller than that of the fluorescence band.

In a rigid medium, reorientations of the solvent molecules may not occur to the same extent as in a liquid. Hence, the band separation of a fluorescent dye is smaller in a rigid polymer matrix than its liquid monomer (Sah and Baur 1980). This separation can be increased by changing the environment of the dye molecules within in the polymer in such a way that the absorption and emission bands are shifted by different amounts. For example, doping the polymer matrix with molecules of high mobility, the band separation can be increased without changing the magnitude of the absorption band appreciably (Sah 1981).

Chapter 3

Luminescent–Concentrators

A **luminescent–concentrator (LC)** (Levin, Cherkasov, and Baranov 1988) is a non-imaging optical device for collecting and concentrating light energy. As shown in figure 3.1, it is essentially a planar optical matrix that is embedded with a luminescent material. Photons incident on the LC are absorbed by this material at the molecular or ionic level. A significant number of these *luminescent centers* then emit new photons at longer wavelengths, a large fraction of which are then trapped within the LC and guided to its edges by **total internal reflection (TIR)**. The purpose of this chapter is to describe the general theory behind LCs.

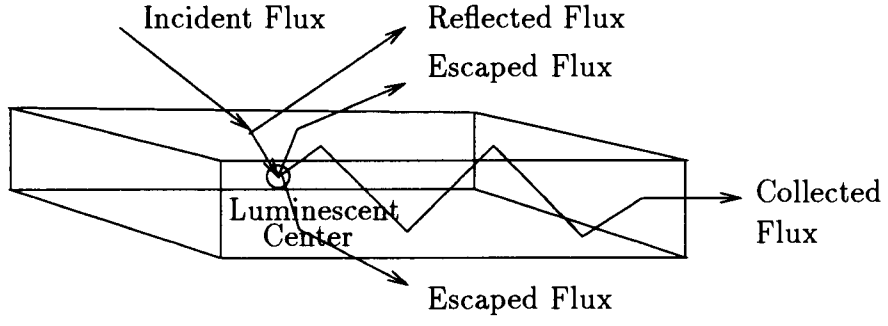

Figure 3.1: Luminescent–Concentrator

3.1 Principle of Operation

Radiant flux incident on an LC is collected and redirected to its edges where it can be used. The concentration and composition of the flux output is a function of the LC geometry and material properties (see appendices A and B) respectively. The cross sectional view of the LC element considered in this chapter is shown in figure 3.2. Here d is thickness, L is length, n_1, n_2 and n_3 are the refractive indices of the *upper cladding*, *core* and *lower cladding* materials respectively and C is the molar concentration of the luminescent material embedded in the core.

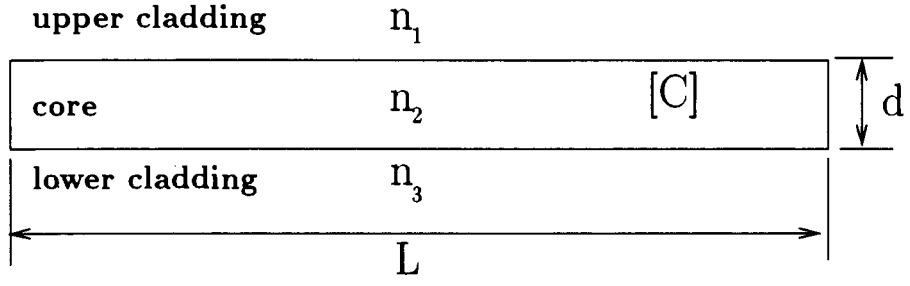

Figure 3.2: LC Cross Section

Figure 3.3 illustrates the major pathways available to photons in an LC. Here, the **flux input** represents an external photon source. **Reflective losses** from the input surface decrease the number of photons transmitted into the LC, while **absorption losses** account for the loss of incident flux outside the absorption band of the luminescent material. Depending on the quantum efficiency, a portion of the photons absorbed are re-emitted. These luminescent photons may be captured by TIR or may add to the **critical cone losses**. Photons emitted inside the critical cone may be recaptured due to scattering, incomplete TIR or re-absorption by other centers. Re-absorbed photons are either re-emitted or added to the **self absorption losses**. **Transport losses** account for photons absorbed by the matrix or that escape due to incomplete TIR. Finally, **reflective losses** at the output edges of the LC claim a further portion of the re-emitted photons. The **flux output** represents the luminescent photons that escape from the edges of the LC.

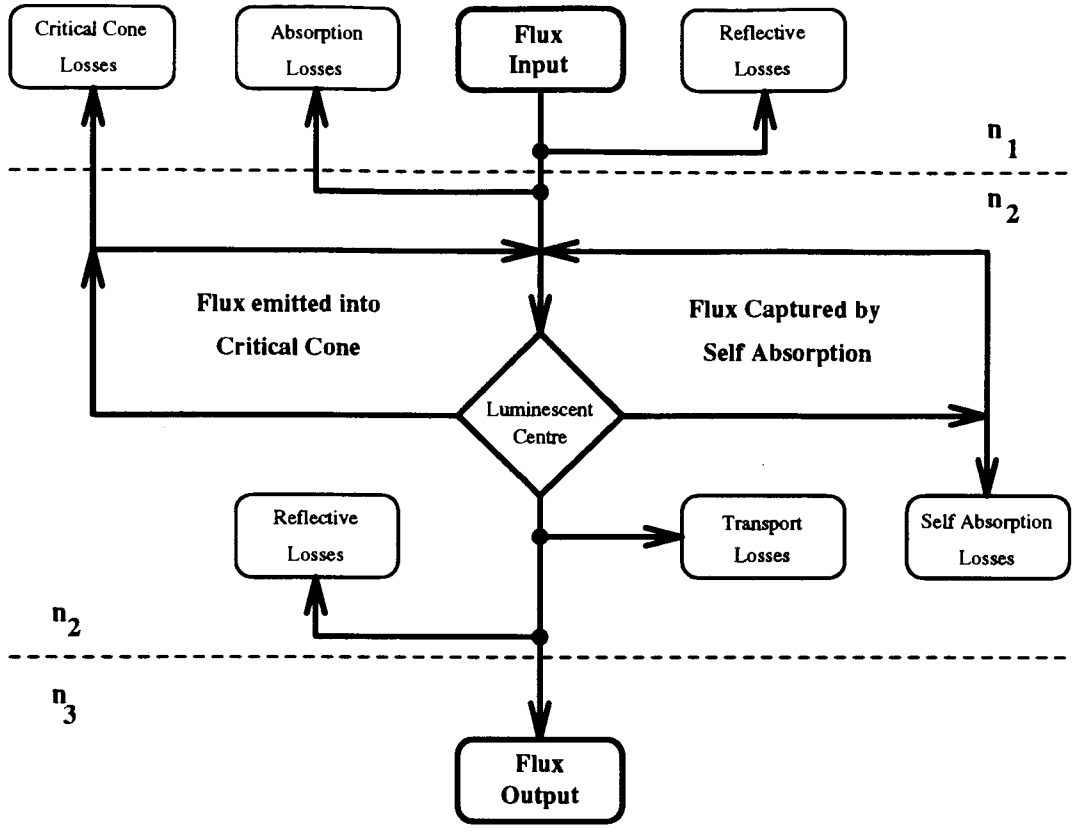

Figure 3.3: Photon Flow Diagram

3.1.1 Flux Input

Photons incident on the surface of an LC can have a variety of spectral and angular distributions depending on the nature of their source. By modeling these photons as a series of optical rays, this flux input Φ_i [W] can be described in terms of incident angle θ_i and wavelength λ_i. The total flux incident of the LC surface therefore is just the sum of these rays over all possible angles and wavelengths. Of course, the fraction of this flux that is available for absorption by the LC is reduced by surface reflections.

3.1.2 Surface Reflection and Transmission

The amplitude reflection coefficient for transverse electric (TE) and transverse magnetic (TM) light are given by the Fresnel equations (Driscoll and Vaughan 1978, page

10-7)

$$\begin{aligned} r_{TE} &= \frac{-\sin(\theta_i - \theta_t)}{\sin(\theta_i + \theta_t)} \\ r_{TM} &= \frac{\tan(\theta_i - \theta_t)}{\tan(\theta_i + \theta_t)} \end{aligned} \tag{3.1}$$

where θ_t is the angle of transmission and is related to θ_i by Snell's law

$$n_1 \sin(\theta_i) = n_2 \sin(\theta_t) \tag{3.2}$$

Using these, the intensity reflection coefficients *(probability of reflection)* may be found from (Driscoll and Vaughan 1978, page 10-9)

$$\begin{aligned} \Gamma_{TE} &= r_{TE} r_{TE}* \\ \Gamma_{TM} &= r_{TM} r_{TM}* \end{aligned} \tag{3.3}$$

where $r_{TE}*$ and $r_{TM}*$ are the complex conjugates of r_{TE} and r_{TM} respectively. For unpolarized light, this becomes (Driscoll and Vaughan 1978, page 10-8)

$$\Gamma = \frac{(\Gamma_{TE} + \Gamma_{TM})}{2} = \frac{1}{2}\left[\left(\frac{\sin(\theta_i - \theta_t)}{\sin(\theta_i + \theta_t)}\right)^2 + \left(\frac{\tan(\theta_i - \theta_t)}{\tan(\theta_i + \theta_t)}\right)^2\right] \quad [-] \tag{3.4}$$

With $\theta_i = 0$ (normal incidence) this is simply (Driscoll and Vaughan 1978, page 10-8)

$$\Gamma_{\theta_i=0} = \left(\frac{n_1 - n_2}{n_1 + n_2}\right)^2 \quad [-]$$

The intensity transmission coefficients *(probability of transmission)* for TE and TM light are given by the equations (Driscoll and Vaughan 1978, page 10-8)

$$\begin{aligned} T_{TE} &= 1 - \Gamma_{TE} \\ T_{TM} &= 1 - \Gamma_{TM} \end{aligned} \tag{3.5}$$

and for unpolarized light by

$$T = 1 - \Gamma \quad [-] \tag{3.6}$$

The amount of flux transmitted into the LC is therefore given by

$$\Phi_t = \Phi_i T \quad [W] \tag{3.7}$$

Using equation 3.6, T was plotted as a function of θ_i for $n_1 = 1$ and $n_2 = [1.2, 1.6, 2.0]$.

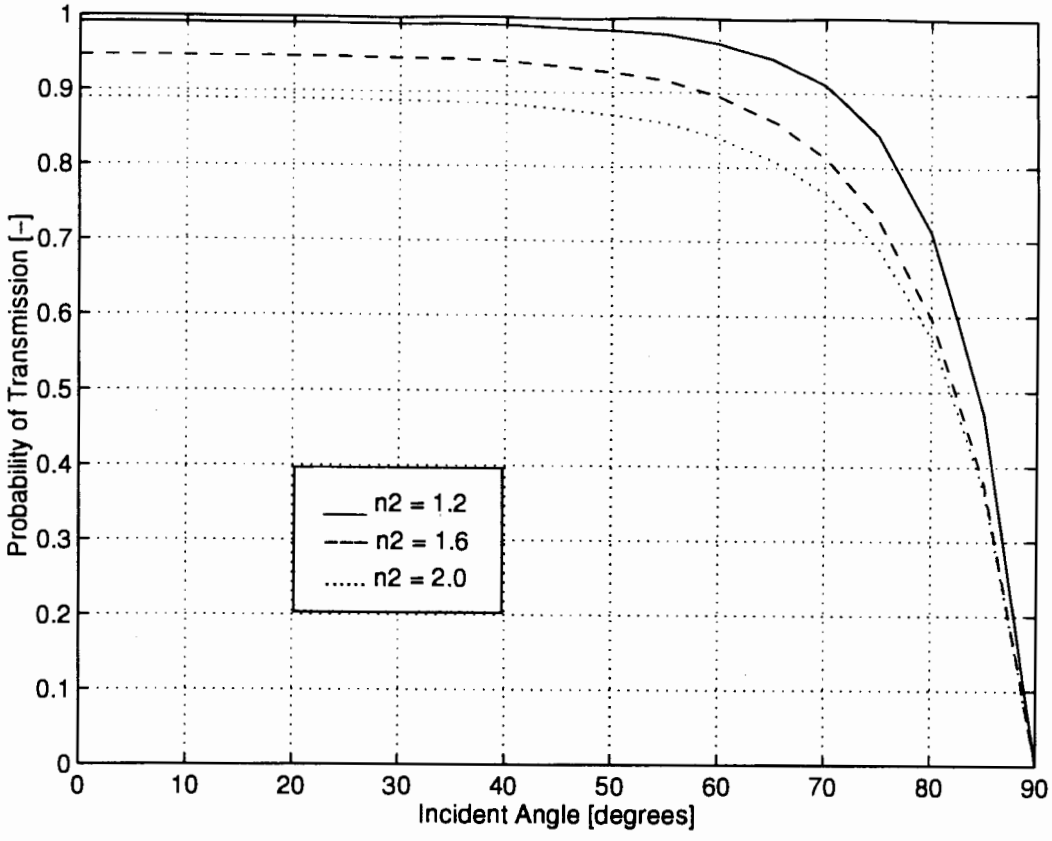

Figure 3.4: Probability of Transmission

3.1.3 Absorption

Φ_t will be partially absorbed by both the luminescent and matrix molecules with an efficiency (*probability of absorption*)

$$Q_a = \frac{\Phi_a}{\Phi_i} = \frac{\alpha(\lambda)}{\alpha_t(\lambda)}(1 - e^{-\alpha(\lambda)l_s}) \quad [-] \tag{3.8}$$

where Φ_a represents the flux absorbed by the luminescent material and

$$\alpha_t(\lambda) = \alpha(\lambda) + \alpha_m(\lambda) \quad [cm^{-1}] \tag{3.9}$$

denotes the combined absorption coefficient for the LC. Here $\alpha(\lambda)$ is the absorption coefficient for the luminescent material and $\alpha_m(\lambda)$ is the absorption coefficient for the matrix. l_s is the pathlength traveled by the flux inside the LC and is independent of d. Hence, the amount of useful flux Φ_a absorbed is just Φ_i, times T, times the fraction

$\frac{\alpha(\lambda)}{\alpha_t(\lambda)}$ that specifies how much of the total absorbed flux was absorbed by the luminescent centers [1], times the probability of absorption (from the Beer–Lambert relation of equations 2.4 and 2.5), integrated over all angles of incidence and wavelengths.

In a similar process, photons traveling inside an LC may be absorbed by matrix molecules. This **Matrix absorption** also behaves according to the Beer–Lambert relation, and hence can be calculated from its molar extinction coefficient as a function of wavelength. Although this form of absorption is a component of the transport losses (see section 3.2.1), it is significant only over long average pathlengths. Therefore, for a sufficiently small LC, matrix absorption losses are considered negligible (Roncali and Garnier 1984b).

In accordance with Lambert's cosine law, it can be shown that Φ_a is nearly proportional to the cosine of the angle of the incident flux. That is, the decrease in Φ_a for large angles of incidence is due mainly to the decrease in the effective area exposed to the incident flux given by the actual area times $\cos\theta_i$ (Batchelder, Zewail, and Cole 1979).

3.1.4 Emission

In an LC containing a single luminescent material, the most important energy transfer processes are fluorescence, phosphorescence and internal conversion. Only the luminescent emission is collected by the LC and its strength is a function of the the quantum efficiency η (*probability of emission*) of the absorbing species. Furthermore, the direction of this emission is approximately isotropic, and hence a large fraction of the re-emitted photons are trapped within the LC by TIR (Hermann 1982).

Depending on the size of the *Stokes shift*, there may be a degree of overlap between the absorption and emission spectra of the luminescent material. This overlap allows a luminescent photon to be re-absorbed by another luminescent center. Phenomenon resulting from this re-absorption are called **self absorption effects** (Batchelder, Zewail, and Cole 1979). For example, since most of the overlap of the absorption and emission bands occurs at the high energy end of the emission spectrum (Zewail and Batchelder 1983), as the luminescence passes through the LC, each generation

[1] Flux absorbed by the matrix is lost as heat, while that absorbed by the luminescent material may be re-emitted.

of re-emitted photons will be progressively red-shifted (with respect to the preceding generation). Therefore, all but the first generation of luminescent photons will be spectrally non-uniform (Batchelder, Zewail, and Cole 1979).

3.1.5 Total Internal Reflection

Photons incident at an angle θ to the surface between two dielectric media with refractive indices n_a and n_b are said to undergo TIR provided $\theta \geq \theta_c$ where θ_c is the **critical angle** given by Snell's law

$$\theta_c = \arcsin\left(\frac{n_b}{n_a}\right) \tag{3.10}$$

and the flux is incident from media n_a with $n_b < n_a$ (there is no TIR when the flux is incident from the low index side). For $\theta \geq \theta_c$ there is no real solution for the angle of the transmitted photons. This implies that there is no transmission and hence that $\Gamma = 1$ (total reflection). Furthermore, no power crosses the interface so that TIR represents a means to confine light in one region of space (Syms and Cozens 1992).

The cone formed by all rays of flux originating at the point of luminescence and forming an angle θ_c with one of the surfaces inside the LC is called the **critical cone**. It describes the geometrical fraction of luminescence that is emitted at an angle $\theta < \theta_c$ (flux not trapped by TIR) (Batchelder, Zewail, and Cole 1979). For isotropic re-emission, the fraction L of rays laying on or inside of the critical cone of one surface of the LC can be calculated by finding the ratio of the area that subtends this cone $A_{cone} = 2\pi r^2(1 - \cos\theta_c)$ to the area of a sphere of the same radius $A_{sphere} = 4\pi r^2$ (Hermann 1982)

$$L_{cc} = \frac{A_{cone}}{A_{sphere}} = \frac{2\pi r^2(1 - \cos\theta_c)}{4\pi r^2} = \frac{1}{2}(1 - \cos\theta_c) \tag{3.11}$$

Using Snell's law, at the upper surface of the LC structure considered here, this becomes

$$L_{2,1} = \frac{1}{2}\left[1 - \left(1 - \left(\frac{n_1}{n_2}\right)^2\right)^{\frac{1}{2}}\right] \tag{3.12}$$

while at its lower surface it is

$$L_{2,3} = \frac{1}{2}\left[1 - \left(1 - \left(\frac{n_3}{n_2}\right)^2\right)^{\frac{3}{2}}\right] \tag{3.13}$$

Finally, for both surfaces, the fraction of re-emission lost through the critical cones is

$$L = L_{2,1} + L_{2,3} = \frac{1}{2}\left[2 - \left(1 - \left(\frac{n_1}{n_2}\right)^2\right)^{\frac{1}{2}} - \left(1 - \left(\frac{n_3}{n_2}\right)^2\right)^{\frac{1}{2}}\right] \tag{3.14}$$

Therefore, the fraction of rays laying on or outside of the critical cones (*probability of TIR*) is simply

$$P = 1 - L \quad [-] \tag{3.15}$$

Using this equation, P was plotted as a function of n_2 for $n_1 = n_3 = 1$.

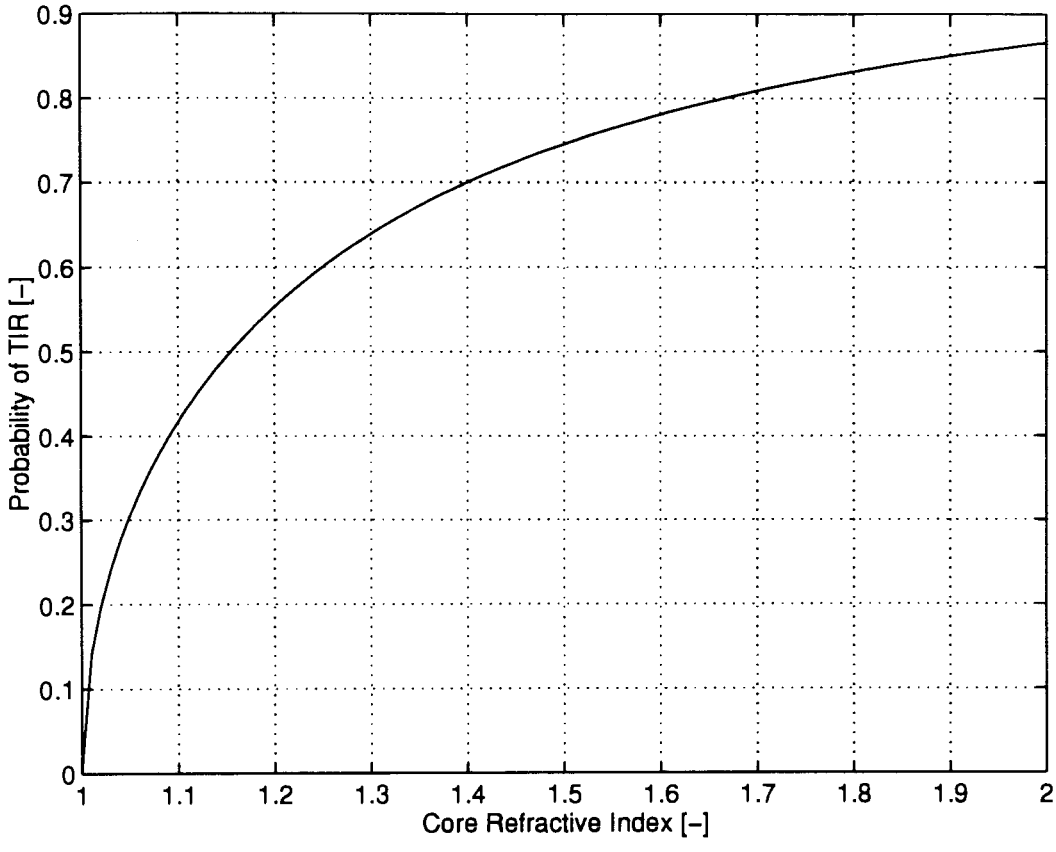

Figure 3.5: Probability of TIR

The **collection efficiency** Q_c is defined as the fraction of Φ_a that is transported to the output edge of the LC (*probability of collection*). Therefore in the ideal case, for an LC with no self absorption or transport losses, $Q_c = P$. In practice Q_c decreases with decreasing thickness. This is due (in part) to an increase in losses resulting from scattering and imperfect TIR proportional to the increase in the total number of internal reflections (Heidler 1981). The most important factor influencing Q_c however,

is the Stoke's shift of the luminescent molecules. Poor efficiency of the collector is a result of high self absorption (see section 3.2.2) (Sah and Baur 1980). For sufficiently small LCs however, self absorption becomes negligible due to the short average path-lengths, so that the ideal collection efficiency can be used (Batchelder, Zewail, and Cole 1979).

Within the critical cones, part of the luminescence can be retained via incomplete transmission at the LC surfaces. However, this effect typically reduces L by no more than 0.01% (Batchelder, Zewail, and Cole 1979). Furthermore, not all of the flux will be trapped by TIR due to surface roughness and undulations (Batchelder, Zewail, and Cole 1979).

3.1.6 Flux Output

The flux output from an LC is a function of the incident angle and wavelength, and is given by the equation

$$\Phi_o = \Psi_o A_e = \Psi_i A_s \eta T Q_a Q_c \quad [W] \tag{3.16}$$

where Ψ_o and Ψ_i are the flux density and A_s and A_e are the areas of the LC surface and edges respectively. The composition of Φ_o is largely determined by the spectral characteristics of the luminescent material. This flux is of great interest in the design of LC devices, primarily due to its concentration and unique spectral properties.

Using equation 3.16, the output flux gain of an LC can be expressed as

$$G_o = \frac{\Psi_o}{\Psi_i} = G_g Q_o \quad [-] \tag{3.17}$$

where

$$G_g = \frac{A_s}{A_e} \quad [-] \tag{3.18}$$

is the **geometric gain** and

$$Q_o = \frac{\Phi_o}{\Phi_i} = \eta T Q_a Q_c \quad [-] \tag{3.19}$$

is the **optical efficiency** of the LC. Due to its planar structure, A_e is less than A_s. Therefore, as long as $G_g > \frac{1}{Q_o}$, Ψ_o will be greater than Ψ_i and the flux incident on the surface of an LC is available for collection in concentrated form at its edges. The magnitude of this concentration can be increased by increasing A_s, decreasing

A_e or by a geometrical trapping effects (shape of LC) (Roncali and Garnier 1984b). However, an increase in G_g (and hence concentration) results in a decrease in Q_c and therefore a decrease in Q_o (Heidler 1981). In any case, G_o is also a function of the LCs ability to absorb and collect flux. Therefore, the actual output flux gain of the LC will always be less than ideal.

Since concentration of photon flux somewhere in a system must come at the expense of an entropy increase somewhere else, the LC is also subject to *thermodynamical limitations.* In an isolated LC surrounded by air, this limitation can be approximated by the inequality (Yablonovitch 1980) (Ries 1982)

$$G_o \leq \left(\frac{\nu_2}{\nu_1}\right)^2 e^{\frac{h(\nu_1-\nu_2)}{kT}} \quad [-] \tag{3.20}$$

where k is Planck's constant, T is temperature (Kelvin), and ν_1 and ν_2 are the frequencies of the absorbed and emitted photons respectively. Hence, the maximum concentration ratio of an LC depends on the Stokes shift. Therefore, G_g must be designed within the constraints of inequality 3.20 and for very high concentration ratios, materials with very large Stokes shifts must be used (Yablonovitch 1980). For rhodamine 6G with $\nu_1 \approx 5.657 \times 10^{14}$ s^{-1} and $\nu_2 \approx 5.353 \times 10^{14}$ s^{-1} (Berlman 1971), $G_o \leq 117.637$.

3.2 Loss Mechanisms

The losses inside an LC can be categorized into two main groups, **transport losses** due to the geometric and material properties of the LC, and **transfer losses** due to the spectral characteristics of the luminescent material.

3.2.1 Transport Losses

Mechanisms of transport loss in an LC include:

- **reflective mismatches** at the output edge
- **geometrical trapping effects** resulting from overall shape
- **incomplete TIR** due to surface roughness and undulations
- **scattering** from impurities and due to optical birefringence

- **matrix absorption** (see section 3.1.3)

In general, these losses can be accounted for by introducing a loss term σ so that (Batchelder, Zewail, and Cole 1979)

$$Q_o = (1 - \sigma)\eta T Q_a Q_c \quad [-] \tag{3.21}$$

3.2.2 Transfer Losses

Mechanisms of transfer loss in the luminescent material include:

- **inadequate absorption bandwidth** (depending on the application)
- **imperfect quantum efficiency** ($\eta < 1$)
- **self absorption**

Self absorption losses can degrade the optical efficiency of an LC. For example, once a photon has been re-absorbed, non-unity quantum efficiency reduces the probability that a photon will be re-emitted. Also, since re-emission occurs in random directions, a fraction of the re-emitted photons will be lost due to transport losses (Olson, Loring, and Fayer 1981). However, since self-absorption occurs at higher rates for long average pathlengths and high dye concentrations, in an LC having sufficiently small A_s and/or C, these losses are negligible (Batchelder, Zewail, and Cole 1979; Olson, Loring, and Fayer 1981).

3.3 Design Considerations

There are a number of considerations in the design of a planar LC. Amongst these are choice of refractive indices, dye concentration, device geometry, optical coupling of the input and output flux and the use of specialized structures such as back reflectors to increase efficiency. The choice of luminescent material used is also important to tailor the LC's spectral output for a particular application (this is discussed in section A.1).

3.3.1 Refractive Indices

For TIR to occur at the interfaces n_2 must be greater then n_1 and n_3 (Harnak 1992, page 399). Smaller differences in the refractive index between the core and cladding require larger cladding thicknesses to maintain TIR. Finding the optimum core thickness therefore, requires a tradeoff between the need for a thin device and the requirement for a thick cladding layer to isolate the optical energy from the absorbing substrate material (Harnak 1992, page 415). Furthermore, the overall efficiency of an LC is a strong function of its ability to collect luminescent photons via TIR. Therefore, increasing n_2 increases the fraction of the luminescence that is trapped and hence the efficiency of the LC (Batchelder, Zewail, and Cole 1979). Maximizing the amount of trapped flux requires maximizing the product TP with respect to n_2 (Goetzberger and Greubel 1977). However, increasing n_2 also has the effect of increasing surface reflection Γ. Therefore, the addition of an *anti-reflection* (AR) coating is desirable in order to improve LC efficiency (see section 3.3.4).

3.3.2 Dye Concentration

Q_a increases with increasing C. This is because increasing the number of luminescent centers in core increases the probability that incident photons will be absorbed. Unfortunately, increasing C also contributes to re-absorption losses (see section 3.2.2) (Olson, Loring, and Fayer 1981) and can result in concentration quenching (see section 2.5). Therefore, the optimal value of C must be determined experimentally.

3.3.3 Geometry

The ability of an LC to concentrate flux is primarily a function of G_g. Therefore, by adjusting A_s relative to A_e (or vice versa), its gain can be tailored for specific applications. For example, in the design of LCs for photovoltaic energy conversion, a fixed G_g has an optimum collector geometry to maximize G_o (Levitt and Weber 1977).

Thickness

Q_a increases with increasing LC thickness d (due to a corresponding increase in l_s) (Levitt and Weber 1977) so that Q_o also increases. Unfortunately, increasing d reduces G_g (see section 3.1.6). Similarly, reducing d results in a decrease in Q_a (due to a corresponding decrease in l_s) (Roncali and Garnier 1984b) and Q_o and an increase in G_g. The decrease in Q_o with thickness is also the result of an increase in the number of internal reflections (proportional to d^{-1}) that results in a net increase in transport losses [2] (see section 3.2.1).

Layout

The layout of an LC is the two dimensional arrangement of its edges with respect to its surface. This effects the performance of an LC primarily by influencing the propagation distances from input to output. For example, a circular LC with its whole perimeter as the collecting edge, provides the optimum collection of the luminescent flux (Roncali and Garnier 1984b). However, geometrical trapping by the LC's edges can also be used to further concentrate or redirect this flux in specific applications. Therefore, by changing the layout of an LC and the position of its photocells, the amount of flux coupled out can be adjusted for particular applications. For example, a triangular LC can be used to reflect trapped flux preferentially out of a single edge while other more exotic layout designs, such as parabolas and toroids, can be used to focus trapped flux on suitably arranged point detectors.

3.3.4 Collection and Coupling

Figure 3.6 shows how input flux can be collected from a source by illuminating the surface of an LC either directly (a) or through an aperture (b). The aperture is used to shield the photocells at the output edge of the LC from direct illumination. In this case, only luminescent flux will reach the output edge of the LC and hence, the output of the photocells will follow the absorption characteristics of the luminescent material. As shown, input reflections can be reduced by an AR coating on the surface of the LC.

[2] As the number of internal reflection increases, the probability for the photons to scatter or to encounter surface defects increases and hence Q_c and Qo decrease (Roncali and Garnier 1984b).

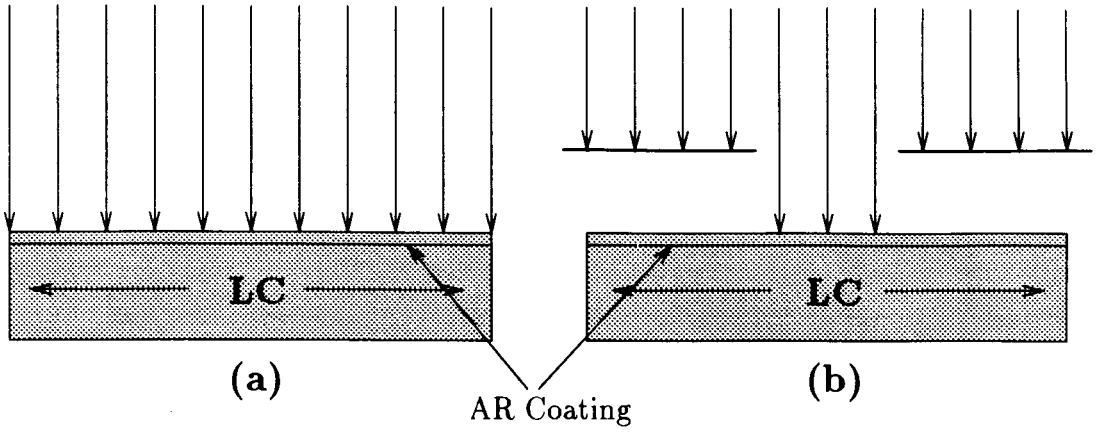

Figure 3.6: Collection of Flux Input

Figure 3.7 illustrates several methods for collecting flux output from an LC. For example, a photocell can be attached directly to the LC's edge (a) or to its top or bottom (or both) surfaces (b). Due to the high index of refraction of the photocell material, TIR in the LC s not possible at the point where the photocell is attached. Therefore, a significant portion of the output flux is coupled into the photocell. Edge coupling maximizes the amount of flux collected, while surface coupling facilitates collection of flux from thin LCs. A third possibility (c) is to create a optical diffusing region on the top or bottom surface of the LC in order to scatter flux propagating inside the LC. As shown, reflective losses at the edge of the LC can be reduced by an AR coating on the surface of the photocell.

3.3.5 Back Reflectors

Practical LC devices can be fabricated using thin films. Unfortunately, these LCs have relatively low absorption efficiencies due to the short pathlengths l_s of the incident flux transmitted into them. The efficiency of these films can be increased by increasing the concentration of the luminescent material or by adding a **back reflector** (see figure 3.8) (Goetzberger and Greubel 1977).

For a specular reflector, if the absorption coefficient of an LC is given by $\alpha(\lambda)$, then it can be shown that during the first pass $1 - e^{-\alpha(\lambda)l_s}$ and during the second pass $(1 - e^{-\alpha(\lambda)l_s})e^{-\alpha(\lambda)l_s}$ of the transmitted flux will be absorbed (Goetzberger 1978). The net effect can be approximated by assuming that the flux reflected by the back reflector

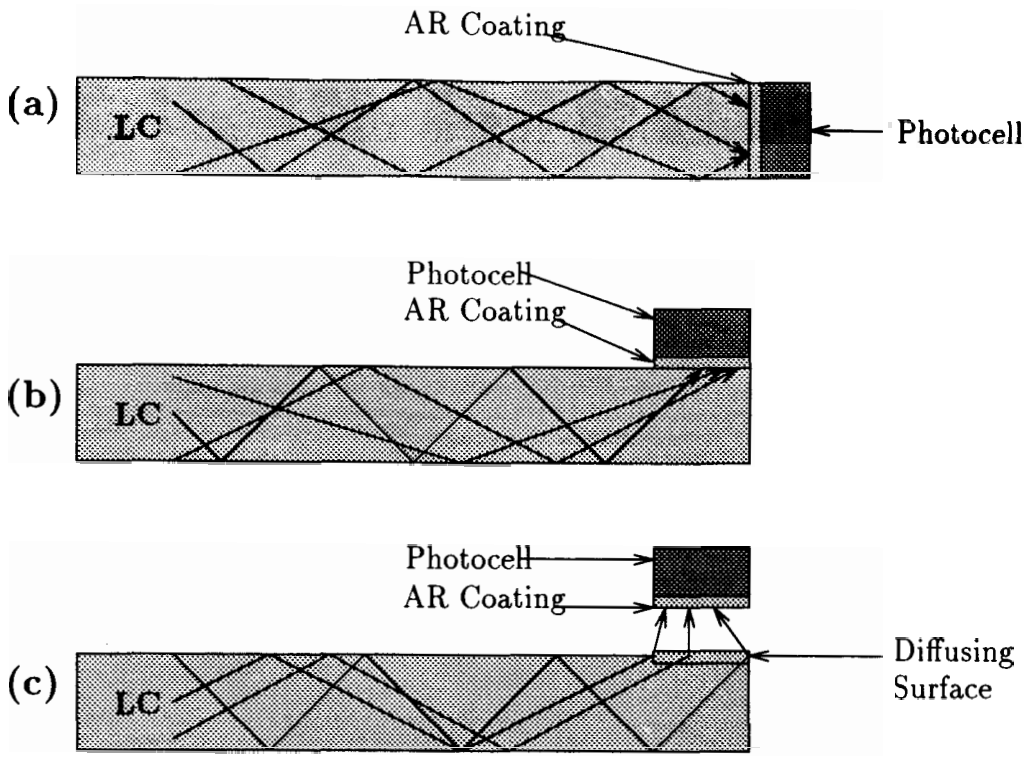

Figure 3.7: Collection of Flux Output

in direct contact with the LC's lower surface [3] is lost through its top surface (neglecting the effect of multiple internal reflections). In this case, the effective pathlength for the propagation of the transmitted flux can be approximated for moderate θ_i by the equation (Batchelder, Zewail, and Cole 1979)

$$l'_s = \frac{2d}{\cos\theta_t} = \frac{2d}{\left(1 - \left(\frac{n_1}{n_2}\sin\theta_i\right)^2\right)^{\frac{1}{2}}} \tag{3.22}$$

The advantage of adding a back reflector is to increase the probability that incident flux transmitted into an LC will be absorbed.

[3] Direct deposition of a reflective material on the surface of an LC will degrade its guiding properties (Roncali and Garnier 1984a).

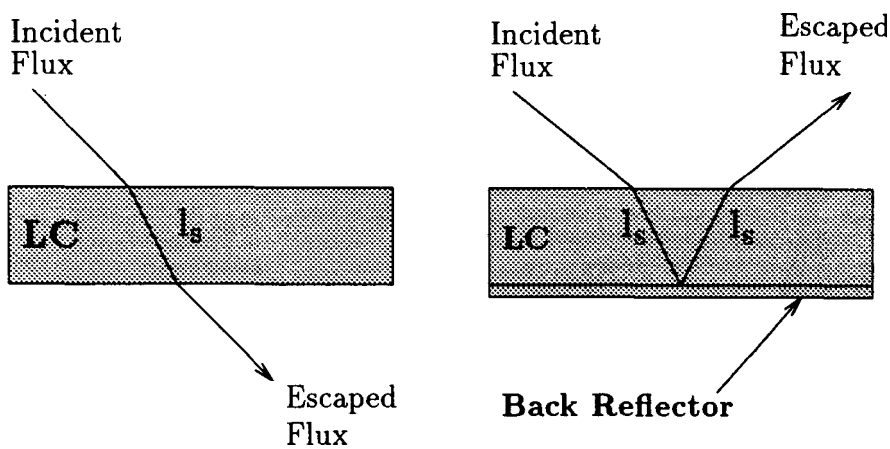

Figure 3.8: Back Reflector

Chapter 4

Integrated LC Photodetectors

LC devices can be constructed using discrete components (individual LCs and photodetectors). To be practical, these components must be large enough to be handled manually. In some sensor applications however, miniature LC devices are better suited. For example, in space based sensing systems where size and weight are the primary concerns. Using techniques of integrated circuit (IC) technology and micromachining it is possible to fabricate these miniature devices on semiconductor or similar substrates. In the case of a simple photosensor, the result is an **integrated LC photodetector (ILCP)**. In this chapter the design, simulation and testing of a prototype ILCP is considered.

4.1 Design

The design used for the ILCP considered is shown in figure 4.1. Here, the substrate is a semiconductor, such as silicon (Si), into which a planar *PN junction photodiode* has been diffused. The cladding is a low index material (in this case SiO_2) which can be thermally grown on the substrate. The thin–film LC consists of a high index material (here a polymer material doped with a luminescent dye) that can be spin coated over the substrate and any associated electronics on the semiconductor substrate. The LC is physically patterned to permit access to the interconnect metalization (not shown) that connects the electronic components of the ILCP to its *external detection circuitry.* Finally, the arrows indicate the direction of light propagation inside the polymer LC. The planar nature of the LC element is complimentary to the planar technology used

to fabricate the electronic components on the semiconductor substrate.

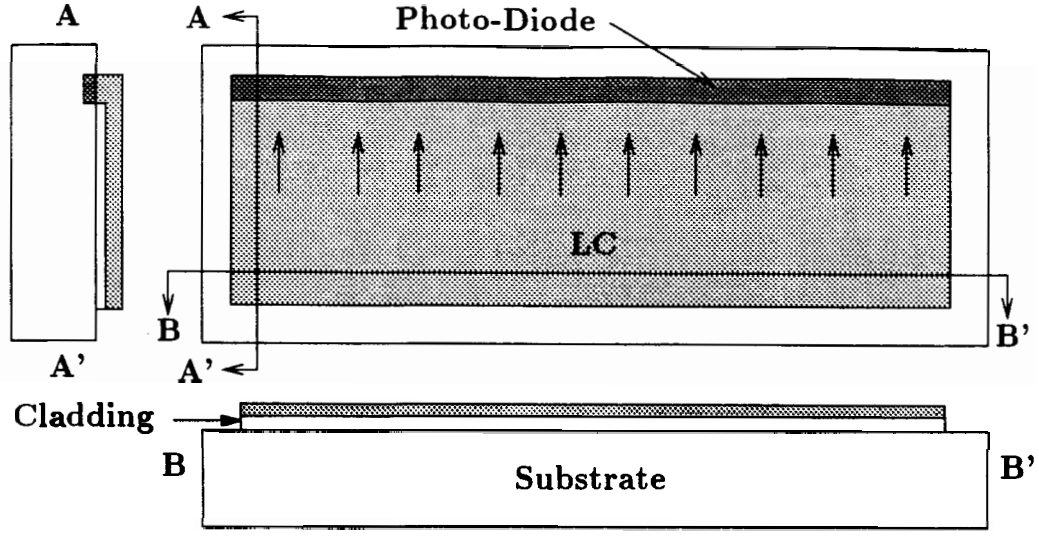

Figure 4.1: Integrated Luminescent–Concentrator Photodetector

4.1.1 Light Pipe versus Waveguide

For the purposes of this work, a **light pipe** is defined as a transparent material system designed for transmitting *broad–band* light along its length. Conversely, a **waveguide** is defined as a material system designed for transmitting *monochromatic* light. In either case, light energy is confined and directed primarily by TIR at physical boundaries.

Since an LC is designed to collect light over a reasonably broad band (depending on the widths of the absorption and emission spectra of its luminescent dye), it is best described as light pipe. However, the dimensions and fabrication of an integrated LC on a semiconductor substrate are comparable to those used in the formation of slab waveguide structures for photonic applications. Furthermore, since light is confined by the same mechanisms in both structures, it is instructive to consider some of the properties of waveguides in more detail.

The characteristics of light propagation through a waveguide are determined by radiation patterns in the plane transverse to the direction of travel. Depending on the waveguide thickness and for a given wavelength, only a finite number of these patterns

or **modes** are allowed. The number of modes that can propagate in a waveguide is an increasing function of thickness and a decreasing function of wavelength. For example, the approximate number of (TE or TM) guided modes m allowed in an asymmetric slab waveguide is given by the equation (Tamir 1988, page 16)

$$m = \frac{2d}{\lambda}\sqrt{n_2^2 - n_3^2} \quad [-]$$

where d is the guide thickness, λ is the wavelength of the propagating light and n_2 and n_3 are the refractive indices of the core and lower cladding respectively. The upper cladding $n_1 = 1$ (air). Using this equation, the concentration of guided modes as a function of d and λ for a polymethyl methacrylate (PMMA) core on an SiO_2 substrate was calculated and plotted in figure 4.2. The more modes that are supported, the more energy is carried for a given flux density.

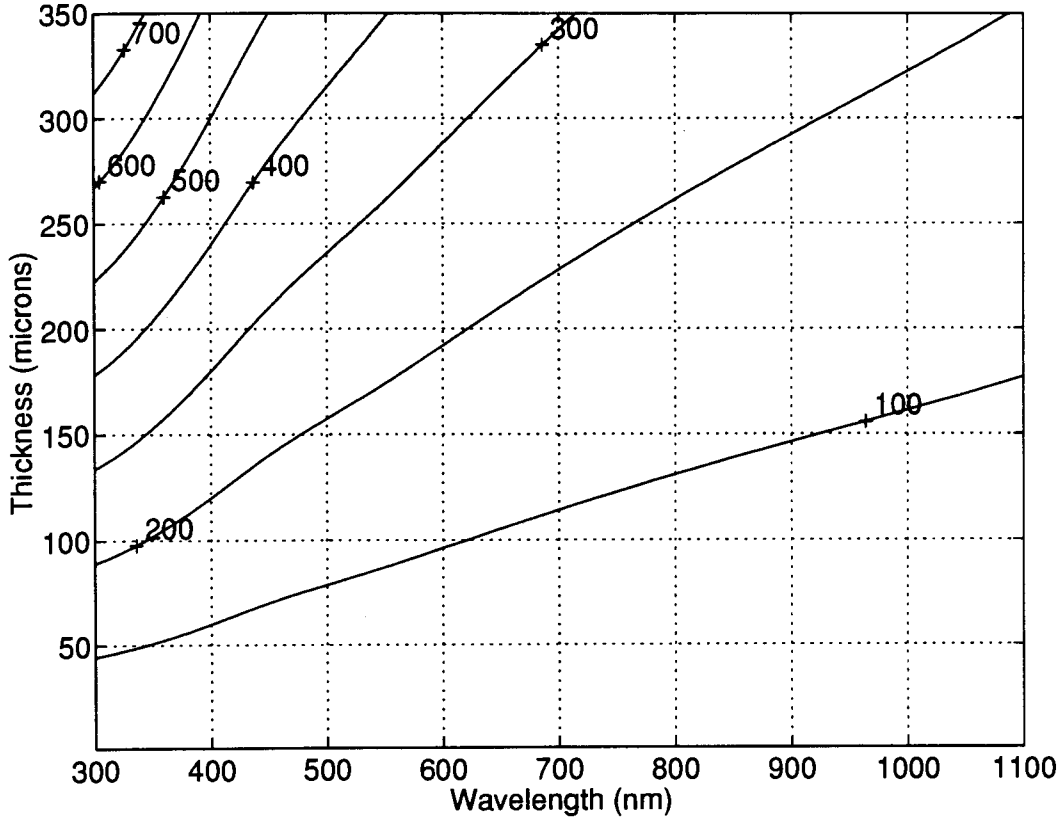

Figure 4.2: Modal Concentration in an Asymmetric Slab Waveguide

4.1.2 PN Junction Photodiodes

In figure 4.1, light captured by the LC propagates inside the core (between the cladding layers) to the PN junction photodiode at the edge of the device. At this point, the cladding layer is removed so that the LC comes in direct contact with the surface of the photodiode. Since the refractive index of the semiconductor is much greater than that of the core material, TIR is no longer possible and a large fraction of the propagating light energy will be transmitted into the photodiode.

A planar PN junction photodiode consists of two layers of semiconductor material with an internal potential barrier that produces a depletion region. Incident photons are absorbed by the semiconductor and create electron-hole pairs. These minority carriers then diffuse to the junction where they are swept through the depletion region, thus creating a forward bias and producing either an open circuit voltage or a short circuit current (Dennis 1986, page 80) that can be detected by external circuitry.

A semiconductor photodiode can only absorb photons with energy greater than its bandgap according to the relation

$$\frac{hc}{\lambda} \geq E_g \quad [eV] \tag{4.1}$$

where h is Planck's constant, c is the speed of light, λ is the wavelength of the incident photon and E_g is the bandgap energy required to excite an electronic transition in the semiconductor used for the photodiode. Using this equation, the cut off wavelength λ_c of the photodiode is defined as

$$\lambda_c = \frac{hc}{E_g} \quad [m] \tag{4.2}$$

Si photodiodes, can absorb only photons with an energy greater than their bandgap of 1.1 eV. This corresponds to a cutoff wavelength of approximately 1100nm. Assuming that for $\lambda <= \lambda_c$ the diode quantum efficiency (number of electrons generated per photon absorbed) is unity and for $\lambda > \lambda_c$ it is zero and that the incident light has equal energy at all wavelengths, we can plot the ideal responsivity of a Silicon PN junction photodiode as shown in figure 4.3. The responsivity of a Newport 818-SL commercial photodiode is also shown (Newport Corporation 1991, page 5). In practice, Si photodiodes can detect photons from the near ultraviolet (UV) through to the near infrared (IR) with a peak at about 900 nm (Dennis 1986, page 96). However,

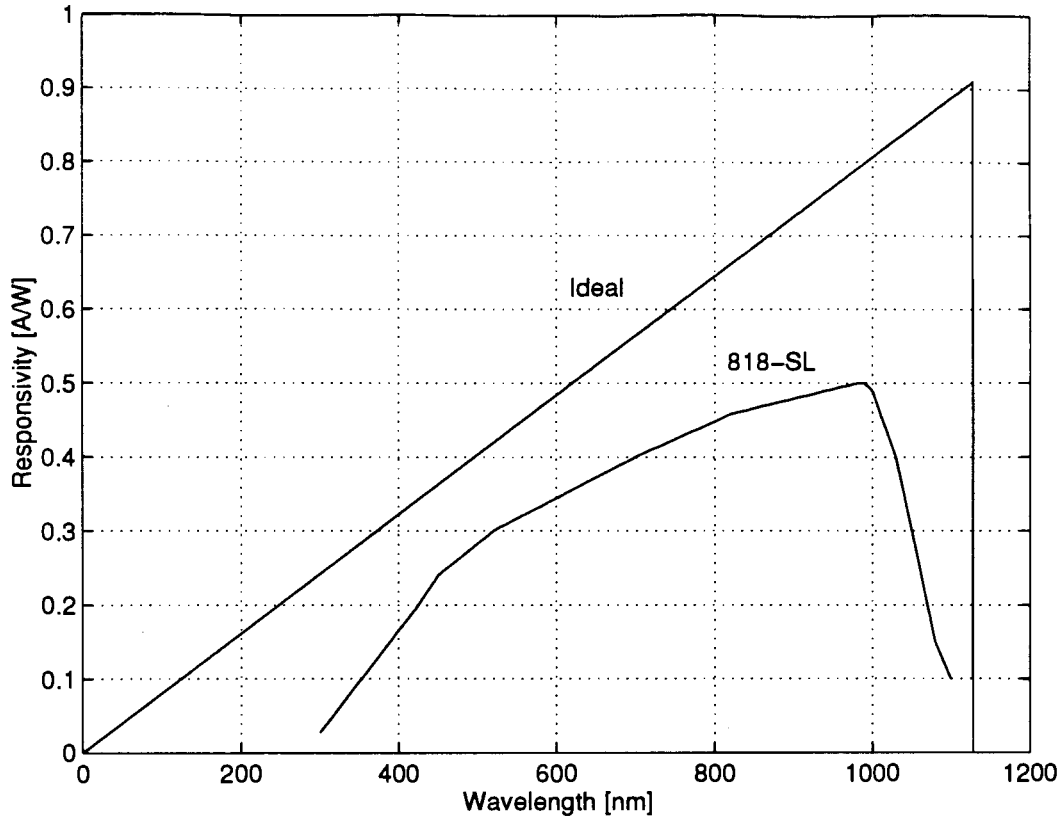

Figure 4.3: Silicon Photodiode Responsivity

they are not suitable for detecting short UV wavelengths or IR wavelengths above the bandgap cutoff.

4.1.3 External Detection Circuitry

A PN junction photodiode can be operated in either of two modes:

1. **Photoconductive: (Biased)** for fast response times in high speed applications
2. **Photovoltaic: (Unbiased)** for low noise applications at low frequencies

However, the major advantage of junction photodiodes over other detectors is that in the photovoltaic mode they require no bias supply. Consequently, there is a considerable simplification of the associated electronics (Dennis 1986, page 84). For example, a simple transimpedance amplifier circuit like that shown in figure 4.4 provides near zero load impedance and allows high output voltages that can easily be monitored.

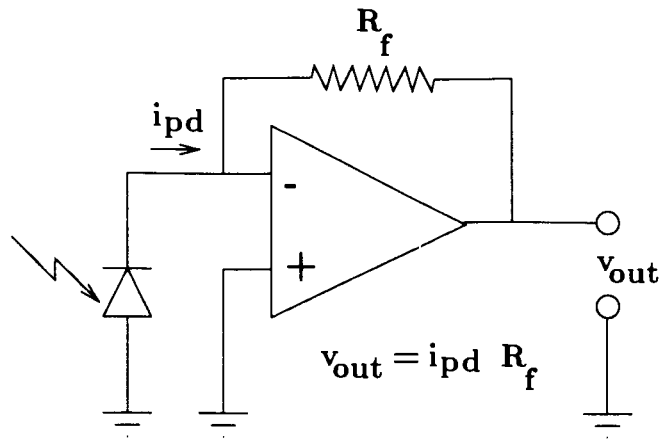

Figure 4.4: External Detection Circuitry

In this work, all the devices fabricated were operated in the photovoltaic mode using similar circuitry.

4.2 Simulation

An LC and an ILCP were simulated in MATLAB [1] using a two dimensional **ray–optic** algorithm. This method is a simple approach with great intuitive appeal, although it is not as complete a description as that provided by electromagnetic theory. The ray–optic approach permitted handling the simulation in a realistic way so that the device performance could be easily evaluated.

The objective of the simulation was to estimate the probability of flux propagating a distance L (from the point of incidence) through the LC and either escaping through its end or being transmitted into a planar photodiode at its edge. The various possible fates of the incident rays in the ILCP (reflection and refraction at the various surfaces and absorption and re-emission by the dye) were handled in the appropriate order and the probabilities at each step were calculated.

Both dye doped and undoped LC elements were simulated to investigate the contribution of non-total internal reflections and the effect of unabsorbed flux propagating to the LC output. The simulation results detail the spectral composition of output

[1] MATLAB is a product of The MathWorks, Incorporated, 24 Prime Park Way, Natick, MA 01760.

flux as a function of incident angle θ_i and wavelength λ_i. The details of the calculations performed are outlined below.

4.2.1 Modeling Structures

The LC element and ILCP structure were modeled is shown in figure 3.2 and 4.5 respectively. In either case, d is the LC thickness, L is its length, n_1, n_2 and n_3 are

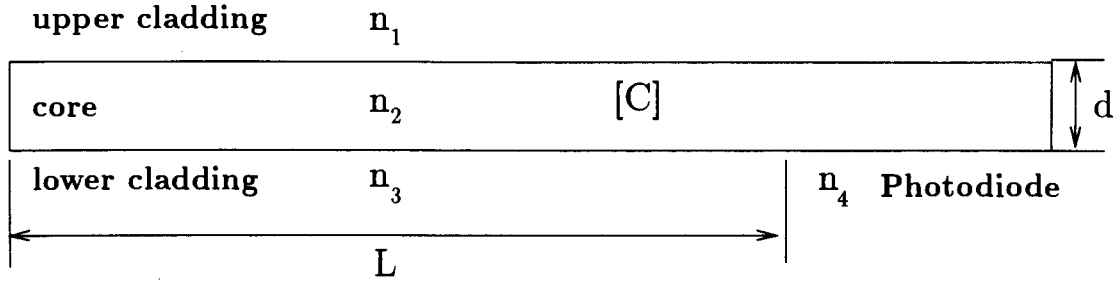

Figure 4.5: ILCP Cross Section

the refractive indices of the upper cladding, core and lower cladding respectively and C is the molar concentration of the fluorescent dye in the core matrix. In the case of the ILCP, n_4 is the refractive index of the semiconductor substrate (photodiode). Here, $n_4 > n_2 > n_1$ and n_3. The upper cladding layer was modeled as air, the core matrix as PMMA, the bottom cladding layer as SiO_2 and rhodamine 6G was selected as the fluorescent dye. The substrate was modeled as intrinsic silicon. The core material was assumed linear, homogeneous and isotropic, all scattering processes were ignored and unless otherwise noted, $C = 2.36 \times 10^{-3}$ moles per liter (0.1% dye concentration by weight) was used. Finally, the results are only considered valid for $\frac{d}{\lambda} \gg 1$.

4.2.2 Flux Input

The probability of flux of wavelength λ_i existing outside the LC was considered unity over all wavelengths and for all angles of incidence (uniform flux distribution) and an equal number of TE and TM polarized rays were assumed (the incident flux was non-polarized). The input flux was modeled as a ray incident the surface of the LC. Finally, θ_i was varied between 0° (normal) and 90° (tangential to the surface).

4.2.3 Surface Transmission

The intensity transmission coefficients were calculated at the upper surface of the LC using equations 3.1 to 3.6 for each θ_i and λ_i. These were then used to determine the amount of flux entering the LC. The transmission angles θ_t of the transmitted flux were also calculated for each θ_i and λ_i using equation 3.2. Here, θ_t is equivalent to the propagation angle θ_p of the incident flux inside the LC.

4.2.4 Absorption and Emission

Once within the LC, the transmitted flux is partially absorbed by the luminescent dye with a probability given by the Beer–Lambert relation (equation 2.4). The path-length l_s between reflections in the LC was calculated geometrically and, using the molar concentration C of rhodamine 6G and its digitized molar extinction coefficients $\varepsilon(\lambda)$ (absorption characteristics) in a methanol solution (Berlman 1971, page 412), the amount of flux absorbed following each pass (from the upper to the lower face of the LC) was determined. In practice ε will vary depending on the state and type of solvent used. The probability of absorption was considered independent of polarization and incident angle and absorption due to the LC matrix material (heat loss) was assumed negligible.

The spectrum of the emitted flux was calculated from the digitized emission spectra of rhodamine 6G in a methanol solution (Berlman 1971, page 412) multiplied by the quantum efficiency $\eta = 0.98$ of the dye (Baczynski, Marszalek, Walerys, and Zietek 1973). In practice, both the spectra of the emitted photons and η will vary depending on the state and type of solvent used. The dye was assumed to emit isotropically in the simulation plane without keeping any memory of the polarization state of the absorbed ray (non-polarized light is emitted). This implies a random orientation of the dye molecules in the LC matrix. The angular span of the emitted rays cover a 2π angle, but only half of the rays were considered (propagation to one side). Solvent effects on the absorption and emission spectra and re-absorption of fluorescence by the dye were neglected (the absorption and emission spectra are independent of matrix material).

4.2.5 Internal Reflections

Using equations 3.1 to 3.4, the intensity reflection coefficients were calculated at both dielectric surfaces inside the LC and for each θ_p and λ_i. These were then used to calculate the amount of incident and luminescent flux remaining inside the LC after each reflection (both TIR and non-TIR). The Goos–Hänchen shift (effect of penetration of the evanescent field in cladding and substrate) was neglected, since the penetration of the evanescent field into the cladding and substrate decreases with increasing core thickness or decreasing wavelength (as more modes are supported) so that the effect is significant only for single mode guides (Tamir 1988, page 17).

4.2.6 Flux Output

The probability of flux propagating to the output of the LC was calculated by summing the probabilities of luminescent and non-luminescent flux reaching a distance L within the LC by internal reflections (as described above). In the LC simulation, the rays that reach the edge of the LC may be reflected or transmitted through the end of the LC as given by equations 3.1 to 3.6 for an incident angle equal to $\frac{\pi}{2} - \theta_p$ (for a vertical output edge). The material at the end of the LC was modeled as air. For the ILCP simulation, the rays that make it to the edge of the LC may be reflected or transmitted at the Si surface again as given by equations 3.1 to 3.6 for an incident angle equal to θ_p. Those that are absorbed may lead to the generation of an electron–hole pair and hence can be detected by the external circuitry.

4.2.7 Results

An undoped (clear) LC element was simulated first. The results indicate that none of the incident flux transmitted into the guiding structure propagate by TIR (as expected). Flux propagation in this case is entirely a result of non-TIR reflections and hence the probability of flux reaching the edge of the guide is a strong function of d and L. For example, using $d = 145$ μm and $L = 500$ μm results in a maximum optical efficiency on the order of 1×10^{-8}. Furthermore, (for $n_2 > n_1$ and n_3), although there is a finite (though exceptionally small) probability of flux propagating by non-TIR to the edge, the angles of incidence to the surface are related to those of the edge

in such a way that the rays are totally internally reflected back into the guide. Hence none of the incident flux is transmitted through the output edge.

An undoped ILCP was simulated next. Again, the results indicate that none of the incident flux transmitted into the guide propagates by TIR. However, in this case (for $n_4 > n_2 > n_1$ and n_3), the probability of flux throughput (although still exceptionally small) is non-zero, since no TIR takes place at the output. Figure 4.6 presents the results of this simulation for $d = 145$ μm and $L = 500$ μm. Reducing d or increasing L

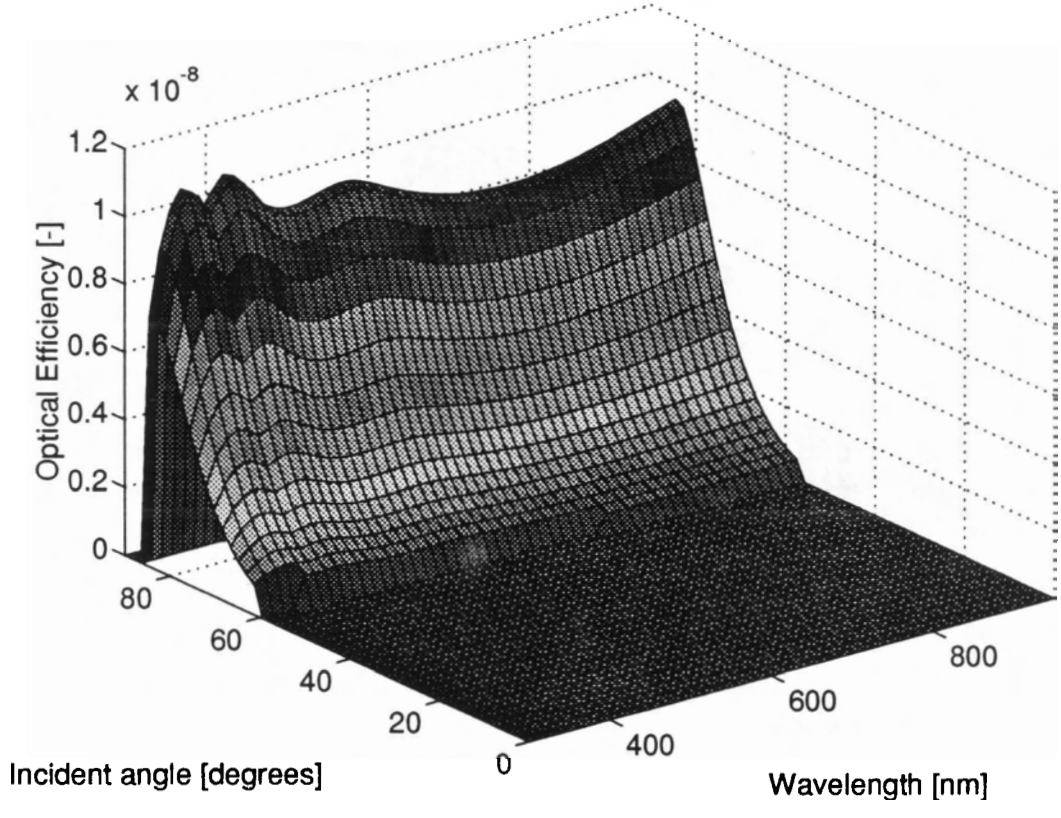

Figure 4.6: Light Guide Simulation results

would further reduce the probability magnitude due to a proportional increase in the number of non-TIR reflections. Clearly, for the device dimensions considered here, collection of incident flux transmitted into the guide purely by internal reflections is negligible.

Finally, dye doped LC and ILCP structures were simulated. In either case the

results indicated that a significant portion of the incident flux transmitted into the guiding structure is absorbed and re-emitted with an angle greater than required for TIR at the dielectric interfaces. For $d = 145$ μm and $L = 1$ cm, the optical efficiency of the LC structure was found to be on the order of 10% while that of the ILCP was on the order of 4%. Figure 4.7 presents the simulation results for the ILCP structure.

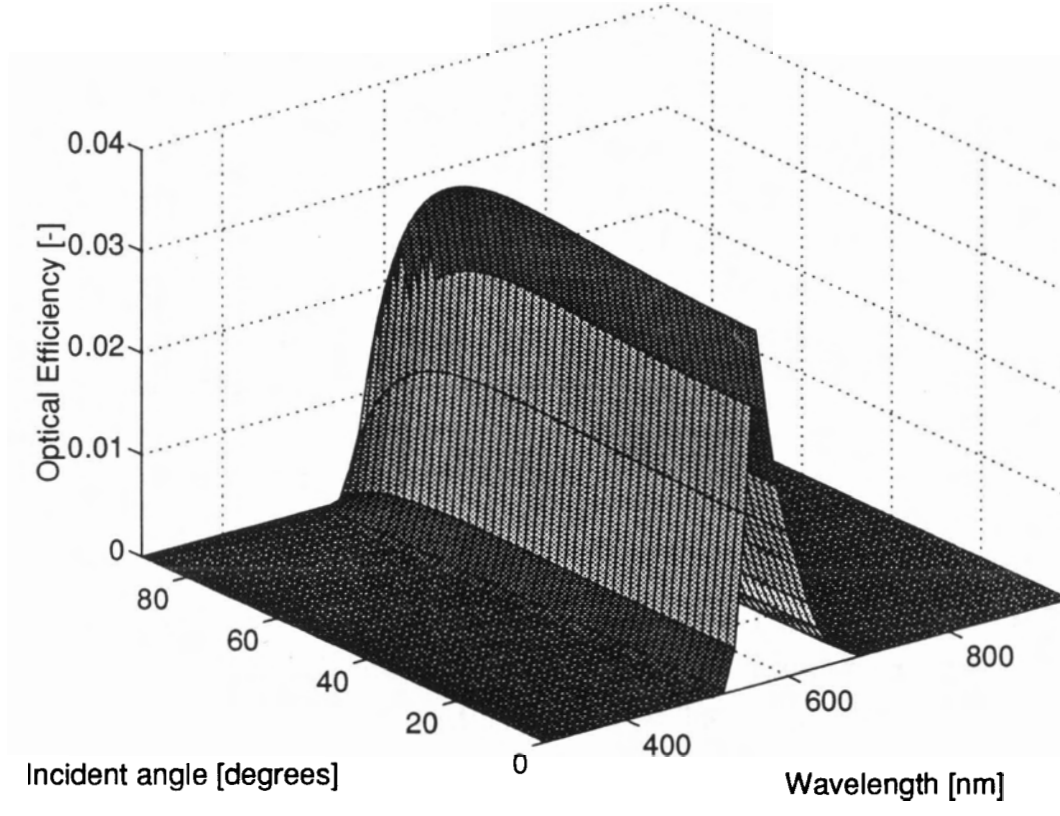

Figure 4.7: ILCP Simulation results

In both the LC and ILCP, luminescent emission from the dye (peak at 560 nm) is the dominant component of the output flux. Hence, flux absorbed by the dye is re-emitted and collected by the photodiode and the responsivity of an ILCP is a strong function of the absorption spectrum of the dye.

4.3 Experimentation

Thin film LC test samples (see appendix section B.2) were evaluated to determine their peak optical efficiency Q_o and gain G_o in terms of thickness d. Next, as proof of concept, prototype ILCPs were fabricated (see appendix C) on a silicon substrate following the design of figure 4.1. As discussed previously, this device consisted simply of several PN junction photodiodes and their interconnect circuitry over which a thin film LC was deposited and patterned.

The IC photodiodes and prototype ILCPs were tested to determine their **responsivity** R as a function of incident wavelength. Here, responsivity is defined as the sensitivity of the detector (Dennis 1986, page 9) and for the purposes of this work was determined using the relation

$$R = \frac{i}{\Phi_i} = \frac{i}{\Psi_i A_s} \quad [A/W] \tag{4.3}$$

as a function of wavelength, where i is output photocurrent [A], Φ_i is the input power (Watts), Ψ_i is the input flux density [W/cm] and A_s is the input surface area of the detector.

4.3.1 Optical Test Bench

In order to test the LCs and ILCPs, light from a 75W high pressure Xe arc lamp was focused onto the 100 μm input slit of an Instruments SA Incorporated HR640 monochromator with an 1800 line/mm grating (reciprocal linear dispersion of 1 nm/mm). The light from its 100 μm output slit was then used to illuminate an LC or ILCP test sample inside a light–tight enclosure. The Xe source was used since determination of the absorption spectra of a luminescent material requires a high intensity, smooth and continuous source. An Hg source may have provided more power (especially in the UV) but the sharp spectral lines characteristic of such sources are undesirable in this case. Finally, a computer data acquisition system was set up to control the monochromator ($\pm$1 nm) and to sample the output of the photodetector via the analog output of a Newport 815 digital power meter ($\pm$3% at 633 nm NBS traceable absolute radiometric accuracy (Newport Corporation 1991)). The set up of the optical test bench described above is shown in figure 4.8.

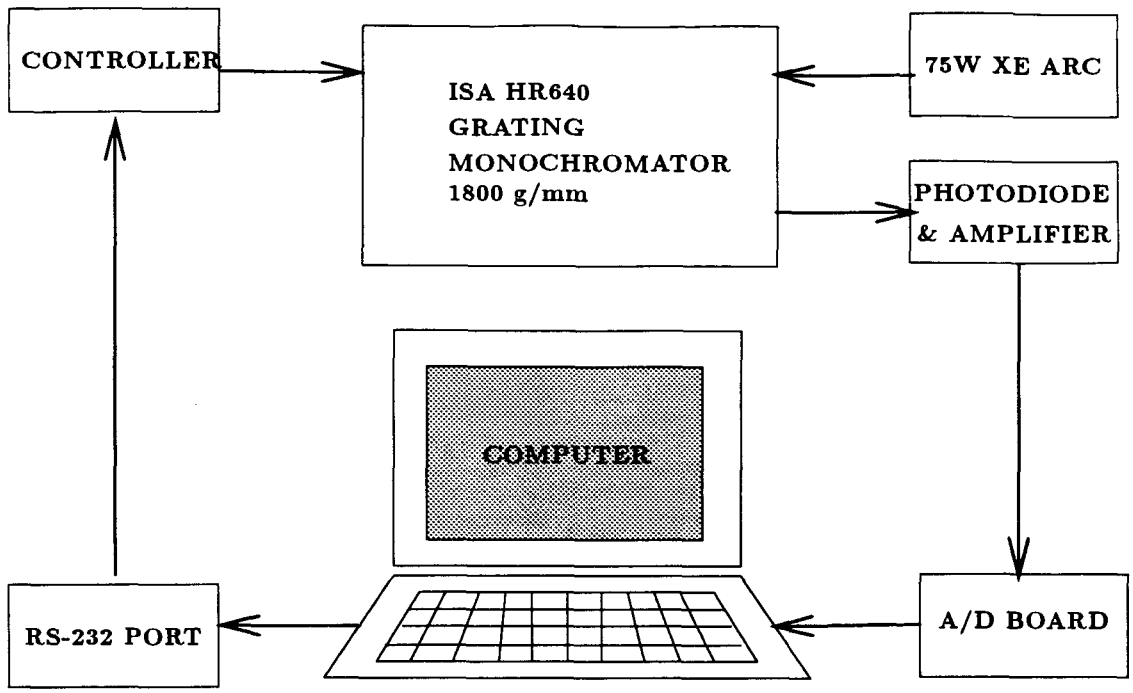

Figure 4.8: Optical Test Bench

4.3.2 LCs

The thin film LCs (see appendix section B.2) were individually cleaved on one side to produce a flat clean edge. Each LC in turn, was then positioned above the surface of a commercial Newport 818-SL photodiode so that only light escaping from this edge could be detected. The photodiode was then connected to the Newport 815 digital power meter and the sample illuminated normal to its surfaces using the monochromator as shown in figure 4.9. Finally, using the data acquisition system described above, the output flux intensity from the cleaved edge (as measured by the photodiode and power meter) was recorded as a function of incident wavelength.

The incident flux intensity was also measured using an 818-SL photodiode (1 cm^2 in area) and used to illuminate a 1 by 3 cm area A_{s_1} on the surface of the LC 1 cm from the cleaved edge. The luminescent flux propagated 1 cm inside the LC core from illuminated region and was emitted 0.5 cm above the surface of the photodiode [2]. For the purposes of this experiment, the area of the output edge A_{e_1} was assumed to be

[2] All measurements made here with an accuracy of ± 0.5 mm.

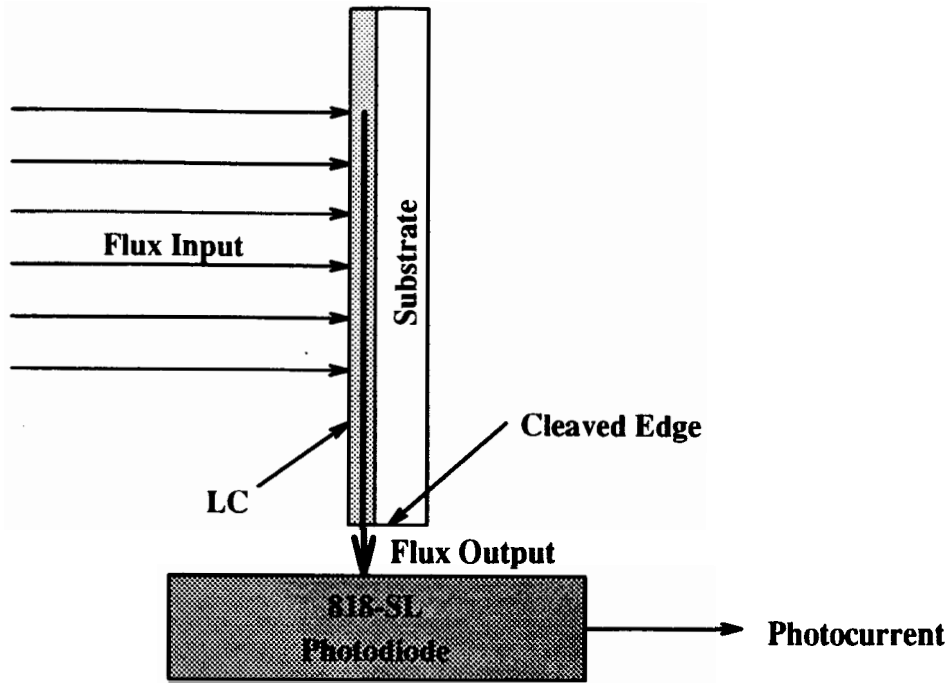

Figure 4.9: Set Up for LC Test Measurements

equal to the diameter of the photodiode (1.13 cm) multiplied by the thickness d of the LC (see appendix B.2). In order to simplify calculations, the rectangular geometry described above was changed to an effective circular geometry as shown in figure 4.10. Here the incident flux intensity was assumed uniform over a circular area $A_{s_2} = \pi r_s^2$ and the output flux intensity was assumed to be uniformly emitted from an edge of area $A_{e_2} = 2\pi r_e d$.

The optical efficiency Q_o of an LC can be found directly by measuring the incident Φ_i and output power Φ_o from equation 3.19 since

$$Q_o = \frac{\Phi_o}{\Phi_i} = \eta T Q_a Q_c \quad [-]$$

Using this relation, the experimental data and the effective geometry described above, Q_o was calculated and plotted in figure 4.11 as a function of LC thickness. For comparison, the LC simulation program was used to predict the theoretical efficiency over the same range of thicknesses and superimposed on the same figure (solid curve).

The geometric gain G_g given by equation 3.18 was calculated for the effective geometry of each LC and is plotted in figure 4.12 (a) as a function of LC thickness.

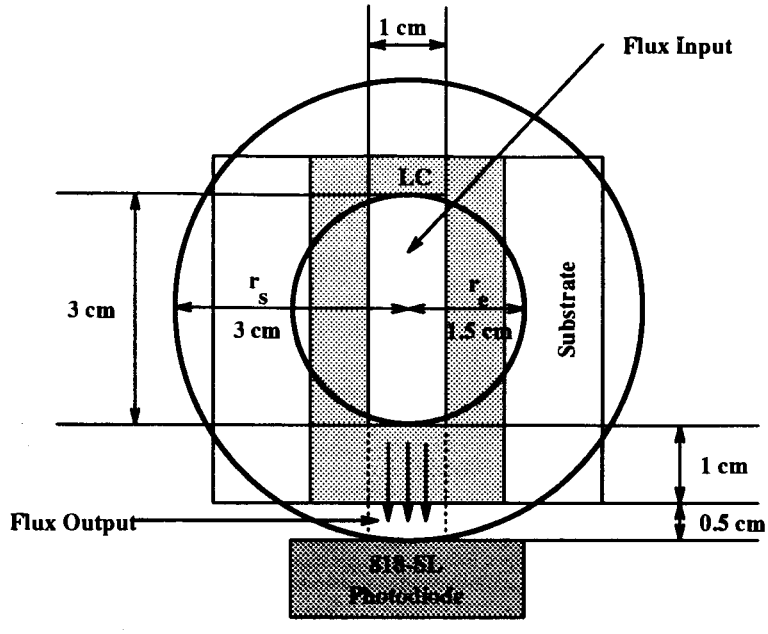

Figure 4.10: Effective LC Device Geometry

Now, $\Phi_o = \Psi_o A_e$ and $\Phi_i = \Psi_i A_s$, therefore

$$Q_o = \frac{\Psi_o}{\Psi_i}\frac{A_e}{A_s} \quad [-]$$

however

$$G_o = \frac{\Psi_o}{\Psi_i} \quad and \quad G_g = \frac{A_s}{A_e} \quad [-]$$

so that the optical gain G_o can be found simply by calculating $G_o = Q_o G_g$. Using the data from figure 4.11 and 4.12 (a), G_o was calculated and plotted in figure 4.12 (b). For comparison, the previous simulation results were also used to predict the theoretical gain for the same range of thicknesses and superimposed over the experimental results (solid curve).

The differences between the theoretical and experimental results presented here can be attributed to non-ideal experimental conditions and the presence of scattering centers and inhomogeneities in the real LC cores. The accuracy of the experimental measurements were degraded by the non-uniform nature of the incident flux, geometrical trapping of the luminescent flux (from scattering centers and at the edges inside the LC), incomplete TIR (due to surface roughness and undulations), self-absorption of luminescence by the dye, and by the matrix material and reflective losses at the surface of the photodiode. Furthermore, the experimental polymer material used to

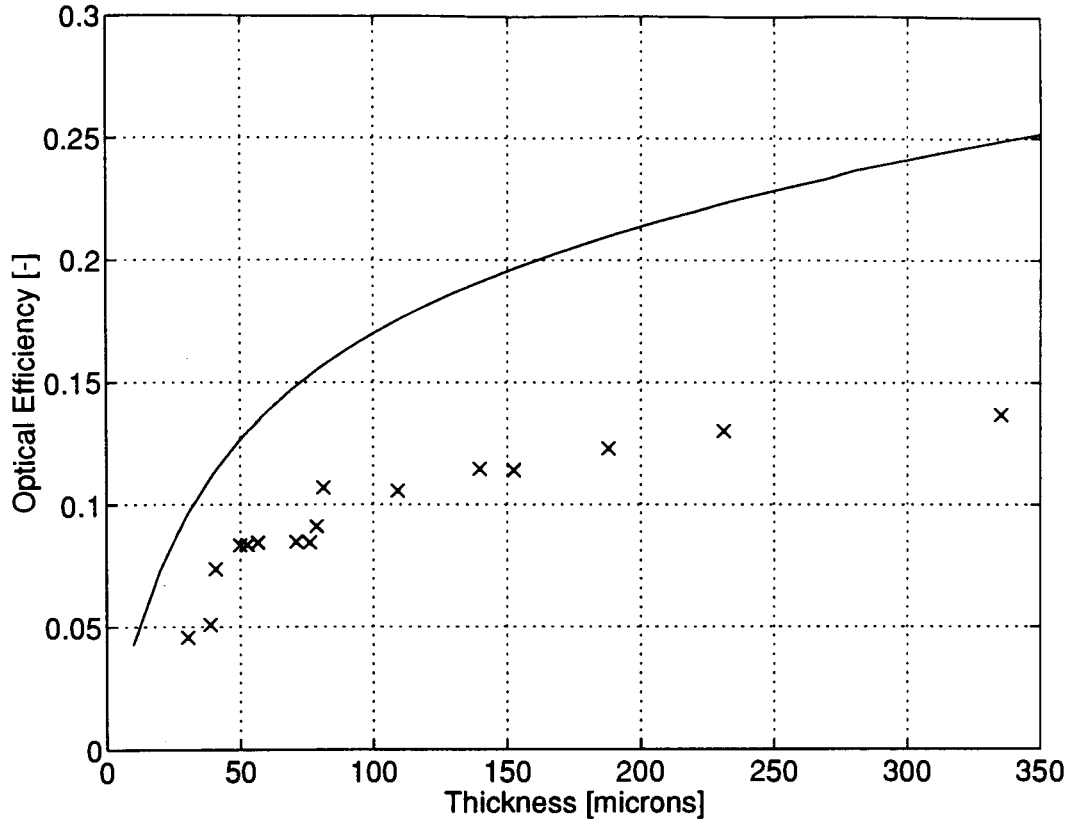

Figure 4.11: Optical Efficiency versus LC Thickness

make the LC cores had a higher refractive index than that of PMMA, so that reflective losses at the surface and output edge of the LC are also greater than predicted by the simulation results.

4.3.3 Photodiodes

The spectral response of the (0.623 cm^2) IC photodiodes (see appendix C) was determined by positioning the bare IC devices behind the output slit of the monochromator. The photocurrent from the diodes was then measured for incident wavelengths between 300 and 9500 nm. The power (W) incident normal to the surface of the diodes was also measured using an 818-SL photodiode (1 cm^2). The data was adjusted for the size difference between detector areas and for the spectral nonlinearity of the Newport photodiode (from the manufacturers specifications – see

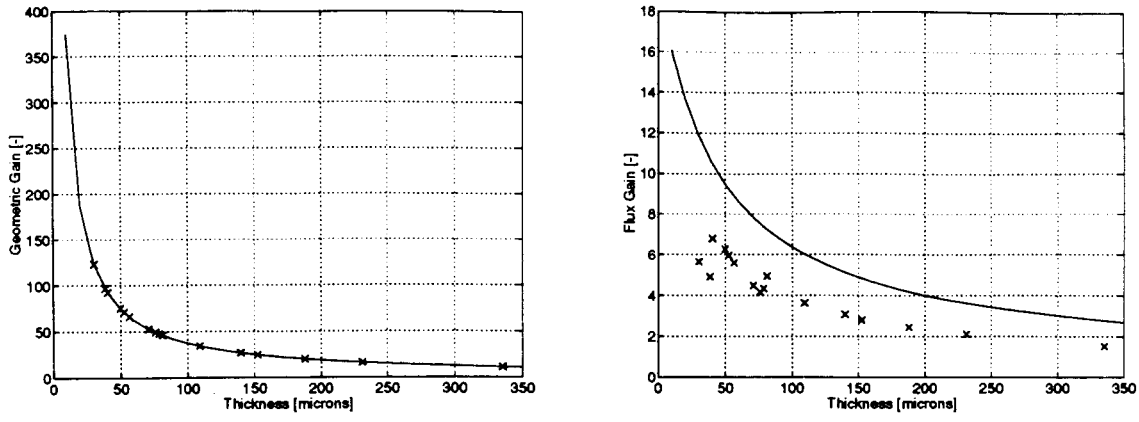

(a) Geometric Gain (b) Optical Gain

Figure 4.12: Output Gain versus Thickness

figure 4.3) and then used to determine the responsivity. A fourth order polynomial was used to fit the experimental data points by the method of least-squares ($R = 1.611 - 9.288 \times 10^6\lambda + 1.484 \times 10^{13}\lambda^2 - 2.450 \times 10^{18}\lambda^3 - 4.485 \times 10^{24}\lambda^4$ with a goodness of fit $r^2 = 0.9575$ (Lancaster and Salkauskas 1986, page 55)) and the results plotted in figure 4.13 (for the sake of clarity the experimental values have been omitted). Finally, the ideal responsivity from figure 4.3 was superimposed over the experimental results for comparison.

The differences between the ideal and experimental results presented here can be attributed to losses that degrade the responsivity of a photodiode. These losses include (Van Overstraeten and Mertens 1986, page 23) the loss of excess photon energy ($h\nu > E_g$) and losses due to metal coverage, surface reflections, incomplete absorbance and non-ideal collection efficiency (not all carriers that reach the junction are collected). Furthermore, silicon photodiodes are not suitable for detecting short wavelengths, since the absorption coefficient of silicon increases for higher frequencies in the visible region. Short wavelength light is unable to travel very far into the semiconductor since most of it is absorbed in only the top 1 μm of the detector surface (this is known as the "dead" region, and is formed during the manufacturing process) (Weiss 1994). Absorption of photogenerated carriers in this dead region results in unacceptably low quantum efficiencies. In general, the minority carrier lifetime decreases with increasing dopant concentration (Van Overstraeten and Mertens 1986, page 49) so

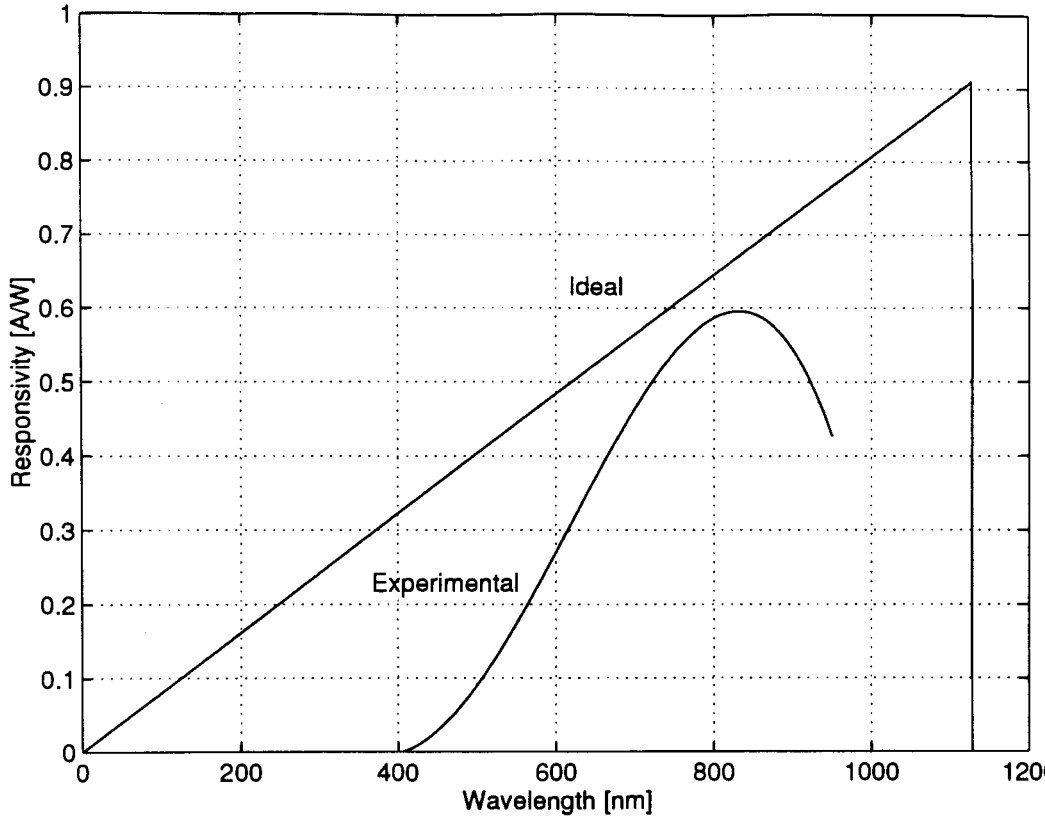

Figure 4.13: Experimental Photodiode Responsivity

that heavily doped photodiodes (such as those fabricated here) there is a further decrease in collection efficiency. Finally, the lack of a surface–passivating layer over the test diodes may have further degraded device efficiencies (Weiss 1994) due the presence of minority carrier trapping centers formed from surface impurities, defects, unfinished and broken chemical bonds.

4.3.4 ILCPs

The responsivity for prototype ILCPs (see appendix C) using rhodamine 6G (absorption peak at 530 nm and fluorescence peak at 560 nm) and coumarin 151 (absorption peak at 382 nm and fluorescence peak at 480 nm), at a concentration of 0.1% by weight, were determined in a manner analogous to that used for the photodiodes. The ILCPs were positioned at the output slit of the monochromator behind a 1 cm^2 aperture so that no light was allowed to fall directly on the photodiodes as shown in

figure 4.14. The distance from the edge of the aperture to the edge of each photodiode

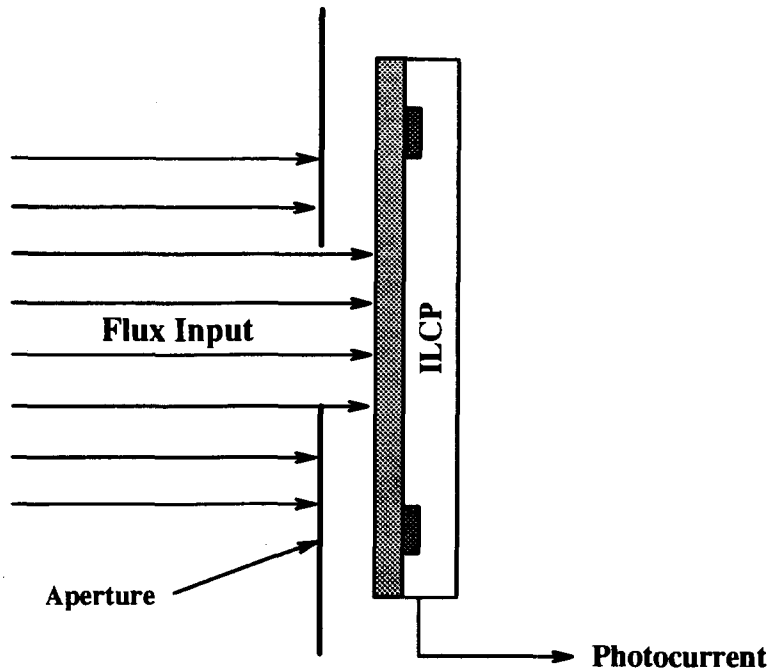

Figure 4.14: Set Up for ILCP Test Measurements

was 0.5 cm. The bonding wires from the ILCP photodiodes were then attached to the transresistance amplifier and the whole set up was connected to the data acquisition system. Finally, the photovoltaic output current and incident power were measured as a function of incident wavelength between 300 and 9500 nm.

The experimental data was adjusted for the size difference between detector areas and for the spectral non-linearity of the Newport photodiode. The data points were then interpolated using a cubic spline technique and the results, plotted in figure 4.15 (a) and (b). The results indicate that the responsivity of the ILCP is a strong function of the absorption characteristics of the dye as expected.

As a final test, the results of the ILCP simulation (optical efficiency versus incident wavelength) using rhodamine 6G for normally incident light were transferred from the emission to the absorption curve. This was accomplished by integrating the simulation output as a function of wavelength and distributing this result uniformly over the normalized absorption spectra (assuming conservation of probability and that the shape of the two curves are invariant from the ideal case). The resulting curve was then multiplied by the least squares fit to the diode responsivity of section 4.3.3 to

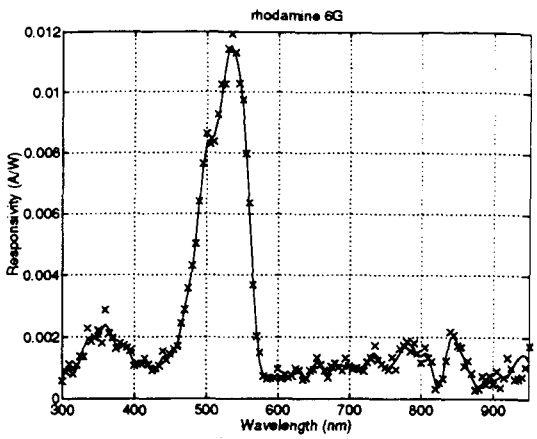

(a) rhodamine 6G

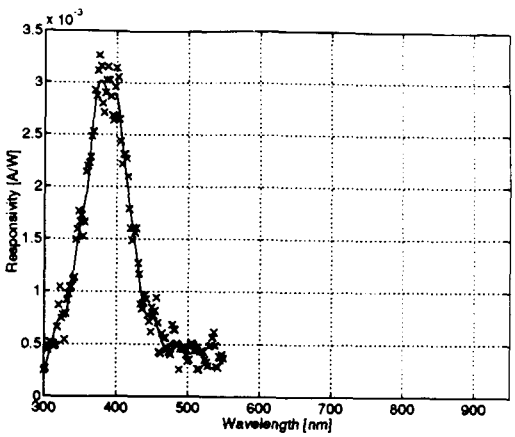

(b) coumarin 151

Figure 4.15: ILCP Responsivity

estimate that of the ILCP. The experimental results and theoretical prediction (solid line) are superimposed in figure 4.16.

The differences between the theoretical and experimental results presented here are the same as those stated for the LCs alone. Again, the accuracy of the experimental measurements were degraded by the non-uniform nature of the incident flux, geometrical trapping of the luminescent flux, incomplete TIR, self-absorption of luminescence by the dye and by the matrix material. Also, as in the case of the LCs, the experimental polymer material used to make the LC cores has a higher refractive index than that of PMMA, so that reflective losses at the surface and output of the LC are greater than predicted by the simulation.

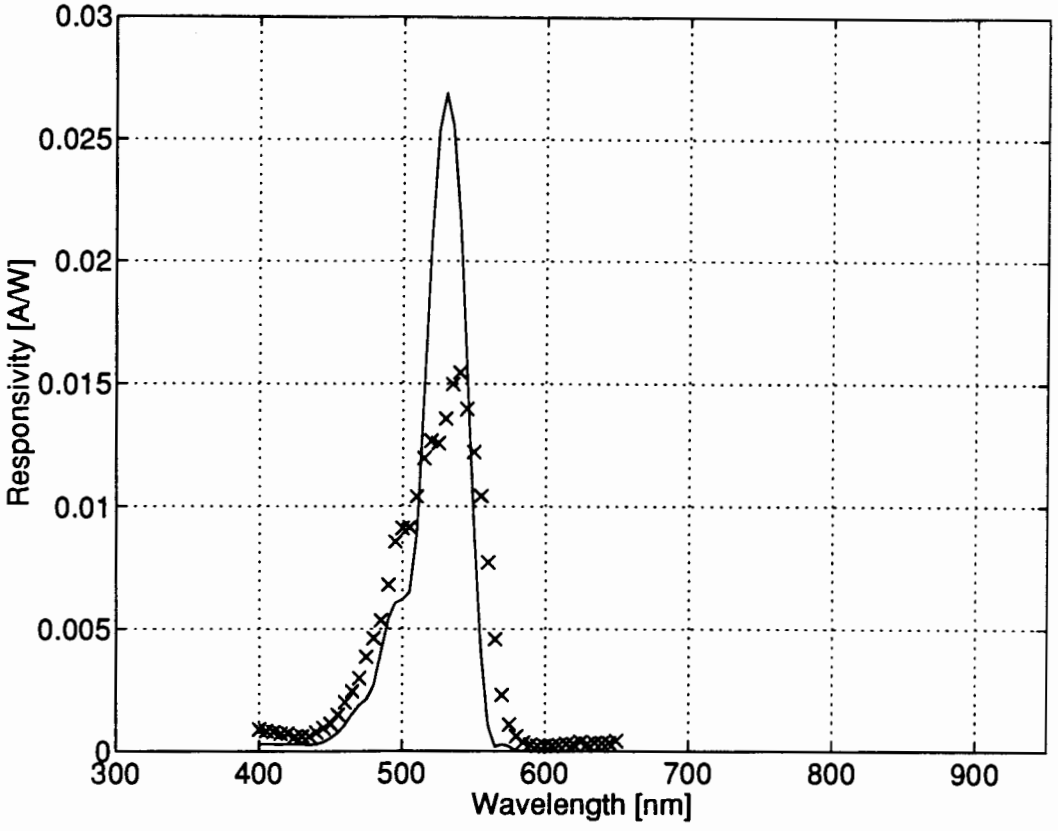

Figure 4.16: Comparison of ILCP Simulation and Experimental Results

Chapter 5

Conclusions

The purpose of this thesis was to document the development of a novel device that uses a LC to collect and concentrate light energy. To this end, the theory and design of an ILCP on a silicon substrate have been discussed and experimental results for several prototype ILCPs presented.

5.1 Contributions

Applied science has borrowed many ideas from biological vision systems for the design of various optical devices and strategies for robotic and machine vision. This work was motivated by the desire to create an artificial photoreceptor with properties similar to those found in nature, that can be fabricated using standard manufacturing processes. The ILCP (at least in part) satisfies these requirements.

5.1.1 Advantages

The ILCP is a versatile device that can be manufactured inexpensively using standard industrial processes. Complex ILCP systems can be fabricated with *optoelectronic integrated circuits (OEICs)* having photodetectors and associated electronics fabricated on the same substrate. Furthermore, due to their integrated nature, ILCPs can be miniaturized for use in compact devices.

The properties of the polymeric materials that were used to make the thin film LC elements (see appendix section B.2), can be easily varied in terms of refractive

index, mixture and concentration of dopant molecules. Furthermore, these low cost materials can be reliably processed inexpensively since the process for forming mask cured guide structures is a low temperature process similar to that used in PC board fabrication and is amenable to high volume production (Harnak 1992, page 280).

Finally, due to the large number of available luminescent materials (see appendix section A.1), ILCPs can potentially be used not only for applications in the visible, but also in the UV and IR regions and in equipment for recording short wave radiation (such as X or gamma rays). The spectral absorption bands of these materials in general, are highly stable and can have widths as small as a few angstroms (Harnak 1992, page 280). Hence, by selecting appropriate luminescent materials, the spectral response of an ILCP can be customized for particular applications. For example, an ILCP can potentially replace complex and costly interference filters in some applications.

5.1.2 Limitations

The main drawback to using ILCPs, is that their spectral responses cannot be chosen arbitrarily since they are a property of the luminescent material. For many cases however, a precise response may not be required so that the spectra of existing materials will suffice. Furthermore, some applications may be based more on the LCs ability to collect and concentrate light than on its spectral response. In these cases, the geometry of the LC device is more important than its spectral characteristics.

Losses and Noise

Losses related to the fabrication process degrade the overall performance of the LC elements. These include: the presence of scattering centers, reflective mismatches, geometrical trapping effects, incomplete TIR, inadequate absorption bandwidth, imperfect quantum efficiency and self absorption of luminescence by the dye and matrix material. In practice, the cured photopolymer core material used in this work (see appendix section B.2) show minimal losses in the visible and near infrared. For example, using this material, optical channel waveguides have been fabricated with losses

less than 0.3 dB/cm at 632.8 nm [1] and, in general, scattering rather than absorption plays a significant role in determining these losses (Krchnavek, Lalk, and Denton 1992). This scatter can result from surface roughness or chemical and physical inhomogeneities.

Losses that can degrade the responsivity of the integrated photodiodes include loss of long wavelengths ($h\nu < E_g$) and excess photon energy ($h\nu > E_g$) as well as loss due to surface reflections, incomplete absorbance and non-ideal collection efficiency (Van Overstraeten and Mertens 1986, page 23). Finally, an exposed surface of any semiconductor contains impurities, defects, unfinished bonds, broken bonds, and so forth. These are excellent trapping centers for moving carriers that further reduce collection efficiency.

Finally, photodetector noise sources (mainly thermal) determine the minimum detectable power that can be measured (Dennis 1986, page 14). Minimizing this for the simple PN junction photodiodes used in this work requires a low dark saturation current that in turn requires a high doping density (Van Overstraeten and Mertens 1986, page 64). In general however, the minority carrier lifetime decreases with increasing dopant concentration, thus reducing collection efficiency (Van Overstraeten and Mertens 1986, page 49) and in order to achieve high quantum efficiency, the junction depth should be small compared to the carrier diffusion length (Dennis 1986, page 84). Hence, a tradeoff has to be made between low noise and high sensitivity.

Reliability

The UV part of terrestrial sunlight (280-400 nm) represents only about 5% of the total radiation. This radiation however, is the most energetic and may be absorbed by polymers that are usually transparent in the visible region (Cheremisinoff 1989, page 546). Not surprisingly therefore, photodegradation has been found to occur in almost every plastic material due to prolonged exposure to sunlight (Cheremisinoff 1989, page 542). The effects of photodegradation include changes in (Cheremisinoff 1989, page 547):

[1] In general, losses ¡ 1 dB/cm are considered reasonable for most practical applications (Krchnavek, Lalk, and Denton 1992).

1. *Mechanical Properties:* drop in tensile strength, elasticity, impact resistance and crazing
2. *Surface Properties:* changes in abrasion resistance, surface quality and wettability
3. *Optical Properties:* discoloration, loss of transparency and gloss

The outdoor service life for unstabilized polymers may be on the order of weeks but can be on the order of years for polymers like acrylics (Cheremisinoff 1989, page 547). A more serious problem in the case of LCs therefore, is photodegradation of the luminescent material (see appendix A.1). In the past, degradation of the concentrator dyes has posed a critical technical barrier to the practical utilization of LCs (Batchelder, Zewail, and Cole 1981). Of course the severity of this degradation will depend on the LC application and its environment.

Repeatability

The experiments performed during the course of this work were repeatable within the limits posed by the ILCP fabrication procedure. For example, the IC processing used resulted in non-uniform results due to varying conditions across the wafers during thermal oxidation, diffusion, drive-in and so on. Hence, variation between the performance of the individual photodiodes was observed. Similarly, the LC processing technique was repeatable from formulation to formulation within the variation of the temperature of the photopolymer and dye solution (higher temperatures resulted in thiner films) and the accuracy to which the spin coating parameters (acceleration and final spin speed) could be maintained.

5.2 Future Work

The possibility of fabricating integrated devices using thin film LC elements for simple spectral light intensity analysis has been demonstrated. Further work to improve the simple design and processing techniques presented here will increase efficiency and reduce losses and hence improve the overall sensitivity and utility of ILCPs in general. Tailoring device geometries and through appropriate selection of luminescent materials, ILCPs can now be used for specific applications. Furthermore, through

continued research, LCs and ILCPs can be applied to a whole range of problems requiring the collection, manipulation, distribution and/or measurement of light.

5.2.1 Design Improvements

Numerous improvements to the simple design presented in this work are possible. For example, following fabrication, the ILCP can be sealed in a low index material to keep its surface free of scattering and absorbing contaminants that can degrade TIR. An AR coating (designed for the peak luminescent absorption wavelength) on the surface of this material and that of the LC element would improve the collection of incident light. Next, using an external aperture and shuttering mechanism to control this flux input would prevent light from falling directly on the photodiodes and time limit photodegradation of the LC under high intensity UV conditions. The exposed LC core can also be fabricated over a mirrored backplane to increase absorption to the incident light. Finally, an AR coating (designed for an appropriate propagation angle and for the peak luminescent emission wavelength) between the LC and photodiode would improve coupling of the flux output.

Other design improvements might employ *poling of the luminescent dye molecules* with a strong magnetic field to align their absorption and emission planes. A *stacked film configuration* with several dyes can be used to increase the spectral range (as in cascade compositions) or for multiple wavelength discrimination (wavelength demultiplexing). *Optical gain devices* (such as active waveguides) can be employed to increase the intensity of the flux output. Finally, the use of an *anti-resonant reflecting optical waveguide (ARROW)* structure would reduce propagation losses, especially in extremely thin LCs.

5.2.2 Technological Improvements

The guiding structures fabricated in this work were UV cured photolithographically using an uncollimated high pressure Hg arc lamp. Using a collimated light source, the resolution of these structures can be increased. It is also possible to produce better and more complex guiding structures via computer controlled direct laser writing. For example, using the base resin photopolymer formulation given in appendix table B.1 and a computer guided argon ion laser, guide losses less than 0.08 dB/cm at 632.8

nm have been reported (Krchnavek, Lalk, and Denton 1992). However, since every portion of the layout is exposed at the same time photolithography is significantly faster. Finally, although the photopolymer material system used in this work provides good adhesion to a variety of substrate materials, it can be improved through the use of adhesion promoters and surfactants (Harnak 1992, page 399). UV stabilizers can be used to prevent the absorption of harmful radiation by acting as UV filters or as scavengers of free radicals (Cheremisinoff 1989, page 547).

5.2.3 LC Applications

Coupling light into waveguiding structures is one of the most challenging problems facing integrated optics technology (Harnak 1992, page 280). An LC element can be conveniently used for this purpose, as shown in figure 5.1 (a) and (b). Here,

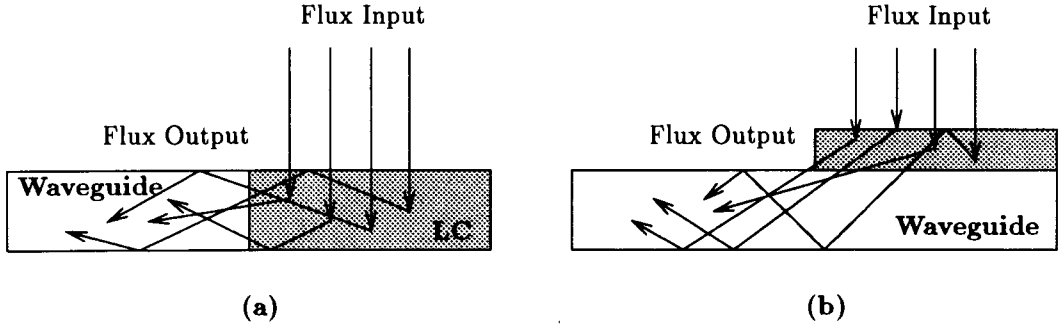

Figure 5.1: LC Light Coupler

light incident on the surface of the LC is guided into the waveguide by matching the refractive indices and butt coupling the LC to the edge of the waveguide (a) or, more conveniently, by depositing the LC on top of the waveguide (b). Using these techniques, light can be coupled from free space into an OEIC system.

5.2.4 ILCP Applications

Due to its unique spectral properties, an ILCP can be conveniently applied to simple colorimetric analysis. By fabricating several ILCPs sensitive to different wavelengths on the same chip, an integrated spectral analyzer can be fabricated. Furthermore, due to their diverse nature, the use of ILCPs is not restricted to colorimetric or

spectral applications. Other applications include the development of **PAR sensors**, **UV dosimeters** and **LASER positioning** and **early vision systems** as detailed below.

PAR Sensor

Plants use the 400 to 700 nm part of terrestrial sunlight for photosynthesis. A photosynthetically active radiation (PAR) sensor is used to measure photosynthetic photon flux density (PPFD) in this waveband. PPFD is a measure of the number of photons incident per unit of time on a unit surface. It is an important measure, since a simple integral relationship exists between the number of molecules photochemically changed and the number of photons absorbed. Plant scientists, horticulturists and other environmental scientists use PAR sensors to measure PPFD in the atmosphere, in growth chambers and in greenhouses (Biggs 1991). An ILCP PAR sensor can be fabricated using a cascade composition of luminescent dyes in a single film. In this case, the absorption characteristics of the dye composition would be tailored so that the ILCP response was band limited to the PAR region.

UV Dosimeter

Terrestrial sunlight with wavelengths less than 400 nm is too short to be detected by the human eye. This UV light is further categorized according to the Commission Internationale de l'Eclairage (CIE) as follows:

1. **UV-A** = 315-400 nm,
2. **UV-B** = 280-315 nm and
3. **UV-C** = 100-280 nm.

Light with wavelengths less than 180 nm (vacuum UV) is absorbed by atmospheric oxygen and in general, UV-C never reaches the earth surface since it is absorbed by the atmosphere. UV-A and UV-B cause tanning (pigmentation) and sunburn (erythema). UV-B is also responsible for the production of vitamin D_3. In high doses, absorption of UV light can lead to photodamage of the skin (photoaging) and eyes (cataract formation), alteration of the skin's immune system (photoimmunology), chemical hypersensitivity (phototoxicity and photoallergy) and skin cancer (photocarcinogenesis)

(Council Report 1989). To allow individuals to protect themselves from these harmful effects, an ILCP UV dosimeter, using UV sensitive luminescent dyes, can be made with an output response proportional to UV intensity. For example, a UV dosimeter might be calibrated to output in terms of the *UV index* shown in table 5.1 [2] (Environment Canada 1993).

Risk:	UV index:	Average time to burn:
Extreme	9.0 or higher	less than 15 minutes
High	7.0 to 8.9	about 20 minutes
Moderate	4.0 to 6.9	about 30 minutes
Low	less than 4.0	one hour or more

Table 5.1: UV index

LASER Positioning System

The proportion of flux output from an incremental length along the edge of an LC is a function of the position and angle of the flux input. Therefore, by comparing the relative magnitude of output from independent photodiodes placed around the periphery of an LC as shown in figure 5.2, it is possible to position the ILCP relative to a the LASER source. In this way a simple ILCP LASER positioning system can be made.

Early Vision system

Integrated circuits are usually two dimensional, whereas nature works more efficiently in three dimensions. The human retina, for example, is a massively paralleled three dimensional imaging system consisting of a layer of sensing cells (rod and cone cells), two layers of processing cells and two layers of interconnection cells. Using a two dimensional array of photodiodes and their associated electronics overlaid with a single contiguous photolithographically defined LC structure and appropriate optical imaging hardware, several early vision mechanisms can be artificially duplicated. For example, by varying the LC dye concentration in this simple three dimensional structure (LC on photodiodes), it may be possible to vary horizontal spreading of the

[2]The UV index is a measure of the UV intensity in full sunlight.

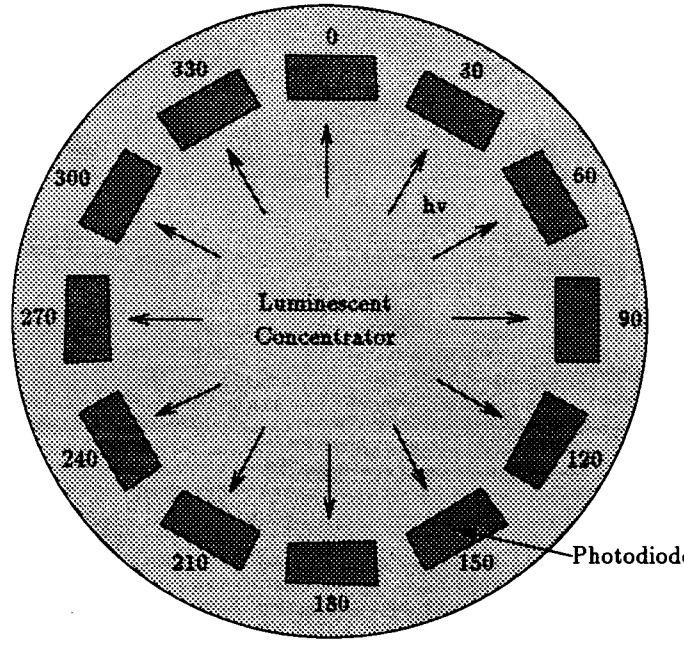

Figure 5.2: ILCP LASER Positioning System

luminescent flux for use as a background adaptation mechanism or to form receptive fields. In this case, the ILCP acts towards its intended purpose, as an artificial photoreceptor.

Appendix A

LC Materials

An LC can be made from glass or crystal doped with inorganic luminescent ions or from polymer containing organic luminescent molecules. The purpose of this appendix is to outline some considerations that must be made when fabricating an LC and to describe a few experimental LCs from the literature.

A.1 Luminescent Materials

Luminescent materials suitable for LC fabrication must exhibit compatibility with the matrix material, high stability, long service lifetime and high quantum efficiency (Goetzberger and Greubel 1977). Furthermore, for efficient collection, incident wavelengths should have a short absorption length (strong absorption), while emitted wavelengths should have a long absorption length (high transmittance) (Weber and Lambe 1976). For low self absorption the absorption and emission wavelengths should be well separated (Goetzberger and Greubel 1977). Finally, to minimize red shifting, the dye should exhibit a relatively broad absorption band and a narrow emission band.

Previous LC experiments have made use of both **organic** and **inorganic** luminescent materials. Other mechanisms such as non-radiative energy transfer processes between different organic molecules or from ligands of suitable rare earth ions to their centers have also been suggested (Goetzberger and Greubel 1977). Finally, it has been proposed that multiple dye (sensitized) LCs may be more efficient than a single dye LC in some applications because they can intercept more spectral energy (Swartz, Cole, and Zewail 1977). Sensitization can also be used to tailor the spectral response

of an LC.

Inorganic Materials

Rare–earth materials such as Neodymium (Nd^{3+}) are suitable for LC applications. In fact, Nd^{3+} doped glass, with several strong absorption bands in the 500–900nm (visible and near infrared) range and emission bands at 880nm, 1060nm and 1350nm is particularly well suited to the Si bandgap (Weber and Lambe 1976; Levitt and Weber 1977) (recall that $E_{gSi} \approx 1100nm$). Furthermore, Nd^{3+} glass quantum efficiencies in the range $\eta = 0.50$ to 0.75 have been reported with attenuation coefficients below $10^{-3}cm^{-1}$ (Weber and Lambe 1976).

Inorganic luminescent materials can be further improved by adding absorbing molecules or ions that transfer energy to the species luminescing at the longest wavelength (Levitt and Weber 1977). For example, Uranyl (UO_2^{2+}) doped glass is a good choice to improve sensitivity in the UV region since it has strong absorption bands below 500nm (peaks at 423nm and below 340nm), emittance in the visible region (peaking at around 507nm) and a quantum efficiency of about 30% at room temperature (Reisfeld and Neuman 1978). For Si photocells therefore, a cascade of UO_2^{2+} to Nd^{3+} would increase the absorption spectrum and hence the collection efficiency of the LC (Reisfeld and Kalisky 1980).

Unfortunately, although inorganic luminescent materials have high stability, they exhibit relatively low quantum efficiencies (Feucht and Burke 1981). Furthermore, LCs made with inorganic luminescent materials in glass, especially those having a complicated composition, are much less accessible than luminescing materials in a polymer matrix (Levin, Cherkasov, and Baranov 1988). As a result, they have not been as extensively studied as organic dyes for LC applications.

Organic Materials

In the past, organic luminescent dyes in PMMA matrices have been used to fabricate experimental LCs. The most attractive feature of these dyes is their high quantum efficiency (typically $\eta > 0.85$) (Batchelder, Zewail, and Cole 1979). Furthermore, these dyes emit visible or near infrared photons and thus are well suited to semiconductors such as Si and gallium arsenide (GaAs) (Weber and Lambe 1976). Unfortunately,

these dyes also tend to dimerize or polymerize under irradiation so that the fluorescence quantum efficiency decreases with time (Lumb 1978, page 117). Therefore, they exhibit degradation and have low chemical stability and lifetimes (Feucht and Burke 1981).

The two basic types of deterioration that occur in organic dyes are thermal and photobleaching (Batchelder, Zewail, and Cole 1979). The effects of thermal bleaching are considered negligible for temperatures below 60°C. However, thermal bleaching is important during exposure to solar radiation when the temperature of the LC can range well above room temperature. For temperatures above 20°C, a rapid decrease in both the absorption and emission bands have been observed. For example, a rhodamine B doped PMMA sample showed a 37% decrease in its absorption peak while similar samples of rhodamine 6G and fluorescein showed changes of 14 and 10% respectively. When the samples were cooled to room temperature, a partial recovery of this thermal bleaching process was observed (Meseguer Rico, Jaque, and Cussó 1981; Meseguer, Jaque, Cussó, and Sánchez 1981).

Photobleaching under extreme UV conditions has been shown to affect LC lifetimes [1] (Goetzberger and Greubel 1977; Batchelder, Zewail, and Cole 1979). It has been suggested that the lifetimes of these dyes can increased through inexpensive protection measures such as the addition of a top cover glass and bottom metallic reflector or through the addition of antioxidants and ultraviolet absorbers. However, the degradation of organic dyes has remained one of the most critical technical barriers to the practical utilization of LCs (Batchelder, Zewail, and Cole 1981).

It has been observed that the fraction of the flux absorbed is quite sensitive to the concentration of the particular dye used. High concentration single dye LCs perform better than lower concentration devices due to increased absorption (Batchelder, Zewail, and Cole 1979). Furthermore, in rhodamine 6G doped PMMA it has been observed that red shifting occurs because the dye absorbs the shorter wavelength luminescence and re-emits into the entire luminescence band. These materials can be improved by adding absorbing molecules or ions that transfer energy to the species luminescing at the longest wavelength (Levitt and Weber 1977).

Multiple dye LCs have been fabricated in PMMA using coumarin 6 and rhodamine

[1] The rate of photobleaching for typical organic dyes has been estimated at 10^{-6} molecules per photon (Batchelder, Zewail, and Cole 1981).

6G (coumarin 6 absorbs at shorter wavelengths than rhodamine 6G and emits into its absorption spectra) at concentrations of 10^{-4} M (Swartz, Cole, and Zewail 1977). This technique was shown to be practical and improved the gain of the LC by at least the ratio of the sum of the absorption areas of the multiple–dye to single–dye LCs. Transfer from rhodamine 6G to m-cresyl violet (rhodamine 6G absorbs at shorter wavelengths than m-cresyl violet and emits into its absorption spectra) in solution has also been studied (Levitt and Weber 1977).

A.2 Matrix Materials

The matrix of an LC is the rigid core material that supports the luminescent molecules or ions. In general, this material must be highly transparent. That is, the matrix should exhibit small absorption and scattering losses (Levitt and Weber 1977). An LC matrix can take the form of a plate, rod or thin film (Baranow 1991). **Glass** and **plastic** are typical matrix materials.

Glass

Glass with various refractive indices is readily available and can be doped with various inorganic luminescent ions (rare earth element doped laser glasses). Furthermore, the glass matrix loss is smaller than that of plastic (Levitt and Weber 1977).

Polymers

A simple LC can be fabricated by dissolving an efficient laser dye in a transparent polymer of good optical quality. Advantages of polymer materials include (Harnak 1992, page 287 and 292):

- low cost
- light weight
- ready variability
- ease of fabrication and processing (by spin coating for example)
- high mechanical and dielectric strength
- high thermal and environmental stability

- compatibility with semiconductor processing

Polymer materials that can be used to fabricate polymer waveguides include (Harnak 1992, page 287) methacrylates (such as PMMA), polyimides and epoxies. In particular, matrix losses as low as 0.08 dB/cm from an aromatic acrylated epoxy on an aliphatic urethane dimethacrylate have been recorded (Harnak 1992, page 280).

Appendix B

Polymers

A number of considerations were made in choosing the polymer material used in this work. These included the need for compatibility with typical IC processing techniques and environments and with the luminescent dye and for good adhesion to the substrate materials. Also, to simplify processing, a material requiring only standard fabrication steps such as spin coating and photolithography was sought. To this end, two basic of material systems were investigated:

1. **Polymer Solvent Systems** and
2. **UV Photopolymer Systems.**

In the case of the solvent systems, rhodamine 6G (443.56582 g/mol) was introduced directly into the solutions, while for the photopolymers it was introduced by way of a concentrated methanol solution. The trial polymer solutions were then spin coated onto glass test slides using a Headway Research model 1-EC10ID-R790 photoresist spinner and the thickness ($\pm$1 micron) and uniformity ($\pm$25 Angstroms) of the resulting films evaluated using a Dektak IIA Surface Profile Measuring System (by Precision Research Instruments, Inc.).

When spin coating polymer solutions, the final film thickness is a strong function of viscosity and spin speed. Film thickness can easily be adjusted by changing the viscosity of the polymer solution. However, fine control over film thickness is best achieved by changing the angular velocity. An inverse power–law relationship generally holds for the thickness dependence on the final spin speed (Flack, Soong, Bell, and Hess 1984). Hence, an increase in spin speed decreases the film thickness. For

a given speed, the film thickness decreases rapidly at first, but then slows down considerably at longer times. What is affected by the length of the acceleration period is the radial uniformity of the film (Flack, Soong, Bell, and Hess 1984). Short acceleration periods result in much more uniform films then for long periods. Using a consistent spin coating process, it is possible to obtain thickness control to within 0.1 μm (Harnak 1992, page 398–399).

B.1 Polymer Solvent Systems

A polymer solvent system consists simply of a bulk polymer material or resin dissolved in a suitable solvent or solvents. The resulting solution can be spin coated and dried to form a thin film. Of course, the surface quality (uniformity) of this film is strongly influenced by the presence and choice of the solvents used. Solvents with low boiling points can lead to radial ridges and unevenness, while those with high boiling points can be difficult to drive out of the film, resulting in cloudiness and material instability. The advantage however, is that the viscosity of the solution can be adjusted by varying the amount of solvent.

Material Processing

The polymer solvent solutions were prepared by gently heating and agitating the solvent or solvents while slowly adding the resin and dye. The mixture was loosely covered to reduce evaporation losses while heating, until the resin and dye were totally dissolved. Next, the solution was allowed to cool to room temperature for several hours and then spin coated using the following procedure:

1. **Clean:** rinse test slide in acetone and spin dry (4000 rpm for 30 seconds)
2. **Prespin:** dispense polymer solution and spin at low speed for even initial distribution (500 rpm 30 seconds)
3. **Spin:** spin at final speed (500, 1000, 1500 or 2000 rpm) until film is dry
4. **Hard Bake:** heat film to remove residual solvent (100°C for one hour)

Finally, a portion of the resulting film was mechanically scraped off the substrate surface and its thickness measured using the profilometer.

Trial Formulations

Preliminary tests involved dissolving bulk polymethyl methacrylate (PMMA) in various organic solvents including methyl methacrylate (MMA), ethyl acetate, acetone, methyl ethyl ketone (MEK), toluene and trichloroethylene. PMMA is an acrylic polymer of MMA with a service temperature up to 200°C (glass transition temperature $T_g = 200°C$). It was chosen because it is readily available in various molecular weights and because it is commonly used as a resist material in electron beam lithography. Solutions of both clear PMMA and PMMA doped with 0.1% commercial fluorescent pigments were formed. For high molecular weight PMMA trichloroethylene was found to be the best solvent. At lower weights MEK, toluene and acetone worked well. However, in most cases, high molecular weight and highly cross–linked polymers did not dissolve easily.

Next, a commercial high molecular weight PMMA resin, Lucite 2041, was dissolved at 2 to 10% solids by weight in various solvents. Using higher solids concentrations resulted in films that were too thick and uneven. Using the low concentration solutions, uniform film thicknesses in the range to 10 μm were formed. However, even for these thin films residual solvents could not be driven out yielding cloudy results. This condition was corrected by increasing the hard bake temperature to 200°C, however at this temperature the polymer ($T_g = 95°C$) and organic dye molecules used were susceptible to thermal degradation.

Finally, a low to medium molecular weight MMA/BMA (butyl methacrylate) copolymer, Neocryl B-725, was dissolved at 40 to 60 % solids by weight in a 1:1 solution of MEK and toluene. Using these formulations, uniform film thicknesses in the range 4 to 20 μm were achieved. Next a layer of polyvinyl alcohol (PVA) and a layer of standard photoresist (Shipley Megaposit SPRZ-1.0L) were spun over the Neocryl to attempt to pattern the films by chemical etching[1]. The procedure used was as follows:

1. **Pattern photoresist mask** by photolithography[2] (expose and develop)
2. **Pattern PVA mask** (rinse in water)

[1] PVA dissolves in water and not in acetone while the photoresist dissolves in acetone and not in water.

[2] The photoresist was developed using Shipley Microposit MR-319.

3. **Strip photoresist mask** and **pattern Neocryl** (rinse in acetone)

4. **Strip PVA mask** (rinse in water)

The results of this processing were encouraging but not acceptable. The process itself was too sensitive to length of rinse times (developing) and the thickness of the PVA and photoresist layers. Edge definition was poor and under–cutting of the PVA and Neocryl layers inhibitive. In order to use this technique, much more work would be required develop the procedure fully.

Results

Spinning uniform thin films using polymer solvent systems was not easy (especially for high molecular weight polymers). Filaments that formed at edges of the substrate tended to adhere to surface and contribute to non-uniformities. Spinning thick films (greater then say 20 μm) was even more difficult because the residual solvents left in the material after spinning could not be driven out. Also, such systems are not suitable for spinning multiple layers because the solvent in fresh layers partially dissolves the material laid down previously resulting in more surface irregularities.

The major problem with using solvent systems was patterning. When using such systems, e-beam lithography and dry etching patterning techniques are commonly used. However such methods are non-standard and costly. Chemical etching was attempted (as described above) however, the resulting processes were complicated and did not produce adequate results. In any case, it is clear that the patterning of films formed using polymer solvent systems requires numerous processing steps that can result in increased optical losses and manufacturing costs. Therefore the use of photopolymers that can be patterned using standard photolithographic techniques was investigated.

B.2 Photopolymers

A **photopolymer** is a polymer system where light initiated changes cause polymerization of a monomer solution resulting in a highly cross–linked material (Harnak 1992, page 145). Such polymers exhibit high reactivity, good optical clarity and good adhesivity to various substrates (Harnak 1992, page 280). Furthermore, as a result

of their high cross-link density these polymers exhibit excellent post-cure stability and are essentially insoluble in organic solvents, infusible and resistant to thermal treatments and resistant to natural weathering (Cheremisinoff 1989, page 596).

The photophysics of UV-polymer interactions are equivalent to those given in chapter 2 for luminescent materials. All the mechanisms are the same, differing only in the possibility of creating free radicals from excited triplet states as shown in figure B.1. These free radicals are subsequently capable of initiating a large number

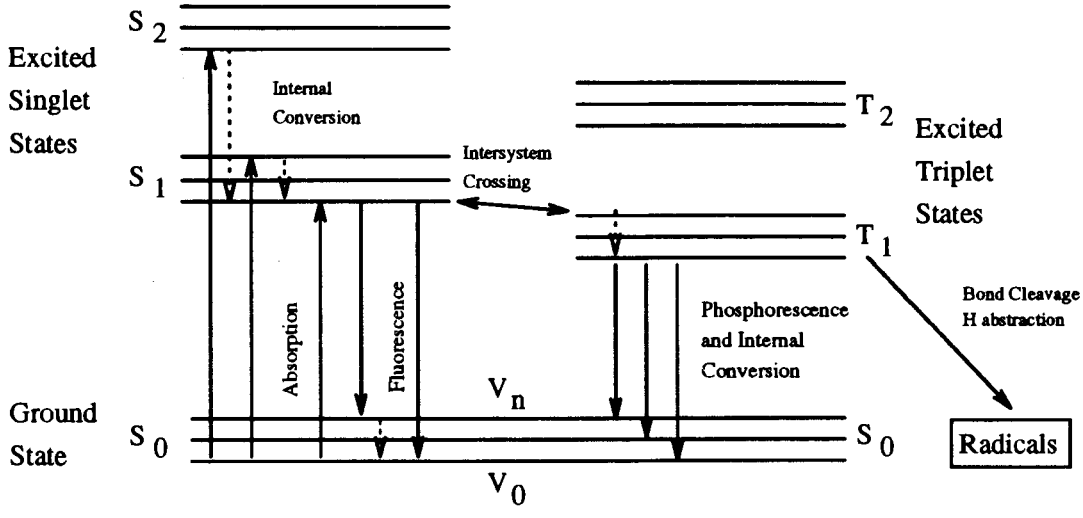

Figure B.1: Creation of Free Radicals for Photopolymerization

of chemical reactions, such as chain scission, cross linking of functionalized polymers, oxidation and polymerization (Cheremisinoff 1989, page 541). However, since most of the monomers commonly employed do not produce initiating species with sufficiently high yield upon UV exposure, it is necessary to introduce a **photosensitive initiator** that will make the polymerization start upon illumination (Cheremisinoff 1989, page 579). Hence, standard photopolymer formulations include both a monomer and a photoinitiator.

Atmospheric O_2 interferes with photopolymerization processes by deactivating both single and triplet excited states via an energy transfer process[3]. This occurs only if the lifetimes of the excited states is longer then 10^{-8} seconds or if those of the radicals is longer then 10^{-7} seconds (Cheremisinoff 1989, page 544). Several methods have been developed to reduce this undesirable effect, such as increasing the light

[3]Molecular O_2 exhibits a high reactivity towards both excited states and free radicals

intensity, the addition of O_2 barriers and scavengers or the addition of surface–active initiators. None of these has yet permitted the up to tenfold increase in cure efficiency that occurs in thin films when O_2 is removed (as in a N_2 environment) (Cheremisinoff 1989, page 591).

UV curing is the process that transforms a monomer into a macromolecule by photopolymerization. The advantages of UV curing over other forms of curing include (Cheremisinoff 1989, page 579 and 597):

- high–solids application
- fast processing rate (rapid reaction rate)
- low energy consumption
- low temperature process (hence low heating of substrate)
- lack of solvent emission
- reduction in equipment and space requirements (small space requirements)
- high product quality

Furthermore, selective UV curing can be used in **photolithographic** or **direct write** processes on standard electronics substrate materials such as epoxy/fiberglass, teflon, ceramic or silicon.

Material Processing

The UV polymer solutions were prepared as described in the next section and spun over glass test slides at room temperature. The wet films were then cured using a 100W high pressure Hg arc lamp. During the preliminary trails, the wet films were cured in air for 10, 15 and 20 minutes. In each case frosted, cloudy and pitted films resulted, indicating incomplete curing of the monomer solutions. Oxygen inhibition was suspected and a N_2 purge chamber constructed. A trial was then repeated in the chamber using a 10 minute cure time and the whole wet film, including the unexposed areas, polymerized. Using shorter cure times of 1, 2 and 5 minutes resulted in good curing and resolution. However, some blurring of edges due to light leaking around the proximity mask was observed. To insure a thorough cure, 5 minutes exposure times were used in all experiments. The UV cured films were then developed using MEK. MEK was chosen because it does not react with the uncured resin, does not dissolve

the cured resin, is reasonably fast acting and does not react with water. Finally the developed films were hard baked at 50°C for one hour to remove any residual solvents from the initial solution and development.

The spin–casting process can produce a significant level of **residual optical stress birefringence** in thin polymer films. This is because in general, polymers in the solid state are still readjusting themselves towards the more stable denser state. This process can be accelerated by **annealing** the polymers at about the *glass transition temperature* of the polymer (Harnak 1992, page 402). Annealing also reduces the internal mechanical stress and may improve the adhesion to substrates. For these reasons, the dry films were annealed in an inert N_2 atmosphere at 145°C for 5 hours[4].

The procedure used to form the thin photopolymer films can be summarized as follows:

1. **Clean:** rinse test slide in acetone as a mild degreasing step and spin dry (4000 rpm for 30 seconds)
2. **Prespin:** dispense polymer solution and spin at low speed for uniform dispersion of resin (500 rpm 90 seconds)
3. **Spin:** spin at final speed (500, 1000, 1500 or 2000 rpm for 30 seconds) and allow wet film to settle for several minutes (about 10 minutes) to minimize bubble formation and to allow the self–leveling nature of the solution to produce a more uniform film.
4. **UV Cure:** cure under 100W high pressure Hg arc lamp in N_2 (5 minutes)
5. **Develop:** rinse in MEK to remove uncured polymer
6. **Hard Bake:** heat film to remove any residual solvents from the solution and development (50°C for one hour)
7. **Anneal:** Annealed films on flat metallic surface (heat load) with a slow ramp up and down (145°C for 5 hours in N_2)

Finally, the film thickness was measured between cured and uncured regions using the profilometer.

[4]Annealing must be performed at less then 200° to prevent thermal degradation of polymer and organic chromophores

Trial Formulations

The first experiments with photopolymers in this work were carried out using commercially available UV adhesives (Loctite Impruv 349 and Loctite 3301 medical grade UV adhesives). These adhesives were originally intended for bonding transparent materials and optical elements. However, it was discovered that similar materials had been used previously in optical applications to fabricate waveguide structures (Hartman, Lalk, Howse, and Krchnavek 1989; Krchnavek, Lalk, and Hartman 1989). Unfortunately, these materials are expensive in small quantities and offer no control over composition. To circumvent these limitations, a custom photopolymer solution was found that can be varied in composition and is made up of easily available and inexpensive bulk materials (Krchnavek, Lalk, and Denton 1992; Nakagawa, Kowalewski, Phelps, Rode, and Krchnavek 1994).

The base resin used was an aromatic (cyclic) acrylated epoxy (Ebecryl 600). This resin is too highly viscous in its pure form to lend itself to efficient curing at room temperature. It tends to gel an then vitrify too rapidly which results in the entrapment of uncured regions within the developing glassy matrix (Krchnavek, Lalk, and Denton 1992). This unreacted monomer or poorly reacted oligomer (incompletely developed polymer chains) can have a plasticizing effect on the polymer with an accompanying lowering of the glass transition temperature, thereby affecting the optical and mechanical properties of the finished waveguide. Uncured monomers can act as optical heterogeneties within the guide, which cause increase in loss and produce an etched or pitted surface after solvent wash (Krchnavek, Lalk, and Denton 1992).

To increase the degree of conversion at room temperature, the resin is diluted with a low viscosity aliphatic (linear) monomer, propoxylated glycerol triacrylate (OTA 480) (Krchnavek, Lalk, and Denton 1992). This serves to delay the onset of gelation and vitrification until a relatively high degree of cross–linking is achieved. The flexible nature of the aliphatic "diluent" monomers imparts enough molecular mobility to the developing three dimensional network that a significantly higher number of the resin end groups are tied together into the final cured structure. Also, the low viscosity monomers act as the vehicle for solubilization and incorporation of the crystalline photoinitiator into the resin system since the undiluted resins are too viscous to allow the dissolution of the photoinitiator without heating.

The curing agent used was 1-Hydroxycyclohexyl phenyl ketone (Irgacure 184), a non-yellowing, highly efficient photoinitiator developed for curing unsaturated resin and monomer systems such as those based on acrylates and methacrylates (Krchnavek, Lalk, and Denton 1992). Irgacure 184 exhibits a broad UV absorption spectrum over the 200–400 nm range, resulting in an excellent balance of surface and through cure properties. In addition it exhibits an excellent shelf stability in formulations and hence reduces the chance of premature polymerization during storage.

The base formulation used (UV1 – density 1.176 g/ml) is detailed in table B.1[5]. 0.1% by weight rhodamine 6G was added to UV1 by way of a concentrated methanol

Resin:	Constituent:	Chemical Composition:	Density: (g/ml)	%wt
UV1	Ebecryl 600	Epoxy diacrylate	1.202	69.3
	OTA 480	Propoxylated glycerol triacrylate	1.084	29.7
	Irgacure 184	1-Hydroxycyclohexyl phenyl ketone	——	1.0

Table B.1: UV Polymer Base Resin Formulation

solution. The resulting mixture was heated to 60°C to form uniform solution and to get rid of bubbles. The solution was then allowed to cool to room temperature over several hours.

It was discovered that the concentration of methanol affected the final thickness of the spun films. Adding more methanol resulted in a less viscous solution and hence thiner films. Several formulations of UV1 with different methanol and photoinitiator concentrations were made up as detailed in table B.2. According to the application

Resin:	Base:				
	E600: (%wt)	O480: (%wt)	I184: (%wt)	Rh6G: (%wt base)	Methanol: (%wt base)
UV2	69.3	29.7	1.0	0.088	0.000
UV4	68.6	29.4	2.0	0.103	3.002
UV3	67.9	29.1	3.0	0.084	6.667
UV5	67.2	28.8	4.0	0.107	9.042

Table B.2: UV Polymer Test Resin Formulations

[5]**Ebecryl 600** and **OTA 480** were obtained from UCB Radcure Incorporated, 131 Revco Road, North Augusta, South Carolina 29841. **Irgacure 184** was obtained from Ciba–Geigy Canada Limited, P.O. Box 2000, 7030 Century Avenue, Mississauga, Ontario L5M 5N3.

notes, Irgacure 184 should be evaluated at a concentration of from 1–6 % by weight in clear and pigmented systems. The optimum concentration will depend on resin formulation, type of dye and level and type of curing lamp. However, film thickness should also be considered when determining the ideal photoinitiator concentration. Generally, an inverse relationship exists between coating film thickness and photoinitiator concentration required for satisfactory cure. For example, in thick films, a high photoinitiator level may not allow for sufficient light penetration to the lower portion of the coating, resulting in an unsatisfactory through cure. In thin films, higher concentrations will be needed to overcome increased air inhibition. Adding more Irgacure 184 to the less viscous solutions, resulted in a better curing of thin films, harder surface, better adhesion to the substrate (no pealing) and improved chemical resistance.

Results

Using the profilometer, the average thickness of the spun films was measured with respect to a horizontal zero at the surface of the substrate is shown in figure B.2 as a function of spin speed (a) and methanol concentration (b). In both cases an

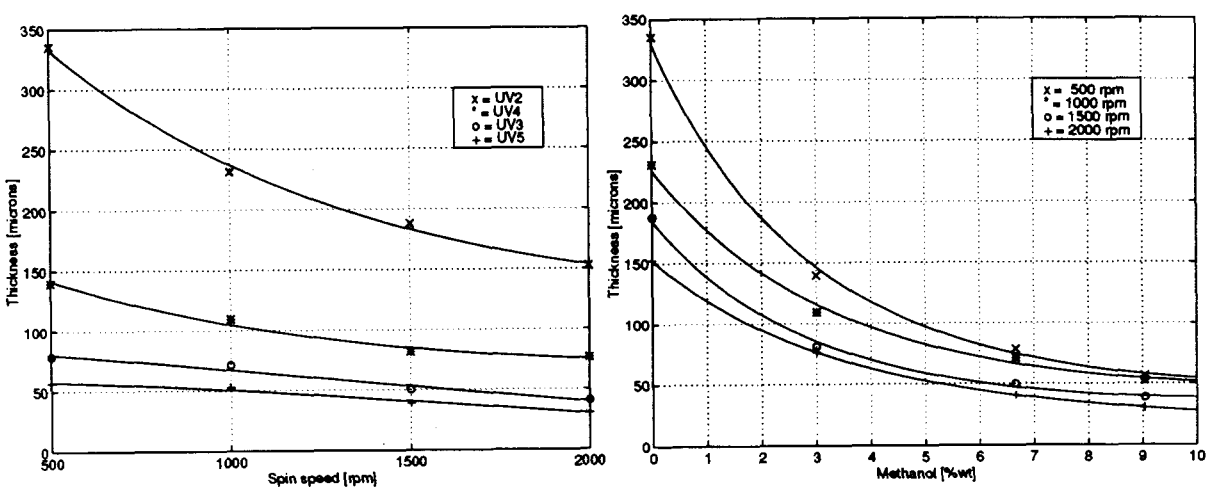

(a) (b)

Figure B.2: Thickness of UV Cured Films

exponential empirical estimate has been fit to the data points using a second order least squares approximation. The results indicate that the thickness of the final film is a strong function of both angular velocity and viscosity (as expected).

The *arithmetic average roughness* R_a for the films is shown in figure B.3 as a function of spin speed (a) and methanol concentration (b). Here, R_a is a measure of the finer irregularities of the surface texture as given by the average deviation from the mean profile height. The data points were averaged by concentration (a) and spin speed (b) and in both cases fit to a linear empirical estimate using a first order least squares approximation. The results indicate that the uniformity of the spun films improve as a function of angular velocity (as expected) and methanol concentration. The latter improvement is probably due to a decrease in the surface tension of the solution with a proportional decrease in viscosity.

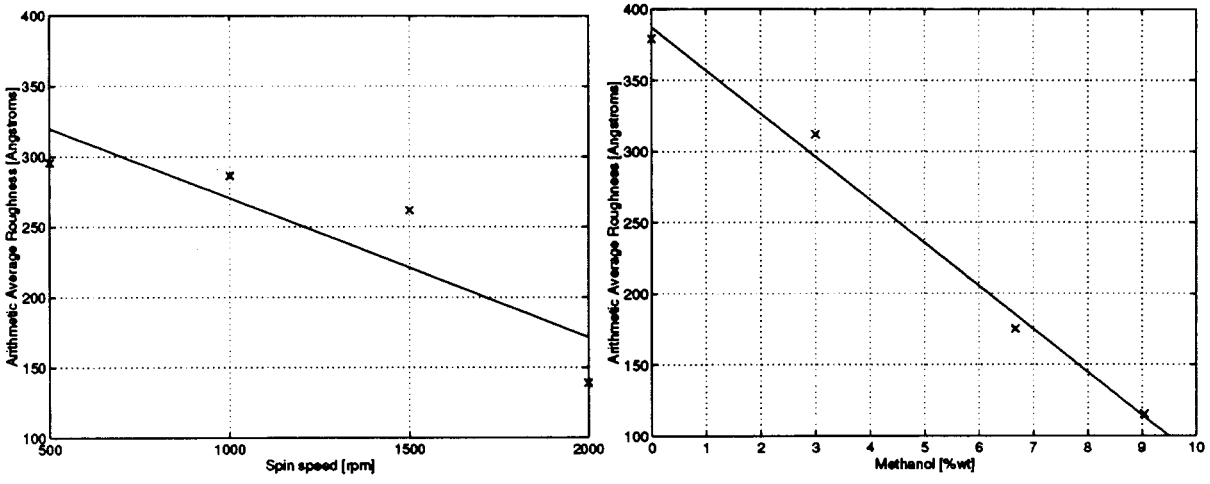

(a) (b)

Figure B.3: Arithmetic Average Roughness of UV Cured Films

Appendix C

ILCP Fabrication

Two main processing steps were used in the fabrication of the prototype ILCPs:

1. **IC Processing:** photodiodes and interconnect metalization and
2. **LC Processing:** creation of the LC guiding structure.

A photograph of one of the prototype ILCPs is shown in figure C.1.

C.1 IC Processing

Several photodiodes were diffused into two Si wafers using standard planer IC technology. During this processing, an SiO_2 cladding layer was also formed by a combination of wet oxidation and RF sputtering. Given the high refractive index of the photopolymer core material used in in this work, SiO_2 was a convenient choice for cladding layer. This oxide layer was subsequently etched from the surface of the photodiodes for the metalization contacts and to facilitate collection of the LC guided light. The details of the IC processing performed are as follows:

1. **Si Wafers:** Two 4 inch n-type <100> 30–60 Ohm·cm silicon wafers (labeled A and B).
2. **RCA Clean 1:** The wafers were cleaned using the standard RCA process with an oxide strip in hydrofluoric acid.
3. **Oxidation 1:** (cladding layer) Used 15 minutes dry, 4.5 hours wet then 15 more minutes dry oxidation in a Tempress furnace at 1100°C.

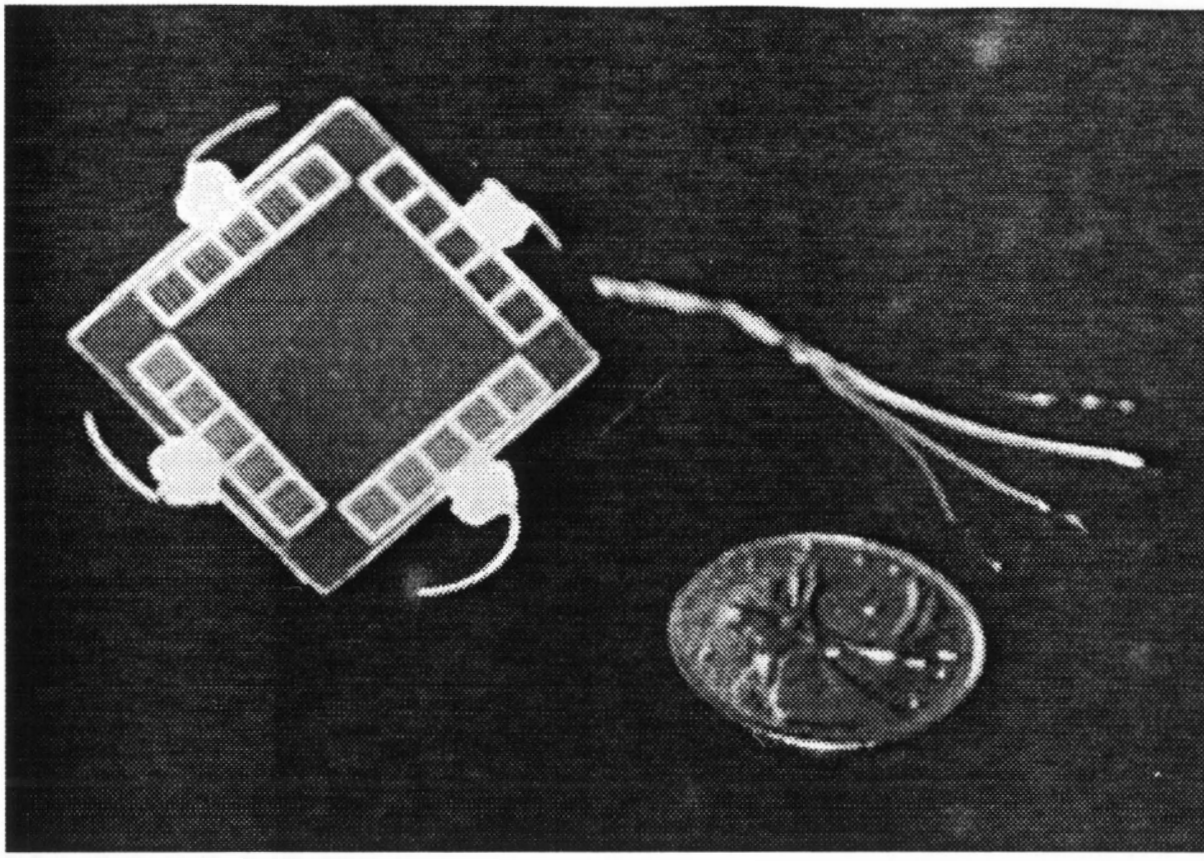

Figure C.1: Prototype ILCP

4. **Mask 1:** (oxide strip) Standard photolithography using a Quintel Corporation 100 W high pressure Hg mask–aligner was used to form an oxide mask for boron diffusion. The oxide was striped using buffered oxide etch (BOE) full strength for 11–12 minutes. The oxide thickness, measured with the profilometer and a Rudolph Research AutoEL^R–II automatic ellipsometer, for wafer A was 1.034 μm and for wafer B was 1.023 μm.
5. **RCA Clean 2:** The wafers were cleaned using the standard RCA process.
6. **Boron Diffusion:** (diode formation) Used boron (p-type) diffusion at 1100°C for 1 hour.
7. **RCA Clean 3:** The wafers were cleaned using the standard RCA process.
8. **Drive–in/Oxidation 2:** (cladding layer) Used 15 minutes dry, 30 minutes wet and then 15 more minutes dry oxidation at 1000°C.

9. **Oxide Sputtering:** (cladding layer – wafer A only) Used reactive ion RF sputtering in O_2 in a Corona Vacuum Coaters sputter coater system to deposit 0.5–0.7 μm of SiO_2.

10. **Mask 2:** (oxide strip) Standard photolithography was used to form oxide cuts for the metalization interconnect contacts. The oxide was striped using BOE full strength for 11–12 minutes. The oxide thickness measured for wafer A was 1.832 μm and for wafer B was 1.369 μm.

11. **Top Metalization:** Al was deposited on the top surface of the wafers by DC sputtering (for the interconnect metalization). The Al thickness, measured with the profilometer, for wafer A and B was 1.3 μm.

12. **Mask 3:** The wafers were cleaned in hot acetone vapors and standard photolithography used to pattern the Al interconnect metalization layer.

13. **Bottom Metalization:** AL was deposited on the bottom surface of the wafers by DC sputtering (for the substrate contact). The Al thickness measured for wafer A and B was 0.65 μm.

14. **Annealing:** The wafers were cleaned in hot acetone vapors and the metalization layers annealed in the oxidation furnace at 400°C for 30 minutes in N_2.

15. **Cleave:** Finally, the wafers were cleaved into four 5 cm square chips per wafer.

The chips produced were quite large to facilitate spin coating of the thin film LCs. These LCs could have been deposited and patterned prior to cleaving so that smaller chips could have been fabricated. To facilitate several experiments using the same wafers however, large sized chips were used.

C.2 LC Formation

The processing used to form the LC cores was equivalent to that described in section B.2:

1. **Clean:** rinse Si chips in acetone as a mild degreasing step and spin dry (4000 rpm for 30 seconds)

2. **Prespin:** dispense polymer solution and spin at low speed for uniform dispersion of resin (500 rpm 90 seconds)

3. **Spin:** spin at final speed (500, 1000, 1500 or 2000 rpm for 30 seconds) and allow wet film to settle for several minutes (about 10 minutes) to minimize bubble formation and to allow the self–leveling nature of the solution to produce a more uniform film.
4. **UV Cure:** cure under 100W high pressure Hg arc lamp in N_2 (5 minutes)
5. **Develop:** rinse in methyl ethyl ketone to remove uncured polymer
6. **Hard Bake:** heat film to remove any residual solvents from the solution and development (50°C for one hour)
7. **Anneal:** Annealed films on flat metallic surface (heat load) with a slow ramp up and down (145°C for 5 hours in N_2)

Finally, the contact pads on the ILCPs were accessed for testing by wire bonding using Acheson Electrodag 415 conductive epoxy.

Appendix D

Glossary

π–electrons: electrons that exist as a consequence of a particular configuration of carbon atoms in the molecule that result in the formation of **π–orbitals** (Becker 1969, page 4).

π–orbitals: electron molecular orbitals formed from a combination of appropriate p atomic orbitals (Lumb 1978, page 96).

absorption: (electronic excitation) an energy transition from the ground to an excited state when an incident photon is absorbed (Berlman 1971, page 10–11).

absorption spectra: depicts the vibrational spacing of lowest excited singlet state in a luminescent molecule (Lumb 1978, page 104).

bimolecular process: a process that occurs in a concentrated or aggregated system due to interactions between molecules of the same species (homo-polar) or in mixed molecular systems due to interactions with molecules of different species (hetero-polar) (Birks 1970, page 34).

branching: bifurcation of a polymer chain.

cascade composition: a mixture where *donor* luminophors luminesce at short wavelengths and *acceptor* chromophores luminesce at longer wavelengths (Krasovitskii and Bolotin 1988, page 12).

chromophore: a molecule or group of molecules that absorbs radiation (Berlman 1971, page 21).

co-polymers: polymers composed of two or more different mers (Van Vlack 1987, page 211).

critical angle: the minimum angle of incidence for total internal reflection.

cross–linking: in polymers, when molecules are tied together in three dimensions causing restrictions with respect to plastic deformation and so on (Van Vlack 1987, page 216).

delayed fluorescence: fluorescence originating from the triplet state that has an emission spectrum identical to the normal prompt fluorescence spectrum (Lumb 1978, page 100) (Berlman 1971, page 12).

diffusion controlled process: a process where the diffusion of reacting molecules toward one another is the rate determining step (Lumb 1978, page 127–128).

emission spectra: a plot of the distribution of luminescence as a function of wavelength for a given excitation that depicts the vibrational spacing of the ground state (Lumb 1978, page 104).

energy level diagram: (*Jablonski diagram*) a diagram that depicts the energy transitions in a luminescent molecule (Berlman 1971, page 9)).

energy migration: is the transfer of electronic excitation energy between molecules or groups of the same species (Birks 1970, page 518).

energy transfer: is the transfer of electronic excitation energy of a molecule or group of molecules to another molecule or group of a different species (Birks 1970, page 518).

excimer: a transient excited dimer formed via collisional interactions between an excited and unexcited molecule (Berlman 1971, page 54). An excimer is a distinct molecular system that can undergo photophysical processes similar to unimolecular processes (Birks 1970, page 335) the only difference being that it has a repulsive ground state (Lumb 1978, page 136).

exciplex: an excited molecular complex that (like an excimer) exists only in an excited state. The term exciplex is restricted to an excited complex of definite stoichiometry in order to distinguish it from a solvated excited molecule interacting with an indefinite number of unexcited molecules forming its solvent environment (Birks 1970, page 420).

excitation spectra: spectra that shows the variations in luminescence emission with changes in excitation wavelength (Lumb 1978, page 106).

fluorescence: Transitions between an excited singlet and the ground state that result in the immediate emission of a photon (Berlman 1971, page 10–11).

Franck–Condon factor: the transition probability between states of different multiplicity (Lumb 1978, page 137).

Franck–Condon principle: the energy transition following the absorption of a photon occurs too rapidly for the atomic nuclei to alter their spacing until the molecule reaches its excited state (Lumb 1978, page 104).

glass transition temperature: the temperature below which a polymer becomes rigid and various other of its properties change significantly (such as thermal expansion coefficient, rigidity, and viscoelastic modulus) (Van Vlack 1987, page 221).

Goos–Hänchen shift: a lateral shift of the reflected ray at the interface between two dielectric media as a consequence of the phase shift between the incident and reflected rays (a function of the angle of incidence) (Tamir 1988, page 17).

Hund's rule: for every excited singlet state there is a corresponding triplet state of lower energy(Lumb 1978, page 99) (Becker 1969, page 6).

internal conversion: (electronic relaxation) a transition from an highly excited state to the lowest excited state, where energy is lost as heat (Berlman 1971, page 10–11).

intersystem crossing: energy transitions between excited single and triplet states (Berlman 1971, page 10–11).

Kasha's rule: the luminescence of an aromatic molecule occurs only from the lowest excited electronic state of a given multiplicity (Birks 1970, page 162).

lightpipe: a transparent material system designed for transmitting *broadband light* along its length primarily by TIR at its physical boundaries.

luminescence: the emission of light that is not due to *incandescence* (Merriam–Webster Incorporated 1985).

luminophor: a molecule or group of molecules that emits radiation (Krasovitskii and Bolotin 1988, page 3).

matrix: the rigid transparent material that supports the luminescent molecules or ions in an LC (typically glass or plastic).

molecular complexes: formed when an electron acceptor is added to a solution containing a luminescent species that behaves as an electron donor via a process known as a **charge transfer absorption transition** (Birks 1970, page 403).

organic materials: compounds composed of carbon and hydrogen atoms (Merriam–Webster Incorporated 1985).

phosphorescence: a transition between the lowest excited triplet and ground state where a photon is released (Berlman 1971, page 10–11).

photodetector: a device that can be used to detect radiant light energy at either a specific or over a broad range of wavelengths and to produce an output signal that is proportional to the amount of energy absorbed (Dennis 1986, page 5).

photoluminescence: occurs when a molecule is excited by electromagnetic radiation (photons) to a state where it itself emits such radiation. This type of luminescence can emanate from either organic or inorganic materials.

photophysical process: a physical process (that is, one that does not involve a chemical change) resulting from the electronic excitation of a molecule or system of molecules by non-ionizing electromagnetic radiation (photons) (Birks 1970, page 29).

photoreceptor optics: the study of how the physical properties of photoreceptors (their structure, arrangement, orientation, shape, size, refractive index and membrane properties) influence their absorption of light and optical characteristics (Menzel and Snyder 1975).

polyfunctional monomer: a monomer that can form three dimensional or *network* polymers (Van Vlack 1987, page 214).

polymers: large or *macromolecules* made up of many repeating subunits or *mers* (Van Vlack 1987, page 197).

quantum efficiency: the probability that an excited molecule will follow a given pathway whether radiative or non-radiative (Lumb 1978, page 109).

radiationless processes the result of conversion of electronic energy to vibrational energy between states of the same or different multiplicity, without the emission of a photon. These processes are in competition with the radiative processes responsible for luminescence emission and can be roughly understood as the dissipation of energy in the form of heat (Lumb 1978, page 123).

radiationless transition: a horizontal transition a potential energy diagram that involves crossing or tunneling from the potential surface of the initial electronic state to the surface of the final electronic state (Birks 1970, page 155).

radiative transition: a vertical transition between surfaces corresponding to different electronic states a potential energy diagram (Birks 1970, page 155).

responsivity: the sensitivity of a photodetector; generally quoted in either Volts or Amps per Watt (Dennis 1986, page 9).

singlet state: an electronic state with an angular spin momentum of zero and a level multiplicity of one (Krasovitskii and Bolotin 1988, page 6).

spectral responsivity: a measure of a photodetector's output responsivity with respect to the incident wavelength (Dennis 1986, page 12).

Stokes shift: the loss in energy that results in a shift in wavelength between the absorbed and emitted radiation (Berlman 1971, page 57).

triplet state: an electronic state with an angular spin momentum of unity and a level multiplicity of three (Krasovitskii and Bolotin 1988, page 6).

uni-molecular process: a process that occurs in isolated molecules (Birks 1970, page 30).

UV curing: using UV radiation to polymerize monomers or cross–link of *functionalized polymers*, especially in the hardening of thin films (Cheremisinoff 1989, page 579).

Vavilov's law: states that the quantum efficiency is independent of the initial vibrational and electronic states into which the molecule is excited. That is, the properties of a molecule in dilute solution are independent of the initial vibrational and electronic state to which it is excited (Birks 1970, page 142).

vibronic state: a molecular electronic level superimposed with vibrational and rotational sub-levels associated with the motion of the main molecular skeleton (Birks 1970, page 44–45) (Berlman 1971, page 9).

vibronic transition: an energy transition between vibronic states (Birks 1970, page 44–45) (Berlman 1971, page 9).

waveguide: a material system designed for transmitting *monochromatic light* primarily by TIR at its physical boundaries. A waveguide designed to carry only one propagating mode at a given wavelength is said to be *single–moded.* A waveguide designed to carry more then one mode is *multi–moded.*

References

Adams, D. (1984). *So Long and Thanks for All the Fish.* Michelin House, 81 Fulham Road, London SW3 6RB: William Heinemann Ltd.

Baczynski, A., T. Marszalek, H. Walerys, and B. Zietek (1973). The influence of molecular parameters on laser properties of dye solutions. *Acta Physica Polonica A 44*(6), 805–812.

Baranow, V. (1991, August). Luminescent concentrators as spectral elements. *Soviet Journal of Optical Technology 58*(8), 472–474.

Batchelder, J., A. Zewail, and T. Cole (1979, September). Luminescent solar concentrators. 1: Theory of operation and techniques for performance evaluation. *Applied Optics 18*(18), 3090–3110.

Batchelder, J., A. Zewail, and T. Cole (1981, November). Luminescent solar concentrators. 2: Experimental and theoretical analysis of their possible efficiencies. *Applied Optics 20*(21), 3733–3754.

Becker, R. S. (1969). *Theory and Interpretation of Fluorescence and Phosphorescence.* New York: Wiley Interscience.

Berlman, I. (1971). *Handbook of Fluorescence Spectra of Aromatic Molecules* (Second ed.). New York: Academic Press.

Biggs, W. W. (1991). Radiation measurement. Radiation Measurement Instruments Catalog LMI-1291, LI-COR, Incorporated, 4421 Superior Street, P.O. Box 4425, Lincoln, Nebraska 68504 USA.

Birks, J. B. (1970). *Photophysics of Aromatic Molecules* (1 ed.). London: Wiley-Interscience, John Wiley & Sons Ltd.

Cheremisinoff, N. P. (Ed.) (1989). *Handbook of Polymer Science and Technology*, Volume 3 Applications and Processing Operations. New York: Marcell Dekker, Inc.

Council Report (1989, July). Harmful effects of ultraviolet radiation. *Journal of the American Medical Association 262*(3), 380–384.

Dennis, P. (1986). *Photodetectors - An Introduction to Current Technology.* Updates in Applied Physics and Electrical Technology. New York: Plenum Press.

Driscoll, W. G. and W. Vaughan (Eds.) (1978). *Handbook of Optics.* McGraw-Hill Book company.

Environment Canada (1993, March). UV and YOU. Brochure En56-97/1992E, Health and Welfare Canada, Communications Branch, Jeanne Mance Building, Tunney's Pasture, Ottawa, Ontario K1A 0K9.

Evenson, S. A. and A. H. Rawicz (1994, June). Integrated luminescent–concentrator photodetector. In G. A. Lampropoulos (Ed.), *International Conference on Applications of Photonic Technology – Sensing, Signal Processing and Communications*, Toronto, Ontario, Canada. IEEE/IEE: Plenum Press, New York.

Feucht, D. L. and J. R. Burke (1981). Advanced photovoltaic research in the u.s. In *Proceedings of the Symposium on Materials and New Processing Technologies for Photovoltaics*, Volume 81–3, pp. 271–280. The Electrochemical Society, Inc.

Flack, W. W., D. S. Soong, A. T. Bell, and D. W. Hess (1984, August). A mathematical model for spin coating of polymer resists. *jap 56*(4), 1199–1206.

Goetzberger, A. (1978). Fluorescent solar energy collectors: Operating conditions with diffuse light. *Applied Phyics 16*, 399–404.

Goetzberger, A. and W. Greubel (1977). Solar energy conversion with fluorescent collectors. *Applied Phyics 14*, 123–139.

Harnak, L. A. (Ed.) (1992). *Polymers for Lightwave and Integrated Optics.* New York, New York: Marcel Dekker, Inc.

Hartman, D. H., G. R. Lalk, J. W. Howse, and R. R. Krchnavek (1989, January). Radiant cured polymer optical waveguides on printed circuit boards for photonic interconnection use. *Applied Optics 28*(1), 40–47.

Heidler, K. (1981, March). Efficiency and concentration ratio measurments of fluorescent solar concentrators using a xenon measurment system. *Applied Optics 20*(5), 773–777.

Hermann, A. (1982). Luminescent solar concentrators – a review. *Solar Energy 29*(4), 323–329.

Krasovitskii, B. and B. Bolotin (1988). *Organic Luminescent Materials* (Second ed.). Weinheim (Federal Republic of Germany): VCH Verlagsgesellschaft.

Krchnavek, R., G. Lalk, and R. Denton (1992, May 1–3). Photo-polymerized acrylic waveguides for optical interconnects. In C. Ward, J. Stamatoff, and W. Wang (Eds.), *Materials for Optical Information Processing Symposium*, Pittsburgh, PA, pp. 95–100. Material Research Society.

Krchnavek, R. R., G. R. Lalk, and D. H. Hartman (1989, December). Laser direct writing of channel waveguides using spin-on polymers. *Journal of Applied Physics 66*(1), 5156–5160.

Lancaster, P. and K. Salkauskas (1986). *Curve and Surface Fitting: an introduction.* Computational mathematics and applications. London: Academic Press.

Leibovic, K. (Ed.) (1990). *Science of Vision.* Springer–Verlag New York Inc., New York, New York.

Levin, M., A. Cherkasov, and V. Baranov (1988, March). Luminescent light concentrators. *Soviet Journal of Optical Technology 55*(3), 180–189.

Levitt, J. and W. Weber (1977, October). Materials for luminescent greenhouse solar collectors. *Applied Optics 16*(10), 2684–2689.

Lumb, M. D. (Ed.) (1978). *Luminescence Spectroscopy.* London: Academic Press.

Menzel, R. and A. W. Snyder (1975). Introduction to photoreceptor optics – an overview. In A. Snyder and R. Menzel (Eds.), *Photoreceptor Optics*, pp. 1–13. Berlin Heidelberg: Springer–Verlag.

Merriam–Webster Incorporated (1985). *Webster's Ninth New Collegiate Dictionary.* Markham, Ontario: Thomas Allen and Son Limited.

Meseguer, F., F. Jaque, F. Cussó, and C. Sánchez (1981). Temperature effects on the efficiency of luminescent solar concentrators (lsc) for photovoltaic systems. *Journal of Luminescence 24*(25), 865–868.

Meseguer Rico, F., F. Jaque, and F. Cussó (1981). Thermal damage in luminescent solar concentrators (lsc) for photovoltaic systems. *Journal of Power Sources 6*, 383–388.

Nakagawa, K., T. Kowalewski, C. Phelps, D. Rode, and R. Krchnavek (1994, January). Optical channel waveguides based on photo-polymerizable di/tri acrylates. Preprint: SPIE OE/LASE '94, Optical Interconnects II, Los Angeles, CA.

Newport Corporation (1991). Newport 815 power meter. Manual P/N 5185-04, Revision B, IN-11833 (9-91), Newport Corporation, Fountain Valley, CA.

Olson, R., R. F. Loring, and M. Fayer (1981, September). Luminescent solar concentrators and the reabsorption problem. *Applied Optics 20*(17), 2934–2940.

Reisfeld, R. and Y. Kalisky (1980, January). Improved planer solar convertor based on uranyl neodymium and holmium glasses. *Nature 283*, 281–282.

Reisfeld, R. and S. Neuman (1978, July). Planar solar energy convertor and concentrator based on uranyl-doped glass. *Nature 274*, 144–145.

Ries, H. (1982, March). Thermodynamic limitations of the concentration of electromagnetic radiation. *Journal of the Optical Society of America 72*(3), 380–385.

Roncali, J. and F. Garnier (1984a). New luminescent back reflectors for the improvement of the spectral response and efficiency of luminescent solar concentrators. *Solar Cells 13*, 133–143.

Roncali, J. and F. Garnier (1984b, August). Photon – transport properties of luminescent solar concentrators: analysis and optimization. *Applied Optics 23*(16), 2809–2817.

Sah, R. (1981). Stokes shift of fluorescent dyes in the doped polymer matrix. *Journal of Luminescence 24*(25), 869–872.

Sah, R. and G. Baur (1980). Influence of the solvent matrix on the overlapping of the absorption and emission bands of solute fluorescent dyes. *Applied Physics 23*, 369–372.

Shepherd, G. M. (Ed.) (1990). *The Synaptic Organization of the Brain (3rd ed)*, Chapter 6, pp. 170–213. Oxford University Press, Boston, Massachusets.

Snyder, A., T. Bossomaier, and A. Hughes (1990). The theory of comparative eye design. In C. Blakemore (Ed.), *Vision: coding and efficiency*, Chapter 4, pp. 45–52. Cambridge: Cambridge University Press.

Swartz, B., T. Cole, and A. Zewail (1977, August). Photon trapping and energy transfer in multiple-dye plastic matrices: an efficient solar-energy concentrator. *Optics Letters 1*(2), 73–75.

Syms, R. and J. Cozens (1992). *Optical guided waves and devices.* New York: McGraw-Hill.

Tamir, T. (Ed.) (1988). *Guided – Wave Optoelectronics.* Springer Series in Electronics and Photonics. Berlin Heidelberg: Springer – Verlag.

Van Overstraeten, R. and R. Mertens (1986). *Physics, technology and use of photovoltaics.* Modern energy studies. Bristol: Hilger.

Van Vlack, L. H. (1987). *Elements of Materials Science and Engineering* (fifth ed.). Addison-Wesley Series in Metallurgy and Materials Engineering. Massachusetts: Addison-Wesley Publishing Company.

Weber, W. and J. Lambe (1976, October). Luminescent greenhouse collector for solar radiation. *Applied Optics 15*(10), 2299–2300.

Weiss, S. A. (1994, June). Silicon photodiode efficient in the ultraviolet. *Photonics Spectra 28*(6), 41.

Welford, W. and R. Winston (1989). *High collection nonimaging optics.* San Diego: Academic Press.

Yablonovitch, E. (1980, November). Thermodynamics of the fuorescent planar concentrator. *Journal of the Optical Society of America 70*(11), 1362–1363.

Zewail, A. and J. Batchelder (1983). Luminescent solar concentrators: An overview. In *Polymers in Solar Energy Utilization*, Washington, pp. 331–352. American Chemical Society: American Chemical Society.